Medium power electric generators for wind power application

Damia-2 application status report

Avo Reinap

Division of Industrial Electrical Engineering and Automation
Faculty of Engineering, Lund University

Medium power electric generators for wind power application

This is a reviewing document on design and evaluation of a few types of electrical machines for wind power application. In fact the wind power application as a target for designing and manufacturing electrical machines is excluded in the beginning of DAMIA-2. It is considered that these particularly low speed applications are not the smart goal for a high frequency magnetic material even though the magnetization frequency can be geared up with the high number of poles. Anyhow, a few of the most considerable reasons to return to the wind power applications are

1. the **production technique** as an alternative input to **build large machines** with uncommon layout and assembly

2. the possibility to **improve coreless machine performance** when introducing core parts of a soft magnetic moldable composite (SMMC=SM²C)

1   Review and target specifications

Initially, in the early days of SM²C suitability studies for wind power applications, a direct driven permanent magnet (PM) excited axial flux (AF) synchronous machine (SM) received a considerable amount of attention. After some time the design development turned towards radial flux (RF) PMSM as a more suitable candidate for the wind power application and that due to the mechanical design point of view. There is a prototyped RFPMSM, which inherited the measures $D_o/D_i\text{-}H_{act}$, *310/240-60 mm* respectively, from another – in-wheel application, but which is also matched for the wind power application as a necessary design input for the development process (Ch.2). Opportunely, the AFPMSM with $D_o/D_i\text{-}H_{act}$ *600/400-60 mm*, became actual in the redesigning and evaluation process (Ch.3). As an outcome some more far-reaching concepts are selected for further research in the same size range, when trying to match the needs and requirements for small-scale wind power applications (Ch.4). Next, the wind power application is specified; shortly the different machine topologies and system requirements are reviewed.

1.1   Application specification

Vertical axis wind turbines in the expected speed range of *50* to *200 rpm* with the demand of a few kW of the rated power are the main specification for the target machine. As a result the specification for the mechanical input torque is a few hundreds of Nm at load and a few Nm at start. As an example, machine that provides *200 Nm* and rotates at *100 rpm* has power nearly *2kW*, in reality the power demand is higher and the rotation speed lower. Therefore different machine topologies are revised with the attention towards a high specific torque.

1.2   Machine topology specification

Considering the type of excitation and the arrangements of the armature coils to the excitation field a number of different machine types can be specified (Table 1.1).

Table 1.1 Classification of electrical machines according to coil-to-gap arrangements and the type of excitation

Armature coils arrangements and orientation to air-gap	Type of excitation
Direct coupling to the field • Axial flux machine • Radial flux machine • Axial-Radial flux machine	Single feed: • Reluctance excitation • Induced excitation
	Multi feed • Electric excitation • Permanent magnet excitation
Indirect coupling to the field • Circumferential flux machine • Transversal flux machine	Combined • Hybrid excitation

If the armature coils are directly coupled to the excitation field, then the armature do not need to necessarily have a magnetic core (Table 1.1). By choosing a coreless or lightly coreless stator with permanent magnet excited rotor there is a good opportunity that the machine suits to the application where the direct drive and a low starting torque are one of the requirements. The purpose of the magnetic core is to magnify, guide and to couple magnetically magnetic sources and loads. If the magnetic core carries alternating magnetic field, then the field alternation induces electric field and gives reason to the flow of electric currents exactly like in the connected armature coils of the machine in the generator operation. Therefore, the magnetic core has to have low energy losses such as previously mentioned eddy current losses but also hysteresis losses. As a matter of fact one of the attractive features of SM²C is low core losses, and with combination with coreless machine topologies, the core material and machine production methods becomes highly interesting.

The specific torque and the specific cost are too important factors for the successful product so there is forth to analyze the main factors behind the cost effective torque capability. Permanent magnets are known not only because of their high specific cost but also because of very high energy

density and low energy loss density. The magnets are almost irreplaceable in the small machines ($Do<5\ cm$) and are still quite beneficial in medium size machines ($5<Do<50\ cm$). On contrary larger machines are almost free of permanent magnets as for magnetizing purposes.

The torque capability is not only related to the strength of the excitation field and the armature field at the range under the magnetic saturation but also the loads and power losses due to that. Therefore heat power and cooling is some of the factors that limit the torque capability. It can be considered that at the peak power production, which occurs at the high wind speed, there is also considerably better cooling conditions. The occurrence of the peak loading and cooling has to be adequately considered in the design.

Torque capability

The purpose of a rotating electrical machine is to provide torque – braking or driving in order to convert mechanical energy to electrical or vice versa. The ability to produce the torque depends on electric and magnetic loading of the machine, which is basically the current and flux density in the magnetically coupled coil and core that results not only the flux density but also a magnetic displacement of poles in the air-gap. As an outcome the force density or magnetic pressure between the machine parts is established. From torque production point of view the magnetic shear stress over the gap-area is the quantity that relates the size and torque for the specified arrangement and strengths of the displaced magnets.
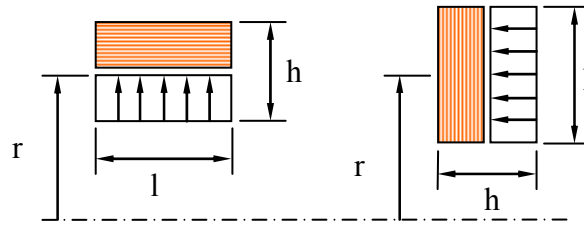

Figure 1.1 Rough dimensioning of a radial flux machine (left) and axial flux machine (right)

The torque capability in relation to the dimensions presented in Figure 1.1 and the selected types of machine topologies are calculated according to 1.1 for radial flux machine and 1.2 for axial flux machine, respectively.

$$T_{em\,EF} = 2\pi\sigma r^2 l \qquad\qquad 1.1$$

$$T_{em\,AF} = 2\pi\sigma\int_{r_i}^{r_o} r^2 dr = \frac{2}{3}\pi\sigma r_o^3\left(1-\left(\frac{r_i}{r_o}\right)^3\right) = \frac{2}{3}\pi\sigma\left((r+0.5l)^3 - (r-0.5l)^3\right) 1.2$$

The magnetic shear stress is selected $\sigma=5000\ N/m^2$ and assumed to be constant over the axial plane between the rotor and the stator in AF-machine. The reason for the low value of magnetic shear stress is that this selected value is based on the design experience of naturally cooled machines with SM2C core and PM excitation. At the same time it is easy to use a multiple of shear stress and to get rough scaling of the torque capability of the machine. The calculated results of torque are shown in Figure 1.2. The machine length l is shown along rotating axis for RF-machine and as a difference between inner and outer radius for AF-machine. Radius r corresponds to an air-gap radius of the RF machine and a mean radius of the inner and the outer radius for the AF-machine.

There are two target sizes, which are marked as a blue circles on the following contour plots (Figure 1.2 - Figure 1.4)

1. Radial flux machine, D_o/D_i-H_{act}, *310/240-60 mm*, which is inherited from in-wheel application and adapted to in-wind application

2. Axial flux machine, D_o/D_i-H_{act} *600/400-60 mm*, which is built and tested by Bo-Henrik Karlsson
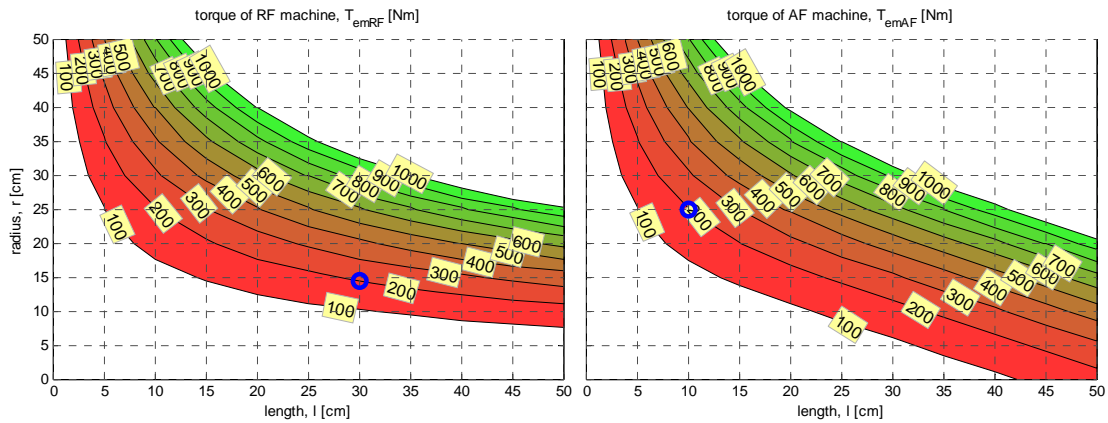
Figure 1.2 Electromagnetic torque of a radial flux (left) and axial flux (right) machine at shear stress of 5kPa

Taking into account the air-gap shear stress area and by selecting the magnetic shear stress the torque and **power** at given speed (of **50 rpm**) can be estimated (Figure 1.3).
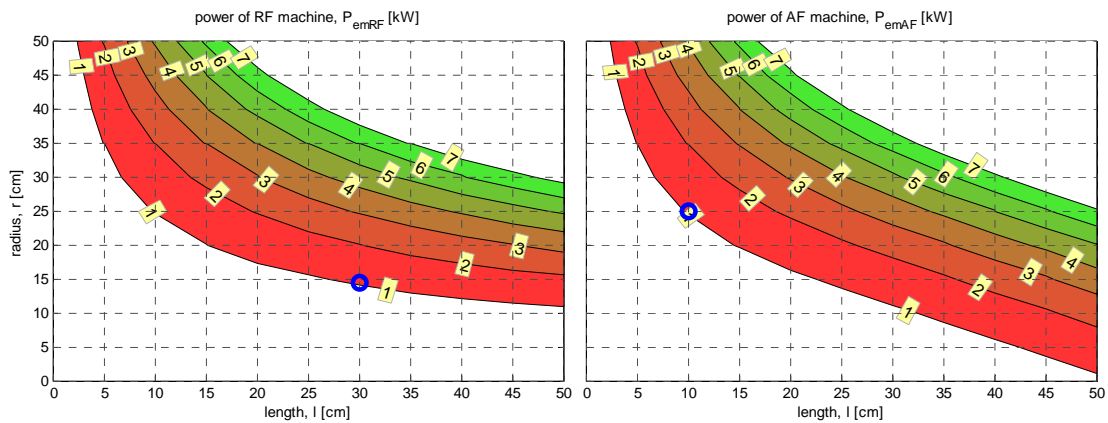

Figure 1.3 Electromagnetic power of a radial flux (left) and axial flux (right) machine at 50 rpm

By selecting the belt thickness for the stator and rotor (*h* in Figure 1.1 selected to be **100 mm** for this example) the approximate **weight** of the electrical machine is estimated (Figure 1.4). in this estimation the equivalent density of the electrical machine is selected to be **7000 kg/m³**.

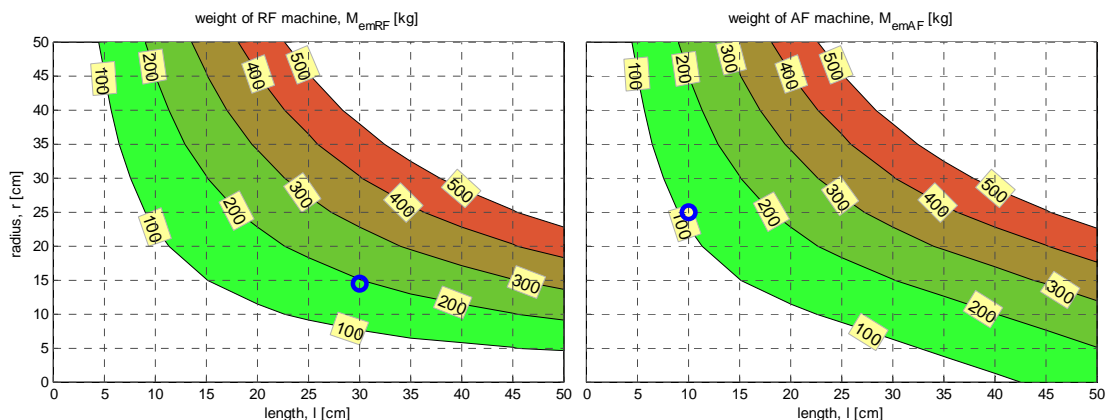*Figure 1.4 Machine material weight of a radial flux (left) and axial flux (right) machine at 7000 kg/m3*

From the previous graphs (Figure 1.2 - Figure 1.4) it is not apparent whether axial flux machine has clear advantages over radial flux machine or not. Basically the larger available shear stress area for constructing axial flux machine or radial flux machine gives the preferences to specific topology of the electrical machine.

Another specific feature for these large machines with high number of poles is the specification of the slotting and winding arrangements so that the electromagnetic torque is maximized and the ripple and cogging torque is minimized. Here are given a number of following examples (Figure 1.5 - Figure 1.6) that target is a modular winding arrangement of a distributed concentrated (non overlapping) winding. Some attractive arrangements of concentrated windings for arbitrarily selected number of poles shown as outer rotor radial flux machine in Figure 1.5 or axial flux machine in Figure 1.6.
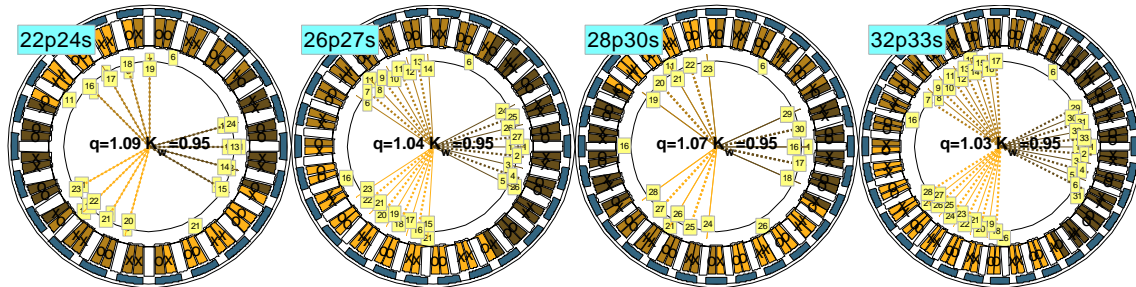

Figure 1.5 Some examples of distributed concentrated winding that forms a modular winding segment in an outer rotor radial flux machine
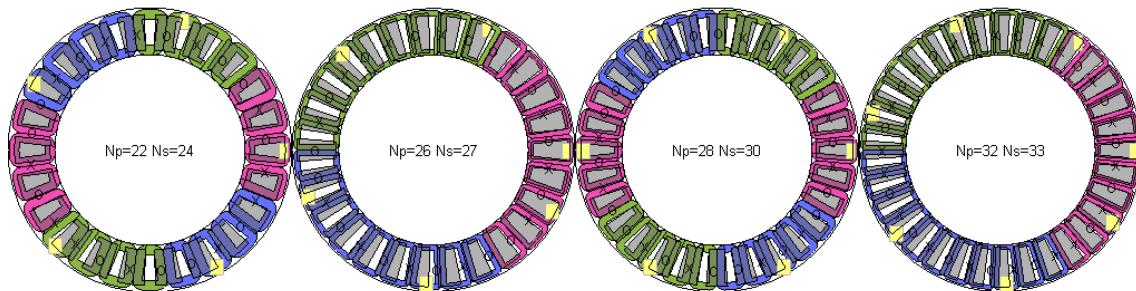

Figure 1.6 Some examples of distributed concentrated winding that forms a modular winding segment in axial flux machine

Previously the air-gap location and dimensions is related to the electromagnetic torque capability and the approximate size of the machine. There are also some suggestions given on how to reduce cogging torque by selecting the number of teeth slightly larger or smaller but not equal to the number of poles. The outcome is modular winding and this is considered to be a smart manufacturing of producing a chain of high fill coils in prior to molding. Consequently, this rough assumption of torque capability determines the size and the air-gap power at a selected speed. Correspondingly the power related to the speed and the torque or voltages and currents is reduced by the internal loads when requiring torque from the motor shaft or generated voltage from the generator terminals. As a result the power capability is shortly studied.

Power capability

As the torque of the machine is related to the size and the power is related to the speed there is also a power factor and power losses that sets the limits to the power conversion. For the sake of simplicity, the power losses are excluded in the first round and the voltage balance is focused only. The action of magnetic induction establishes the back electromotive force E and the (armature) reaction of the stator winding due to current I and reactance X_s determines the terminal voltage U. The generator can be easily expressed as a transmission line with the internal (induced) voltage that the excitation field interacted windings are able to produce and the received voltage in the terminals at different loadings and load current (Figure 1.7).
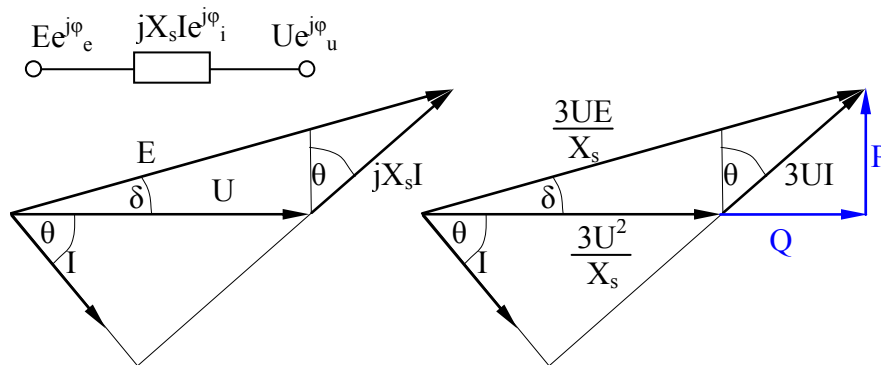
Figure 1.7 Phasor diagram and power transmission of a generator based on internal and terminal nodes

The phasor diagram is extended to power diagram where the maximum extracted power depends on the load angle between the excitation field and the armature field.

$$P_{out} \approx \frac{3UE \sin \delta}{X_s} \quad 1.3$$

The main concern from now is to specify on how the electrical machine is connected to the wind turbine and to the electric load.

1.3   Drive topology specification

From the utilization of the power unit point of view it is important to consider a number of different choices for the connection topology and control strategy as a tradeoff between the installation cost and the amount of extracted power from the wind. Although the main (project) focus is on the subsystem design and manufacturing, which objective is an electrical machine on generator mode, the essential specifications comes from the system level and this is related to the maximization of energy conversion capacity at the minimum weight and cost of the electrical machine and the supplementary devices. Considering the connections from the wind turbine (WT) to the synchronous generator (SG) and from SG to the intermediate link (IL) to the load or the power grid there are following options:

1. mechanical link between WT and SG: direct-drive (DD) or geared-drive (GD)

2. electrical link between SG and IL: passive, semi-active, active light and full

It is important to consider these options not only design but also on the practical evaluation of the prototyped machine.

Mechanical link

It is expected that the machine is directly coupled to the wind turbine in order to reduce the gear box and possible problems related to that. On the contrary, the mechanical transmission can gear up the speed and make electrical machine more useful as a high speed device. Contra rotating system, single stage gear, etc are the possible solutions to reduce the size for the machine, but it is not considered as the option of the reduced complexity for the direct drive system.

Electrical link

There are a few specific issues on how the electric connection of the power system is considered; hereby the man concern is 1) power delivery and control on generator side, and 2) the control realization. Generation connection topology and controllability can be considered as a stand alone or coupled generator, off-grid on on-line coupling. In this project it is considered as a stand alone and off grid power unit that delivers power to 1) three phase resistor bank, 2) dc-link resistor via a diode bridge, or 3) power factor compensated passive electric connection. The estimation of the power harvesting is calculated for a 24-pole 27-coil PM machine that parameters are: $\Psi=2.05Vs$, $R=26Ohm$, $L=0.099H$ used to calculate power across the generator 50 rpm and 200 rpm. The total power includes the power drop in the generator due to winding resistances and the useful power across the load resistor.

The first system arrangement takes advantage of the three-phase resistive load that is connected across the machine terminals via some voltage and current measurement devices (Figure 1.8). The same schematic is used in the practical measurements, when the harvested energy is counted as the power losses across the resistive load. The turbine rotates at certain speed, 50 and 200 rpm in the simulation, when the electric load is connected across the terminals. The voltage and current waveforms of the three-phase system can be distinguished in Figure 1.9.
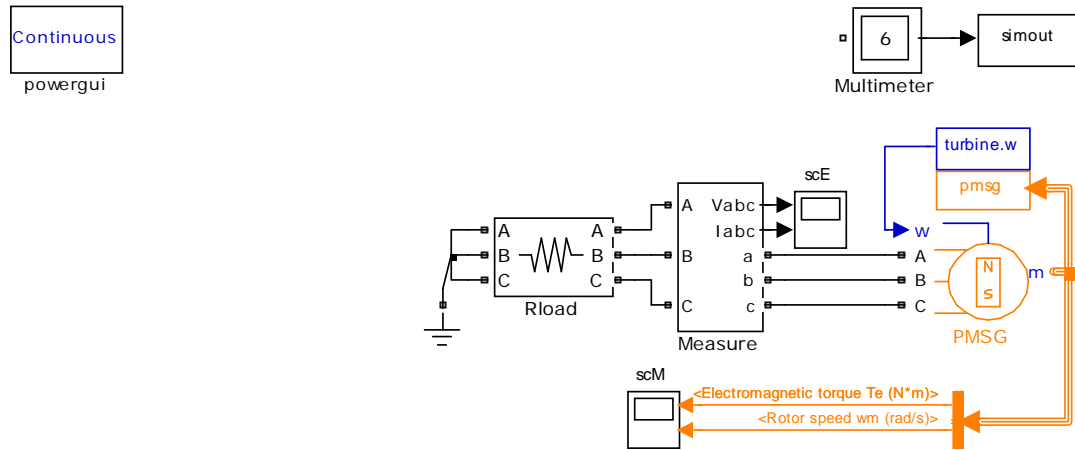

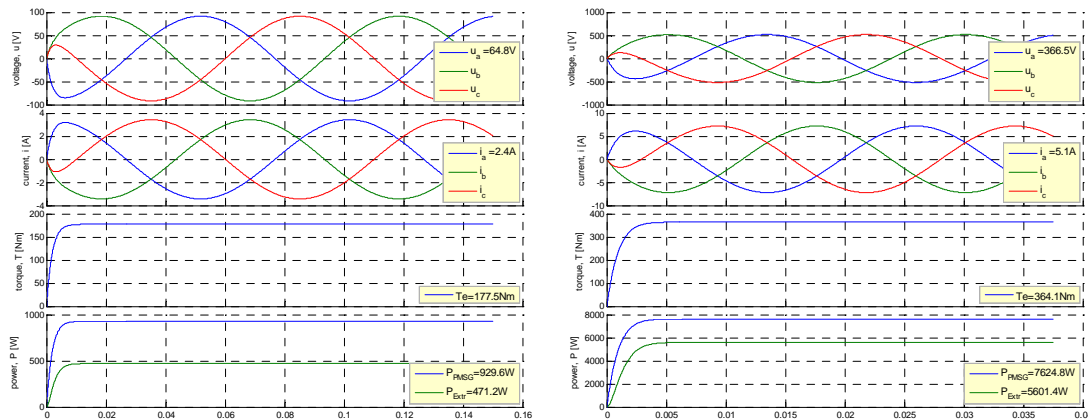*Figure 1.8 PM generator loaded with three phase resistor bank*

Figure 1.9 Voltage, current, torque and power waveforms of the PMSG with the three phase resistor bank at 50 and 200 rpm

The simulation with 50 rpm (Figure 1.9 in the left) shows the results at maximum output power when $R_{load}=abs(R_s+jX_s)=|Z_s|$ so that half of the generated electric power is consumed over internal resistance and half of it over load resistance. The terminal voltage drops by half and the current is half of the short-circuit current. The load angle in this case is 6.7 degrees. At higher speed of 200 rpm a different loading point is selected: $R_{load}=2|Z_s|$ so that the machine does not operate at the maximum loading point with larger current and there is more power dissipated over the load resistance than the winding resistance at the lower current.

The short circuit current is

$$I_{ss} = \frac{E}{Z_s} \qquad\qquad 1.4$$

and at the maximum load point the terminal voltage is half of the induced voltage and current is half of the short circuit current thus

$$P_{out} = \frac{E^2}{4Z_s} \qquad\qquad 1.5$$

The second system arrangement is more conventional passive front end connection of the PMSG (permanent magnet synchronous generator) to the electric load (Figure 1.10). In this layout the varying power input from the wind turbine is rectified to the dc-link that voltage can be varied in order to track the maximum power and used to feed inverter that makes the connection between the grid and the generator possible. Even though, the circuit or part of this circuit is more in use practice in the real devices, it is not used in the practical measurements in this project. The necessary input though is to consider the additional power losses in the generator due to the high harmonic content of the phase currents.
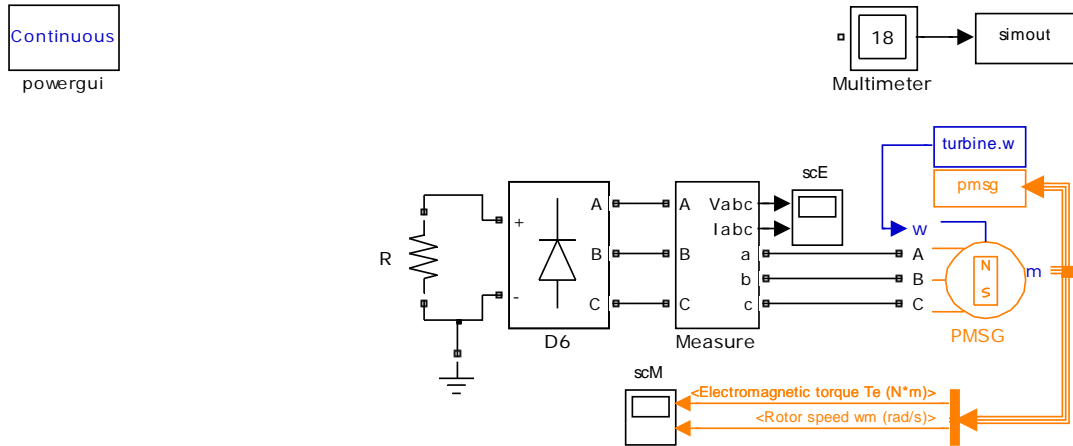

Figure 1.10 PM generator with passive front end – diode bridge rectifier, and resistive load in the dc-link

Figure 1.11 Voltage, current, torque and power waveforms of the PMSG with diode bridge and dc-link resistive load at 50 and 200 rpm

The simulation with 50 rpm (Figure 1.11 in the left) shows again the results at maximum output power when $R_{load}=1.68|Z_s|$ so that approximately half of the generated electric power falls over internal resistance and half of it over load resistance. The forward voltage of $U_d=1V$ and resistance of $R_d=1mOhm$ is specified for the diodes. The load angle in this case is 5.2 degrees. At higher speed of 200 rpm a different loading point is selected where the previous value of the load resistance is doubled. Similar to before the machine does not operate at the maximum loading point with larger current and there is more power dissipated over the load resistance than the winding resistance at the lower current. Small reduction of harvested and the total load power compared to the resistive 3-phase load is observed and the study on the system level is not continued here.

The third system arrangement that is presented here is just a comparison of a various "passive" efforts to get more out from a PMSG (1.4). In this case the reactance of the electrical machine is tried to be compensated with a capacitor bank (Figure 1.12).

Figure 1.12 PM generator with series connected capacitor bank for power factor compensation
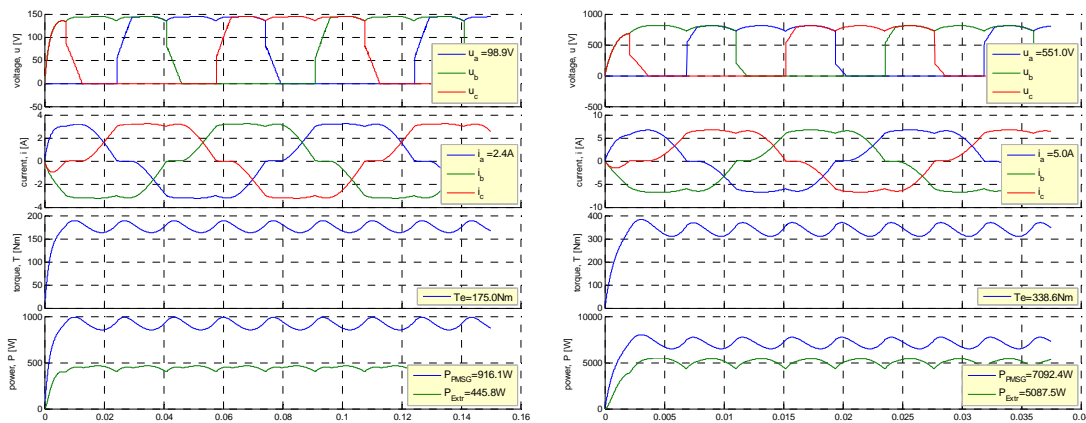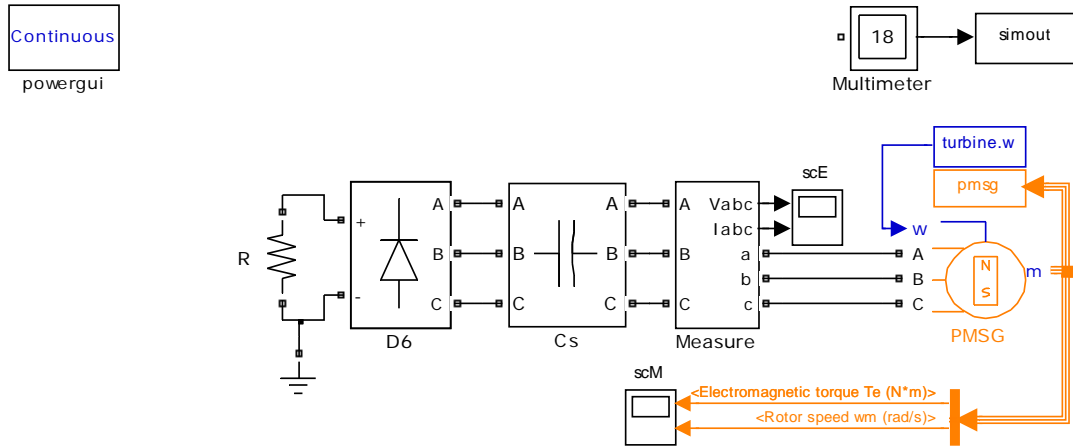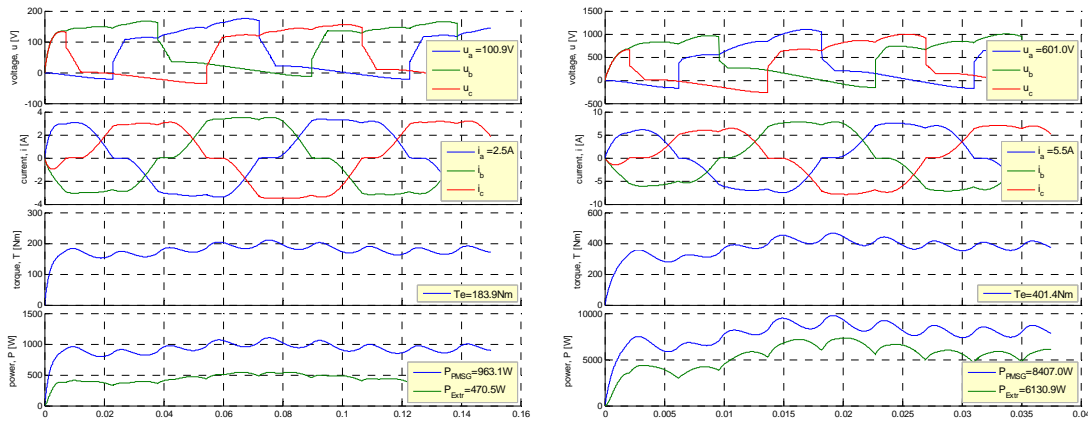

Figure 1.13 Voltage, current, torque and power waveforms of the PMSG with capacitor bank, diode bridge and dc-link resistive load at 50 and 200 rpm

The simulation with 50 rpm (Figure 1.13 in the left) shows again the results at maximum output power when $R_{load}=1.68|Z_s|$ so that approximately half of the generated electric power falls over internal resistance and half of it over load resistance. The load angle in this case is 21.6 degrees. To be repeated: at higher speed of 200 rpm a different loading point is selected where the previous value of the load resistance is doubled. Similar to before the machine does not operate at the maximum loading point with larger current and there is more power dissipated over the load resistance than the winding resistance at the lower current. As a result, this time a small increase of harvested and the total load power compared to the resistive 3-phase load is observed and the study on the system level is not continued here.

As a matter of fact, the system arrangement and right dimensioning so that the investments can ever earned back becomes more important than just providing a PMSG with large size and cost to be able to harvest some power at low speed. Still the goal of this work is provide just an electrical machine and not to carry deeper analysis on the system level. At the same time the short study on system level convinces to dimension and test the machine with a resistive three-phase load.

1.4   Literature review

There is wide range of reported experience such as books, rapports and articles that has an important contribution to the development of the medium power in-wind application that is not limited by the PMSG design but covers various relevant topics, provides comparative analysis and exhaustive experimental works. The literature review is divided into three parts: 1) system realization, 2) generator specification and 3) control implementation. Different converter topologies [3], reviews [7][16], development trends [1] and comparison [6][29][47] has been reported, where part of connection schemes [12][27][34] and system investment analysis [32][37] gives a wide spectrum to this area. Having the focus on the control object – direct drive PMSG reviews [2][5], also on alternative machine topologies, design [52], system analysis [48] and realizations [13][17][22][41][43][46]bring to different issues on power losses [18][56], mounting specification [19] and gearing options [39], where different solutions are presented [24][30][36] and their realization analyzed [25]. When it comes to control [8][14][20] and control design [28] then the variable speed drives and peak power tracking gets a lot of attention [10][11][15][21][23][26][33][38][40][42][44][53][54]. Last but not least, the experimental work related to small [9] or medium [30] size wind turbine system is treated. There is a fraction of available sources that is scanned through for this project.

2 Radial flux machine with SM²C core

Radial flux machines with various winding arrangements are becoming attractive when trying to adapt their size to the torque requirement. The eccentricity can be problematic but manageable for the machines with large diameter. Alternatively, the number of stacked axial flux machines is considered as more demanding solution when it comes to a large air-gap area, huge normal forces, mechanical assembling and support. This can be considered shortly the reasoning behind the different machine types that the radial flux type of synchronous machine gained more attention.

Hereby, the author of this status report acknowledges Lars Brändström from Maskinmontage Syd and Mats Olsson from Examec AB on their valuable contribution.

2.1 Size specification

Soft magnetic moldable composite can be attractive material from manufacturing point of view and challenging choice when carrying out electromagnetic design. The size specification is an interesting issue for the SM²C machines as it is expected that

1. by shortening the magnetization path the low permeability plays less role,

2. shorter magnetization path means more paths per unit of gap peripheral length

3. more magnetization paths leads to higher number of poles

4. higher number of poles introduces to higher magnetization frequency

5. higher magnetization frequency results usually to higher power losses

6. SM²C have inherently low power losses at high frequency

The resulting question is whether the magnetization frequency can be increased so that the loss of the magnetic strength can be compensated with the speed in order to maintain the power. Usually the machine is a direct drive unit to an application that speed is strictly specified. This results that the machine needs to provide the torque that the application requires. Whether it is possible or not, the machine size can be adapted to the required torque and the higher frequency by adapting the gap radius. The adaption of the machine is not only the force and speed but also current and voltage. Usually the magnetic energy is in the air-gap and change of this energy is converted to mechanical work. By leaving this energy change outside the air-gap, which is the low permeability core, means that there are extra sources needed to maintain this energy change.

This is the argumentation behind the adaption of electrical machine to an application and the application requirements. This design experience, which bases on increasing the gap-radius and the machine diameter from Do=270 mm to Do=310 mm, has been one of the preceding practical efforts to meet the torque requirement for SM²C core machines.

2.2 Maximizing torque capability with SM²C core

There are two aspects that the machine design faces with: a) design for manufacturability, and b) design for efficient energy conversion. This seems to be a perfect match for machines with SM²C cores as a) molding process is the same as mounting winding into the core – which is obviously easy, and b) SM²C core has low energy losses – so there are apparently no limits to transfer energy as there is no high frequency brake in the magnetic core and the energy conversion can take place at higher frequency that could lead to a higher power density. The critical moment here is whether the appealing feature of the high power density based on high frequency can be applied for low speed electrical machines where obviously the high torque capability is the indisputable goal.

$$S = \frac{1}{2}U_m I_m = \frac{1}{2}\omega\, B_m J_m A_e A_m = \frac{1}{2}\omega\, B_m J_m \cdot Volume \cdot length \cdot k_p \quad 2.1$$

The equation 2.1 describes a (apparent) power of the magnetically coupled system (such as a transformer), where the voltage is expressed by the magnetic flux and the magnetization speed. Further on the current and the flux are expressed by the flux density over the magnetic conductor area and current density over the electric conductor area (Figure 2.1). The representations of these

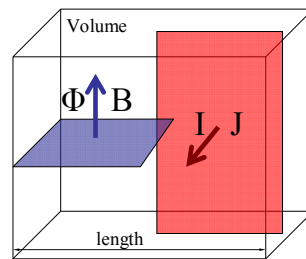areas (Figure 2.1) on two perpendicular planes are rather concentrated and including the returning paths.

Figure 2.1 Visualization of the magnetically active volume with coupled electric and magnetic circuits

According to previous argumentation there frequency limit suppose to be at least *1kHz* in order to consider that as suitable for SM²C, the current density could be at least *5 A/mm²* for the pre-wound and pre-pressed coils and even if the flux density (and magnetic force density) remains low in the core *0.5 T*, the power density is still high. From another side, the torque requirement at the application speed establishes two clear guidelines for design and manufacturing in order to enhance torque capability:

1. pre-wound and pre-pressed coils that include main insulation and have high fill-factor (at least *60%*) within the cross-section area surrounded by the insulation

2. magnetic (and mechanical) support such as SMC blocks that facilitates production but that improves magnetic coupling and performance when using SM²C core

Winding realization specification

Independent of the number of turns the slot has to be filled with copper conductors that in one extreme can be all as a parallel strands or all in all a series connected wire. By following the manufacturing process and starting from the winding that is the central part in the mold no matter how the core is made. There is a range of wires diameters that are most manageable to "soft deform" them into a coil and winding. The specification of the slot area and coil arrangement is shown in Figure 2.2, and the selection of wire diameter result different fill factor is shown in Figure 2.3. These figures of one stator slot, is part of the inner stator in *Ø310 mm* machine that has *28-poles* and *30-slots* (also 30-coils).

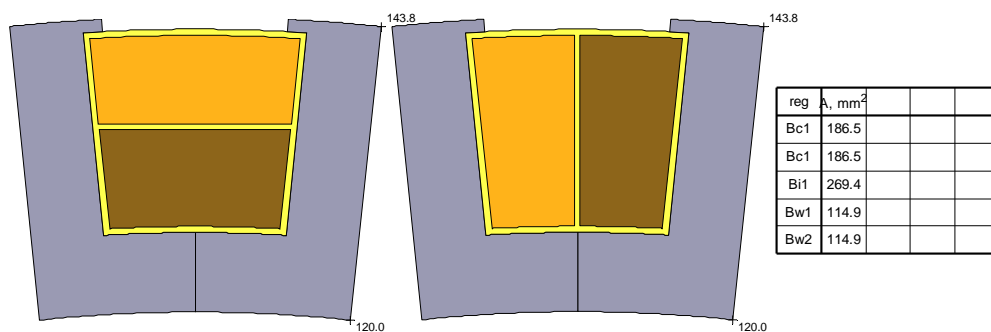| reg	A, mm²		
Bc1	186.5		
Bc1	186.5		
Bi1	269.4		
Bw1	114.9		
Bw2	114.9		

Figure 2.2 Slot area and coil arrangement horizontally or vertically

d_C: 0.650 mm, N: 206 turns, K_f: 57.4 % d_C: 0.800 mm, N: 133 turns, K_f: 56.2 % d_C: 1.000 mm, N: 81 turns, K_f: 53.5 %

d_C: 0.650 mm, N: 230 turns, K_f: 64.1 % d_C: 0.800 mm, N: 149 turns, K_f: 62.9 % d_C: 1.000 mm, N: 92 turns, K_f: 60.7 %
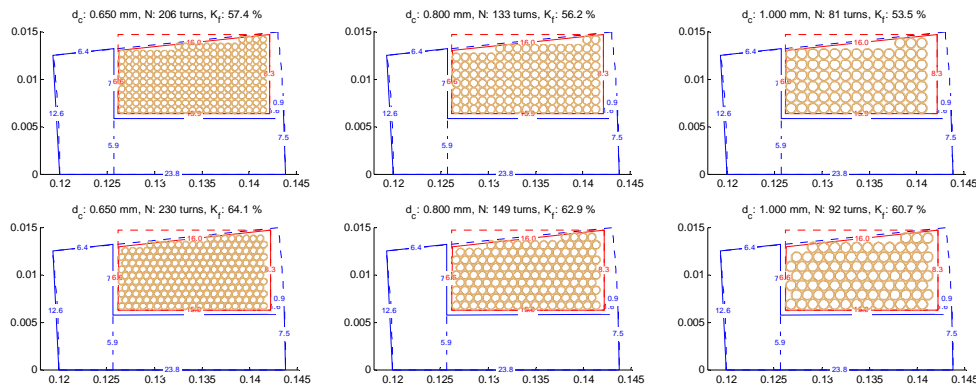
Figure 2.3 Theoretical fill of the half slot

Practical experiences of the predefined coils (Figure 2.3) have resulted to following coil data that is presented in Table 2.1:

Table 2.1 Practically made windings

Winding description	Diameter mm	Number of strands	Number of turns	Turns in half slot
Modular multi-strand	1.25	16	3*	48
Modular multi-strand	0.8	10*	12	120
Single tooth coil	1.0	3	150	90
Modular multi-strand	0.65	70	3	210

*the numeric value is highly probable if not exact

There is some manufacturing uncertainty that complicates the exact evaluation of conductor fill factor. Concerning to the fill factor the end-turn of the modular grows extra on one side when the additional transition turn is conducted from one single tooth coil to another single tooth coil. This extra spice requirement is rather noticeable with low turn coils.

Core variation specification

Initially it is expected that molded SM²C establishes complete AC-core. On contrary, due to the high torque requirement the AC core has to be reinforced with high permeability material in order to increase magnetic flux linkage and torque capability. The convenient selection possibilities are:

1. Compressed SMC piece of a simple geometry that is usually a block that can be used as a tooth with or without coil. The production arrangement is highly influenced whether the coils and windings are produced in-prior or post-prior to the magnetic core.

2. Wrapped magnetic wire that carries magnetic flux in angular or wiring direction. This solenoid of iron-wire is most useful to support the magnetic flux linkage through the cylindrical stator yoke.

The core variation in materials and production techniques introduces a number of different possibilities. The practically experimented choices are presented in the next section.

2.3 28-pole 30-coil RF machine with SM²C core and with or without inserts

This 28-pole 30-tooth machine with 6 phase segments is one of the most practically explored types of machines in Damia-2. The symmetric part of the machine is shown in Figure 2.4. There are 3 different parts in the stator core that are labeled with slightly different grey tones: a) tooth-tip, b) tooth and c) yoke. Practically all these three parts can be made of different materials.
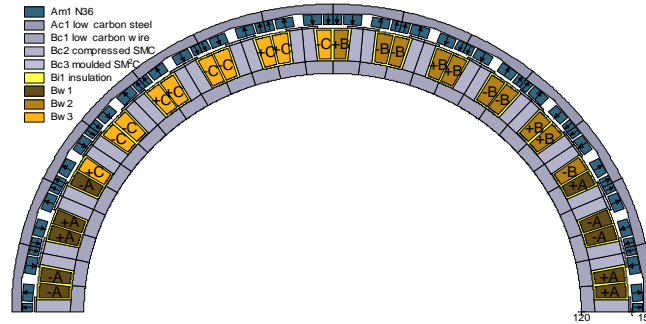
Figure 2.4 Outer rotor 28-pole 30-tooth PMSM

List of prototyped stators

The most practically explored machine types means that there are 5 prototyped stators evaluating different aspects of the production and design. The first is not really counted as this is only used to validate the feedstock – SM²C composition parameters, the molding process and process parameters. The important experimental input to wind power application is the working prototypes 1 and 2. Two additional prototypes are built for in-wheel application, while developing machines for in-wind application. The list of prototyped stators includes:

1. Pre wound and insulated winding segments – 6 units molded into SM²C

2. Pre wound single tooth coils around SMC-3P – 30 units attached into SM²C

3. Premade SM²C core with SMC teeth and SM²C tooth-tips used to make low turn winding

4. Pre-wound stator yoke with SMC teeth and SM²C tooth-tips and low turn winding

The difference between stator 2 and 3-4 is the number of turns that is relatively high for the stator-2 and low for the stator-3 and stator-4 (Table 2.1). The high number of turns facilitates the production of the winding. There are also some attractive features when establishing the main insulation layer around the winding. Namely the classical approach of insulating the tooth and feeding the wire on top of the tooth is more convenient but also secure than the new approach of coating the complete winding or molding the insulation material as the main insulation (liner) of the machine. The alternative production step of molding the insulation system before molding the core influences the whole production of the machine. The molded insulation system or the coated windings defines the geometric shape of the winding segments, assembling the inserts into the mould and the complete magnetic core after the molding. As a result, the alternative way of producing stator core introduced many challenges related to the winding production and the creating and inspecting the main insulation system. Furthermore the magnetic reinforcement of the AC-core has created a new set of challenges and also challenging outcomes.

Machine parameter estimation

The machine parameters such as magnetic flux linkage due to rotor magnets Ψ, stator winding inductance L and resistance R are derived from the measurements. The magnetic flux linkage is calculated from the induced voltage measurements at different speed and compared with results from the finite element analysis (Table 2.2).

Table 2.2 Peak value of flux linkage per turn and modular segment

Description of stator core	2DFE	3DFE	Test
SM²C stator	2.61	2.66	2.16
SM²C yoke and tooth-tip, Som-3P teeth	3.71	3.49	3.73 & 3.48
Som-3P stator	4.58	4.57	-
Wound yoke, Som-3P teeth, SM²C tooth-tip	-	-	3.87

The resistance and inductance is measured of different stator segments with RLC-meter (Aligent U1731A) at 120 Hz and 1kHz. The averaged values at 120 Hz is shown in Table 2.3.

Table 2.3 Resistance and inductance estimation at 120 Hz of four different stators

Description of the prototyped stator core	Number of turns, Nt	Resistance, R [Ohm]	Inductance, L [μH]
SM²C stator	12	0.16	104
SM²C yoke, tooth-tip and Som-3P teeth (1)	150	41.2*	60000*
SM²C yoke, tooth-tip and Som-3P teeth (2)	3	0.033	12
Wound yoke, Som-3P teeth, SM²C tooth-tip	3	0.035	15

* referred to stator-3 measurements as the machines have the same core arrangements

The inductance is rather unchanged when comparing different RLC-meters or the values at different frequencies. The values differ within few pre cent and inductances decreasing slightly with frequency. There is larger discrepancy between the different winding segments. The resistance measurements are more challenging as the difference between the values is considerably larger. As the dc resistance is more than 2 times smaller from the ac resistance, the presented value is reduced by 2 when evaluating the complete phase resistance. There is also another important consideration, namely as the geometric winding specification is the same for all these stators and they differ only from the production and core material selection point of view – therefore the identical winding resistance is considered. The section inductance (Table 2.3) is doubled in order to calculate complete phase inductance and to estimate the power speed characteristics.

Estimated power-speed characteristics

In this section the power speed characteristics of the outer rotor PMSM is calculated for different prototype stators based on the derived parameters. The speed range is selected up to *200 rpm*, which is *46.6 Hz* for the *28-pole H_{act}=60 mm* machine, as the specification of the application speed range at the early days of the project. The derived torque speed characteristics are shown in Figure 2.5.
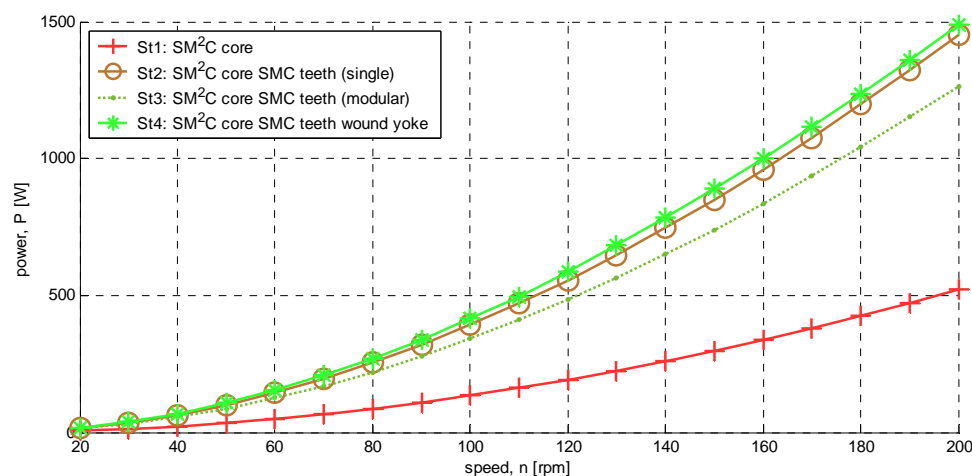

Figure 2.5 Power-speed characteristics of an induced voltage driven RL circuit as a design and production experience from in-wheel application.

Based on the difference on flux linkage and the phase inductance, the magnetically reinforced core, where mainly the SMC tooth is used, shows considerably higher performance. Stator-2 has smaller air-gap therefore also slightly better performance compared to stator-3. Stator-4 could be even better if the magnetic connection between the teeth and yoke is improved.

The suppressed performance of the machine is acceptable if the cost is significantly reduced. Since the permanent magnets take the considerable part of the price it is worth to design machine with high torque capability and with high permeability core. Initially, based on the pure SM²C stator, it is considered that the machine that provides ca 5kW gap power at 1200 rpm can produce the same amount at 200 rpm if the machine is axially 5 times longer H_{act}=300 mm; just the remaining challenge is the power management.

The more reasonable design direction is to **increase gap radius** and adapt the machine construction or RFPMSM according to that, which is main concern in the next section. The power requirement is rather increasing and the speed decreasing according to the development of the application specification.

2.4   RF machine design for wind power application

Based on the previous design and manufacturing experience

1. Distributed concentrated windings that build up **modular windings** is the most suitable approach as

    a.   the winding segments as well as the phase segments can be **produced separately**

    b.   The complete core segment can be made first in order to aid winding production

    c.   Alternatively a number of single teeth with coil can be made in prior to molding

    d.   Modular winding arrangement allows **minimizing cogging**

2. The magnetic core do not need to be completely molded it can be partly molded as the consists of a number of magnetic and **mechanic reinforcement** pieces of simple geometries (inserts) that facilitates both production as well as energy conversion

3. There are no noticeable drawbacks discovered when producing outer rotor with surface mounted magnets. Less advantageous feature is the power losses in the solid rotor core that has to be gained to the excitation speed. Also there is no analysis on how much the inductance differs between modular and more conventional types of windings.

The design of an outer rotor RFPMSM is based on the dimensions of the **existing permanent magnets** 8.5x5.0x60.0 mm. The selected outer radius of the design target is $R_o=300$, *400* and *500 mm*. Figure 2.6 shows the amount of the magnets per pole and the relative coverage of the magnets for three different radii. Lines marked with dots belong to 300 mm machine, asterisks to 400 mm and circles to 500 mm machine respectively.
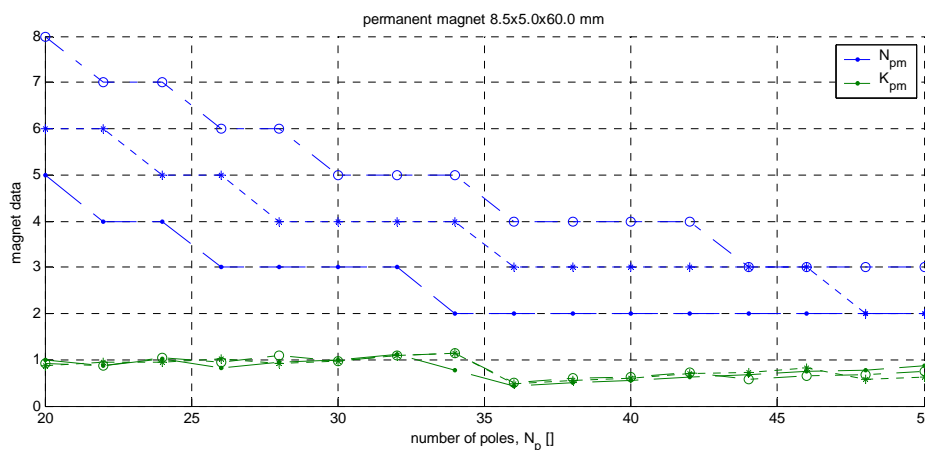

Figure 2.6 Number of magnets per pole and relative fill of magnets

The **stator specification** obeys to the following criteria:

1. the core is made completely from SM²C or alternatively the teeth are made of SMC and the rest of the core is made of SM²C

2. The number of coils N_s is selected as a multiple of 3 from 24 to 45 coils

3. the number of poles N_p are selected as the closest number to the number of coils from this array { 20 22 26 28 32 34 38 40 44 46 50 }

4. The electromagnetic torque is calculated at the external current supply that has the current density of *5A/mm²* over the conductors that fill factor is *60%* inside the insulated slot.

5. Initially the axial active length of the machine is *60 mm* (Figure 2.7-Figure 2.9) that is increased to *300 mm* (Figure 2.10-Figure 2.11),

6. Belt thickness: *h=R$_o$-R$_i$=40 mm*, thickness of rotor *h$_r$=12 mm* and air-gap *g=1 mm*.

Figure 2.7 Electromagnetic torque as a function of poles and teeth for machine with Do=0.6 m with SM²C core (left) and with SMC-teeth as inserts (right)

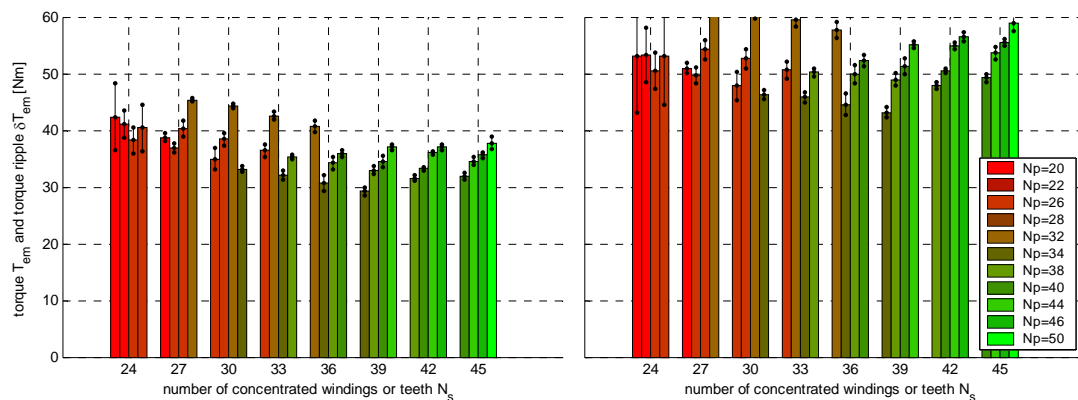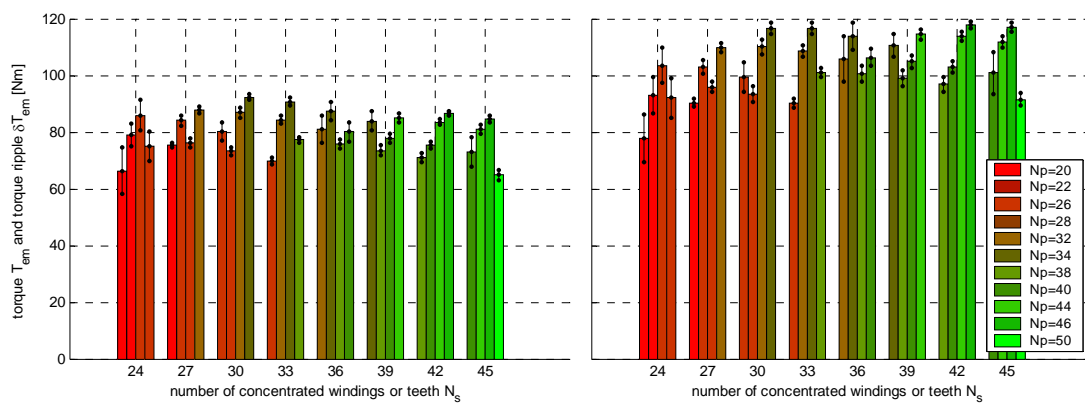*Figure 2.8 Electromagnetic torque as a function of poles and teeth for machine with Do=0.8 m with SM²C core (left) and with SMC-teeth as inserts (right)*
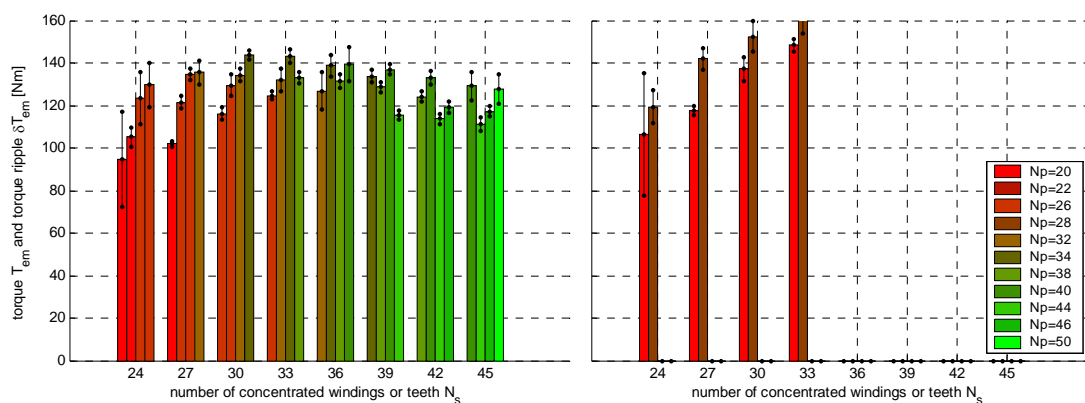

Figure 2.9 Electromagnetic torque as a function of poles and teeth for machine with Do=1.0 m with SM²C core (left) and with SMC-teeth as inserts (right)

Figure 2.7-Figure 2.9 show the torque bars with vertical ripple lines for machines with different pole to coil arrangement, outer radii and core material arrangements. The calculation sequence follows the number of concentrated coils and the number of poles is selected specifically to the number of coils. The calculations for the largest machine size with SMC teeth are incomplete but still considerable as the existing calculations are showing the same difference as before for the smaller sizes between the SM²C stator and the stator with SMC inserts.

The magnetization strength depends on how many existing discrete magnets fits per pole (Figure 2.6). Therefore the torque capability depends on the magnetic flux linkage provided by the magnets and this trend is easily followed in Figure 2.10 and Figure 2.11. In this graphs the initial length of the machine is extended from *60 mm* to *300 mm*.

According to the simulated maximum electromagnetic torque where the applied current is perpendicular to the excitation field (Figure 2.10-Figure 2.11) the magnetically reinforced stator with SMC teeth provides more than 40% torque for Ø600 mm machine and around 30% torque for Ø800 mm machine. The increase of the torque due to the better magnetic core becomes relatively smaller the larger the machine gets.
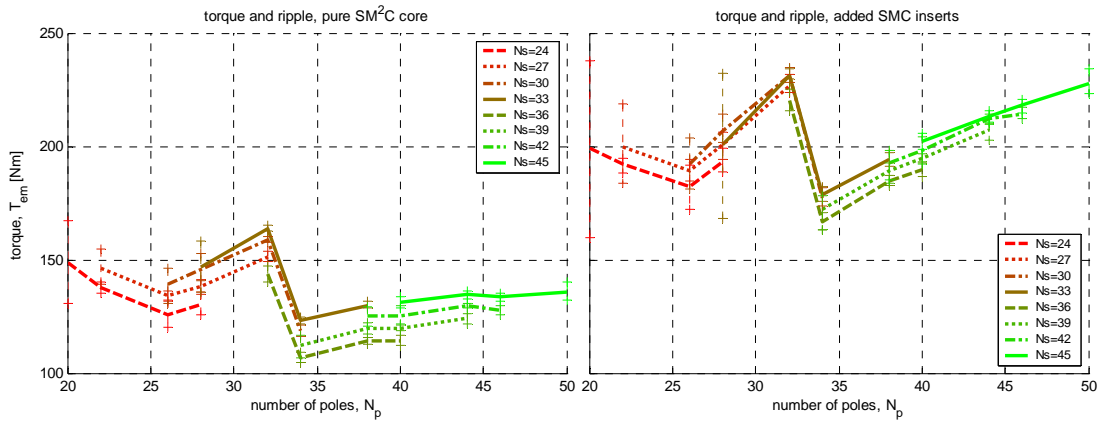

Figure 2.10 Electromagnetic torque as a function of poles and windings for SM²C stator core and the core with SMC tooth inserts
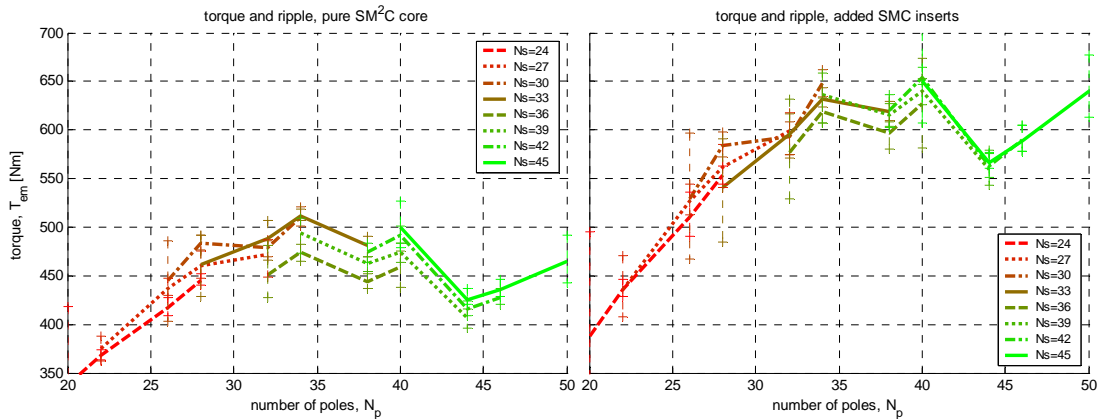

Figure 2.11 Electromagnetic torque as a function of poles and windings for SM²C stator core and the core with SMC tooth inserts

Based on the calculated torque, which is the outcome of the magnet selection, machine size and current density in the coils (*Jc=5A/mm²*), the machine power is calculated at the application speed (Figure 2.12 and Figure 2.13) of *50 rpm*. The amount of conductor losses and the core losses are plotted on top of the gap-power estimation bars. This power estimation does not consider the actual power circuitry and the supply of the reactive power. The graphs rather indicate the active power supply capability and internal consumption at the operation point. The next size (*Ø500 mm*) would increase the torque capability in the range of 700 to 800 Nm and power capability around *4kW* at *50 rpm*.
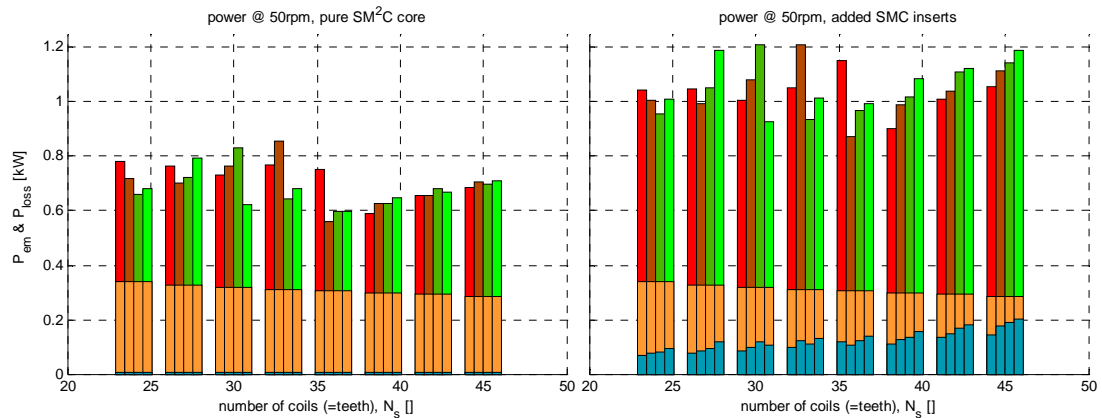
Figure 2.12 Electromagnetic power at 50 rpm as a function of poles and windings for SM^{2}C stator core and the core with SMC tooth inserts for Ø600 mm machine. Power losses in the winding and in the stator core are plotted on top of the electromagnetic power bars.
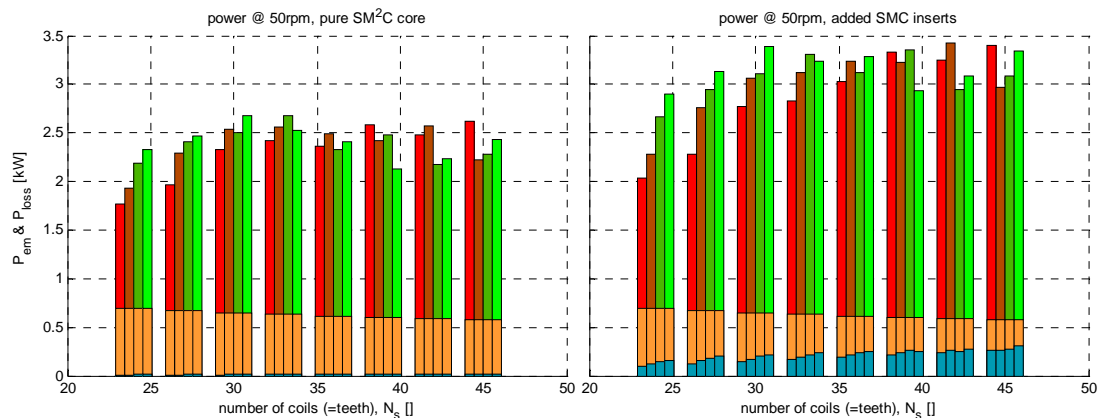
Figure 2.13 Electromagnetic power at 50 rpm as a function of poles and windings for SM^{2}C stator core and the core with SMC tooth inserts for Ø800 mm machine. Power losses in the winding and in the stator core are plotted on top of the electromagnetic power bars.

2.5   Summary

From the practical design for manufacturability experiences on in-wheel application (Figure 2.14) it is suggested to combine single-SMC-tooth coils into modular windings and take advantage of SM^{2}C molding to build a number of large sections of the machine. The remaining challenging part is the cost efficient power harvesting at low rotation speed that directly influences the size and the internal power loss of the electrical machine.

Figure 2.14 Stators with modular windings for outer rotor machine, where SM^{2}C core is presented on the left and SM^{2}C core with SMC inserts on the right.

3   Axial flux machine with and without SM^{2}C core

The opportunity to study a large double-sided axial flux machine and core-less type of machine gives an important input and established a valuable outcome from the project. Hereby, the author of this part report acknowledges Bo-Henrik Karlsson from Villavind AB on his extremely valuable contribution.

The purpose of the redesign is to familiarize the practical issues related to the construction and production of the double (excitation) sided AFPMSM. The aim for the redesign is to provide electromagnetic optimization by maximizing rotor flux linkage and induced voltage and minimizing voltage drop due to self inductance and resistance of the armature coils.

Figure 3.1 Double sided axial flux surface mounted permanent magnet synchronous machine (AFSPMSM)

3.1   Machine specification

There are two concerns on the design of manufacturability: 1) a specification of 3-phase concentrated winding arrangements and dimensions that maximizes the energy transfer, and 2) a determination of manufacturing processes that comfort the practical realization of the machine parts and assembling.

Stator layout selection

The existing 24-pole surface mounted PM system determines the possible coil arrangement for the concentrated or the distributed concentrated winding. As a result of the coil arrangement, the symmetry of three-phase systems as well as the character of the cogging torque is determined. The following coil configurations: 18, 21 and 27 are examined. The winding that consists of 24 concentrated coils does not form a 3-phase system at 24-pole excitation and is omitted in this survey. The selected winding configurations and distribution are shown in the figure below, which also includes 1) 24-pole magnets as a unfilled red and blue contours, 2) distribution of induced voltage vectors and 3) winding factor due to pitch or distribution of the coils.
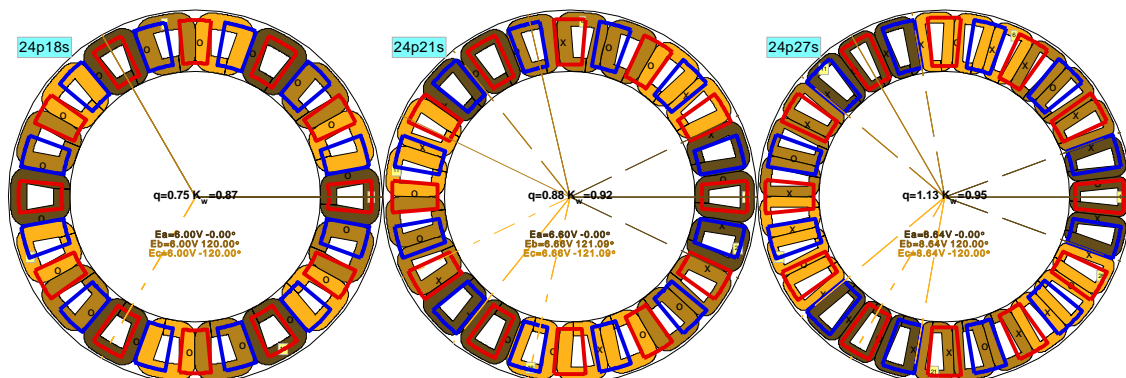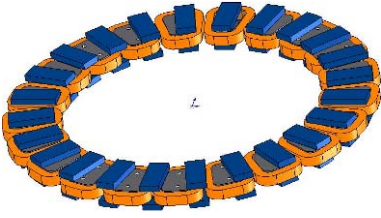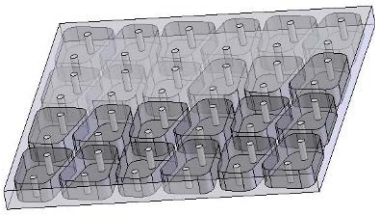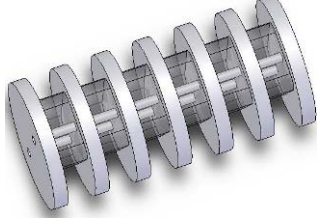

Figure 3.2 Proposed stator layouts of 18, 21 and 27 coils for 24-pole machine

The next important step in the design process is to specify the manufacturing process for the stator. Table 3.1 shows the overview of the manufacturing sequence that is part of the design. The design related issues are presented in the first row and some outcomes of the process outcomes are presented in the second row. The most demanding design step is to specify the number of coils and proportions between the core and the coil (a). Once the shape of the stator core is specified the SM²C block sixe, production and tracks for waterjet cutting is specified (b). This step is processed in the sequence of determining the manufacturing steps for producing the coils (c). The stator poles are cut out from molded SM²C block (d) and have fine surfaces and tolerances. These poles are used as the core for bobbin when manufacturing the coils (e). These coils are placed into a new mold, where the molding of non-magnetic and dielectric material is used to assemble the coils and establish the mechanical strength needed (f).

Table 3.1 Manufacturing process of stator cores and coils

Stator	Stator core	Coil
a	b	c
f	d	e

Next, the original axial flux permanent magnet machine is shortly characterized and the successor introduced.

3.2   Coreless 24-pole 18-coil double sided AF-machine

The initial design 24-pole 18-coil double sided AF-machine and measurement results of the extracted power give a good opportunity to study the specific requirements behind wind power applications for small and local electricity production. As the application needed a new generation machine it is beneficial to use existing parts such as magnetization system (double sided disks with surface mounted PM), mechanical support and wind turbine. The fragment of the first stator is shown in Figure 3.3.

Figure 3.3 Two-coils from the 18-coil 24-pole machine

There machine parameters are extracted from the measurements as well as estimated from 2D FE. According to field experiments, the average value of flux linkages, which is *2.81Vs*, is based on a range of speeds and measured no-load line voltages that average is *146V* at *23.8rpm*. Similarly the machine parameters, such as resistance, inductance and induced voltage, are derived and used to determine generator characteristics. The flux linkage depends on the air-gap length. It is expected that the axial distance between the rotor disks are *27mm*, the magnets are covered with *0mm* dielectric and non-conductive protective construction material and the remaining air-gap is divided between two *4mm* gaps.

The existing coil with a cross section area of *18-19x18.6mm* accommodates *833 turns* that conductor diameter is *0.55mm*. The thickness (along z) is rather constant and the width variation is on the xy-plane. The estimated winding impedance (Table 3.2) bases on the measurements of the two coils (Figure 3.3) and some 2D FE calculations (Figure 3.4, g=1 mm).

Table 3.2 Estimated winding impedance

	Based on 2D FE calculations	Based on the measurements	Introduction of SM²C core
Flux linkage (g=4mm) ψ_1, Vs	3.04	2.81	5.01
Flux linkage (g=1mm) ψ_1, Vs	3.62	-	6.47
Phase resistance Rs, Ohm	150.0	133.2	150.0
Phase inductance Ls, H	0.30	0.34	0.51
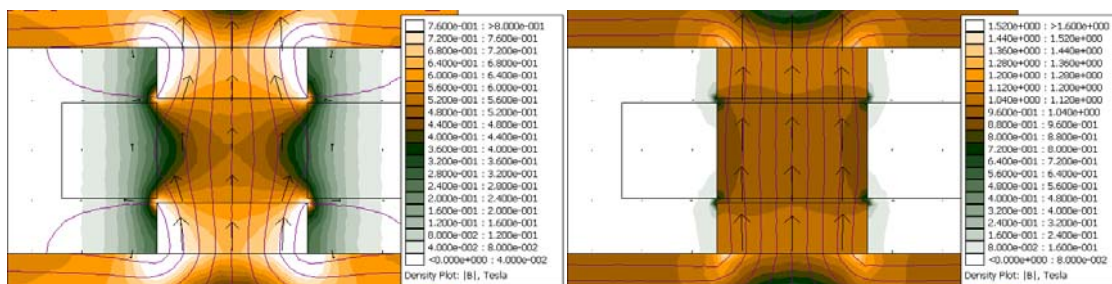
Figure 3.4 2D FE model of axial flux machine with air-core (left, coreless) and with SM²C core (right)

The flux linkage is either calculated from no load voltage measurements or estimated from the maximum flux linkage calculation in the 2D FE Based on the machine parameters the extracted and the total electric (resistive) power is calculated as a function of wind speed and the machine loading (Figure 3.5).
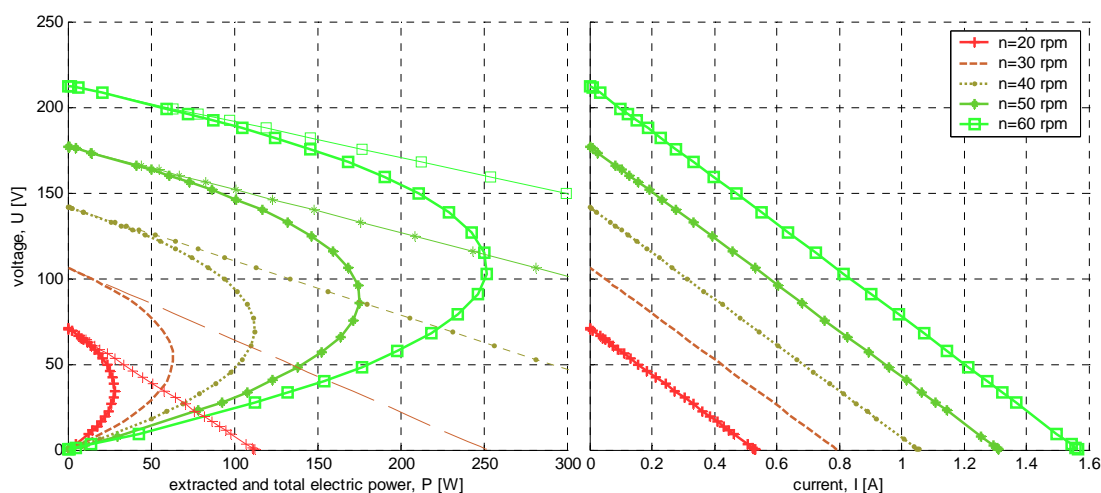
Figure 3.5 Voltage-Power and Voltage-current characteristics as a function of rotation speed. The characteristics are based on experimental machine parameter estimation. Extracted power is shown as solid lines and the total electric power as thin lines on the voltage-power diagram.

The difference between the origin of the machine parameters, the 2D FE or the experimental, shows quite good agreement. At the same time, the quick analysis in 2D FE insists to replace the coreless structure to light magnetic (SM²C) core, the performance of the machine can be improved up to *3 times* (Figure 3.6) if the air-gap is reduced from 4 mm to 1 mm compared to the coreless machine.

The 2D FE model (Figure 3.4) includes *19x19 mm* coil area that length is *0.7 m* and the air-gap is selected as narrow as *1 mm*. The top value of the flux density in the middle of air-gap increases from *0.5 T* to *1.0 T*.
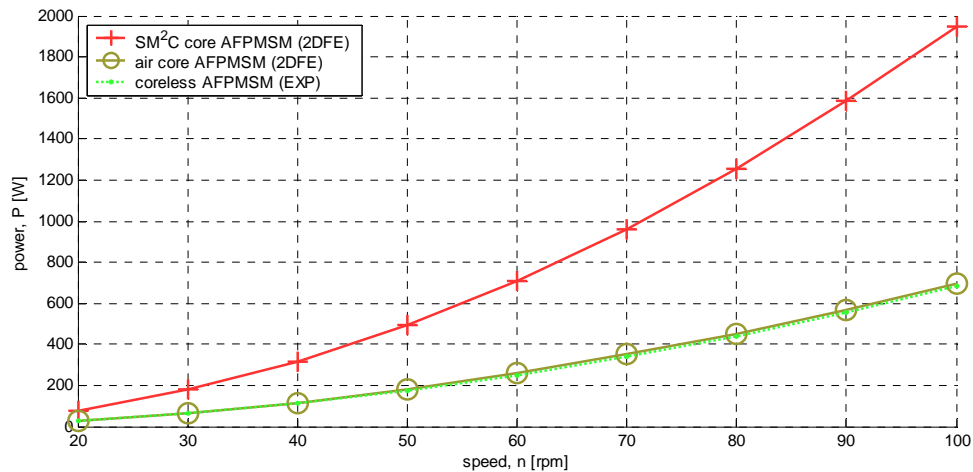
Figure 3.6 Speed-Power characteristic of the axial flux permanent magnet synchronous machine without core (original) and with SM²C core (successor) shows the maximum extracted power as a function of speed for 24-pole machine

3.3   24-pole 27-coil double sided AF-machine with SM²C core

This section goes over the main highlights of the development and assessment of the new stator with SM²C core for the axial flux machine, and describes:

1. the redesign of AFPMSM and how 27-coil stator is selected and dimensioned,

2. the prototyping of the stator, and

3. the verification of the design.

Selection of winding layout

The comparison of the proposed stator layouts (Figure 3.2) for *24-pole* rotors show the induced voltage if a single coil consists of a single turn and induces *1V*. The distribution of coils spreads the induced voltages and the coil pitch or its breadth determines how much flux is linked to the coil. Therefore the winding factor (*Kw*) is a multiple of distribution factor (*Kd*) and the pitch factor (*Kp*). The winding factor shows the magnetic coupling factor as it is referred to the perfect full pitch 24-pole winding that has one (*q=1*) coil per phase and per pole. Practically it would lead to an overlapped 3-phase winding. The comparison of the selected winding layouts in Figure 3.2 is presented in Table 3.3 below.

Table 3.3 Winding characterization of the proposed stator layouts of 18, 21 and 27 coils

Number of coils	18	21	27
Number of coils per pole (q=Ns/Np)	0.75	0.88	1.13
Winding factor (Kw=Kd*Kp)	0.87	0.92 fas-A	0.95
Phase asymmetry (Ea∠φa-Eb∠φb+∠120°)/|Ea|	0%∠0°	1%∠1°	0%∠0°

According to the previous table 24-pole 27-coil machine is most attractive because of high winding factor and three-phase symmetry. Nevertheless, the other candidates are included when

1. Dimensioning of the coils and selecting the number of turns

2. Determining the impedance and the induced voltage of the winding

3. Estimating the cogging torque, load torque and normal forces of the machine

4. Estimating the power output with 3-phase resistive load over rotation speed and coil height

Coil size and number of turns

The coil size is defined by the axial thickness $H_t=16\ mm$, the radial height $L=95\ mm$ where the outer radius $R_{to}=290\ mm$, and the maximum angular width 360/Ns where $N_s = 18$, 21 and 27 (Figure 3.7).
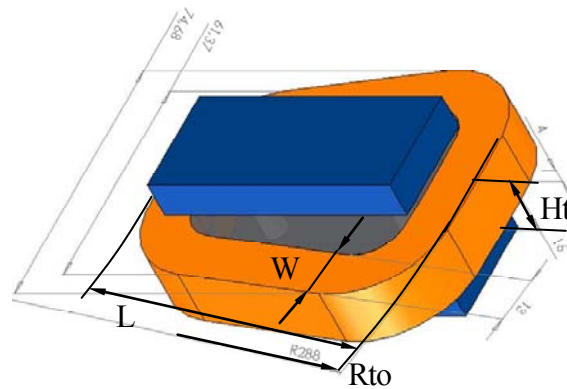
Figure 3.7 Geometric parameterization of a coil

According to the previous definition, the largest coil and tooth area is marked with red dots in Figure 3.8 below. Figures show the geometric layout design, where the blue line creates the connecting surface between the coil and the tooth i.e. the magnetic core. The (blue connecting surface) contours are generated by the step of 2 mm coil layer thickness, where the largest inner radius (R_{ti}) of the coil is $100\ mm$ and the maximum curvature radius (r_t) of the edges is $22\ mm$.
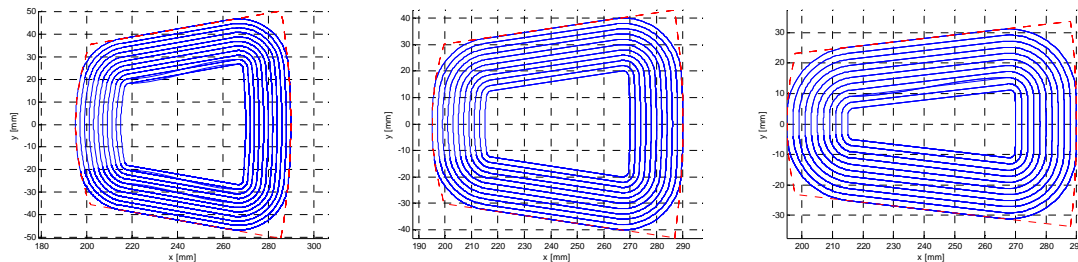
Figure 3.8 Tooth cross sections of 18, 21 and 27 coil stator at different thickness (W) of the coil

Four different winding thicknesses are designated for analysis: 10, 12, 14 and 16 mm, where two different types of winding packing are studied: a) coil with targeted windings where each new turn of the stock is right vertically oriented underlying laps (Figure 3.9, left), and b) the coil fitted windings where each new turn of the stock is between and the underlying laps (Figure 3.9, right). Cross-section of the two types of windings are shown in (Figure 3.9) where the area is chosen *0.5 mm* smaller in each edge due main insulation around the coil. Therefore the electrical conductors are in the cross-section of *15x9 mm* and the main insulation extends it to *16x10 mm*. The wire size diameter is *0.71 mm* and the insulation thickness (or distance between the wires on the insulation thickness is less) is 13% of the wire size diameter. This is basically geometric layout design that purpose is to facilitate the production as well as provide the estimation of the machine characteristics. Table 3.4 Determines the amount of winding turns per cross-section area that depends on packing: quadrilateral or hexagonal wiring and the thickness of the main insulation.

d_c: 0.71 mm, N: 198 turns, K_f: 58.1 % d_c: 0.71 mm, N: 210 turns, K_f: 61.6 %

Figure 3.9 Coil backing: (left) quadrilateral and (right) hexagonal wiring arrangement

Table 3.4 Coil fill description that considers the min insulation of 0.5 or 0.0 mm and quadrilateral or hexagonal wiring of coil.

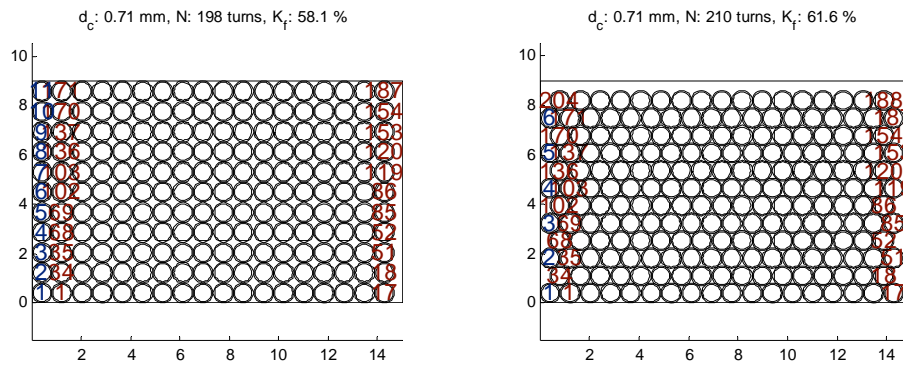| Coil Width or Thickness (W), mm	10	12	14	16
Coil with 0.5 mm thick main insulation				
remaining fill factor due to main insulation, %	84.4	85.9	87.1	87.9
Number of layers in quadrilaterally filled coil	11	13	15	18
Number of turns in quadrilaterally filled coil	198	234	270	324
Fill factor of quadrilaterally filled coil, %	58.1	56.1	54.8	57.0
Number of layers in hexagonally filled coil	12	15	18	21
Number of turns in hexagonally filled coil	210	263	315	368
Fill factor of hexagonally filled coil, %	61.6	63.1	64.0	64.8
Coil without the main insulation				
Number of layers in quadrilaterally filled coil	12	14	17	19
Number of turns in quadrilaterally filled coil	228	266	323	361
Fill factor of quadrilaterally filled coil, %	56.4	54.9	57.1	55.8
Number of layers in hexagonally filled coil	14	16	19	22
Number of turns in hexagonally filled coil	266	304	361	418
Fill factor of hexagonally filled coil, %	65.8	62.7	63.8	64.6

Perfect Air-gap

The rotor magnets as well as the stator coils are molded into the plastic carrier that after hardening gives mechanical support and durability. This non electric and magnetic material covers the magnetic poles of the electro and the permanent magnets. Therefore there are two different air-gaps to be considered in the calculation of the machine characteristics:

1. Mechanical air-gap between the stator and the rotor – 1 mm

2. Magnetic air-gap between the permanent magnet and the coil – 4 mm

Magnetic analysis

Magnetic analysis is based on 3D magnetostatic analysis of a single coil in a double sided AFPMSM, where the air-gap is selected in this particular case to be *4 mm*. The magnetic flux density in the air-gap is within *±0.6T* and in the rotor core is shown between 0.2 and 1.0T (Figure 3.10). The sections are shown for 18, 21 and 27 coil stator with the coil width of 12 mm.
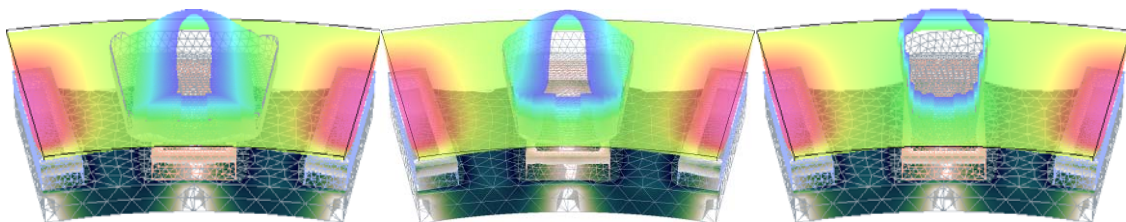

Figure 3.10 Flux density distribution in the core and in the air-gap

According to the flux density between the magnets and the stator teeth the attractive shear stress at *0.6T* is *0.14N/mm²* and with considering the whole magnet cross section area the normal forces between the stator and the rotor is *10.3 kN*. Ideally it is balanced with the forces in the opposite direction between the other axial air-gap between the stator and the double sided rotor.

Winding impedance

Impedance of a three-phase winding is calculated from a single coil by knowing that the phase costs of Ns/3 coils. The calculated values in Table 3.5 are shown at four different thickness or width of the coil band at three different numbers of coils. Resistivity of 1.75e-8 ohm * m and the current density of *5 A/mm²* is used in the resistance and inductance calculation. The supply frequency is selected to 10 Hz and this corresponds to *50 rpm* of rotor speed.

Table 3.5 Estimated winding impedance

	Ns=18				Ns=21				Ns=27			
Coil width W, mm	10	12	14	16	10	12	14	16	10	12	14	16
Tooth area At, cm²	46.6	41.6	36.9	32.4	37.9	33.4	29.1	25.1	26.1	22.1	18.5	15.1
Mean turn length Lt, cm	28.0	27.4	26.8	26.2	25.8	25.2	24.6	23.9	22.7	22.1	21.5	20.9
Number of turns Nt, turns	266	304	361	418	266	304	361	418	266	304	361	418
Phase resistance Rs, Ohm	19.8	22.1	25.7	29.0	21.2	23.7	27.5	30.9	23.0	26.7	30.9	34.8
Phase inductance Ls, mH	82.0	96.6	137	167	84.0	104	134	163	75.0	91.0	119	144
Current at Ls calculation, A	1.50	1.58	1.55	1.53	1.50	1.58	1.55	1.53	1.50	1.58	1.55	1.53

Induced voltage

3D FE magnetostatic analysis of a coil is used to calculate the linking magnetic flux inducing the forces as a function of the rotor position. Coil thickness (W) and pitch (360/Ns) are changed. Figure 3.11 shows the flux linkage per coil and turn, which is used to estimate the flux linkage and induced voltage over the complete series connected coils in a single phase.
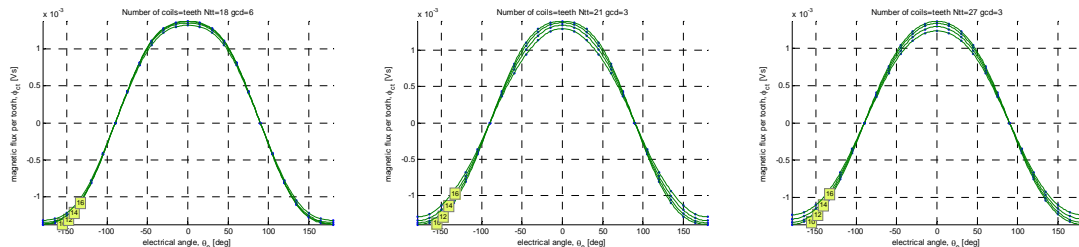
Figure 3.11 Flux linkage per coil as a function of rotor position, coil pitch and coil thickness.

The induced voltage of one phase winding is calculated at 50 rpm and previously estimated number of turns (*Nt*) in a single coil (Figure 3.12). Four different winding thicknesses [10 12 14 16] at *16 mm* coil height is considered in this voltage estimation. Wider coils can assemble more turns and produce more voltage even they link less flux per turn and adds to the self inductance per winding turn.
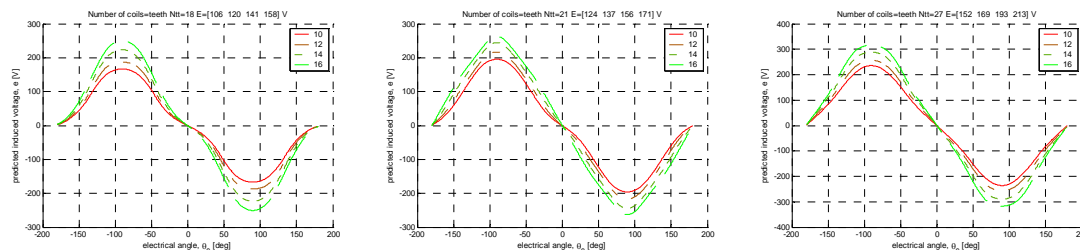
Figure 3.12 Induced voltage per phase at 50rpm and previously calculated number of turns.

RMS value of the induced phase voltage is shown on top of each graph in the same order as the legend shows the different coil thicknesses (W).

Cogging torque

The cogging torque estimation is based on the torque calculations of a single stator tooth (Figure 3.13). Green plus signs along the x-axis visualize the location of the other teeth that their character is added according to the spatial shift of the teeth.
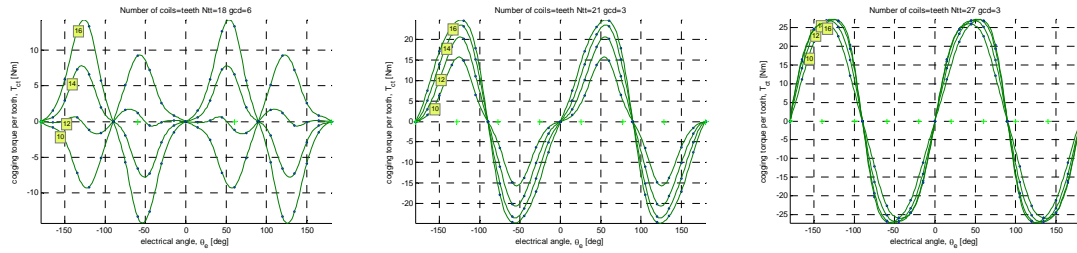
Figure 3.13 Cogging waveform per single stator tooth

The sum of all distributed torque waveforms per single stator tooth gives the resultant cogging (Figure 3.14). As it seen from the figure the cogging torque is largest for the 18-tooth machine. This cogging can be reduced by a careful selection of magnet pitch to coil pitch for 18-coil machine or with a coil to pole configuration that gives the minimum value for the greatest common divisor like it is for the 21 and 27-coil machine.
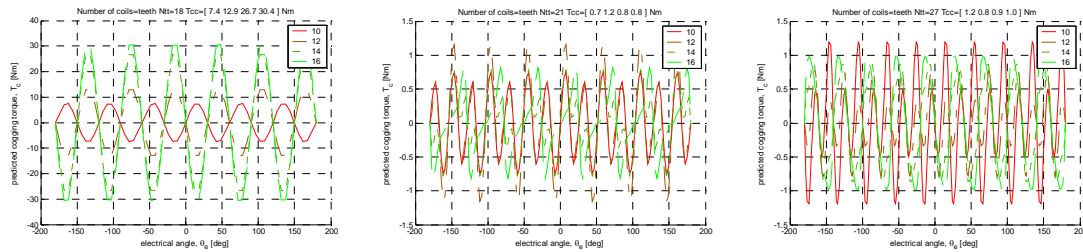
Figure 3.14 Cogging waveform over complete machine

Generator characteristics with 3-phase resistive load

The generator load is selected to be a 3-phase resistive load and the generator characteristics are based on a single phase RLE circuit analysis. This analysis is done for different coil arrangements (N_s = 18, 21 and 27) and coil thicknesses [10 12 14 16] and shown in Figure 3.15 respectively. Table 3.6 summarizes and compares the no-load, maximum load and short circuit operation points at rotor speed of 50 rpm.
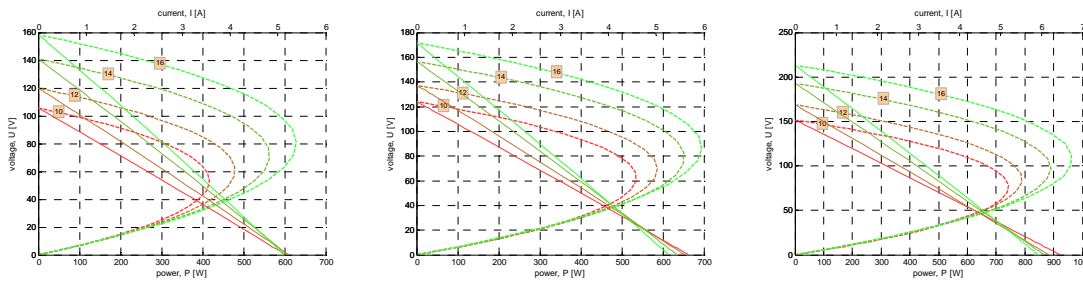
Figure 3.15 Voltage-Power characteristics (dashed lines) and Voltage-current characteristics (solid lines)

Table 3.6 Generator performance with resistive three-phase load

	Ns=18				Ns=21				Ns=27			
Coil thickness W, mm	10	12	14	16	10	12	14	16	10	12	14	16
Number of turns N, turn	266	304	361	418	266	304	361	418	266	304	361	418
Induced voltage Eo, V	105	119	140	157	124	137	156	171	151	168	192	212
Max power per phase Pm, W	138	159	187	209	179	196	218	232	247	263	296	321
Voltage at peak power Um, V	52.6	59.8	72.6	81.3	63.2	70.1	78.3	85.6	74.4	86.1	96.8	107
Current at peak power Im, A	2.6	2.7	2.6	2.6	2.8	2.8	2.8	2.7	3.3	3.1	3.1	3.0
Short circuit current Isc, A	5.2	5.2	5.2	5.1	5.7	5.6	5.4	5.3	6.5	6.2	6.1	5.9

It is worth to consider the thermal loading of the coil for the selected wire gauge, which diameter of 0.71 mm corresponds to 0.4 mm² and the currents of 1, 2 and 4 A results current density of 2.5, 5 and 10 A/mm², which in turn results the specific heat power 75, 300 and 1200 W/dm³ in the current carrying conductor at average resistivity of 2.4e-8 Ohm·m.

Power output as a function of rotor speed

Short-circuit current, open circuit voltage and maximum 3-phase power over resistive load are shown as a function of rotor speed and coil thickness for three stator configurations with Ns=18 (Figure 3.16), 21 (Figure 3.17) and 27 (Figure 3.18).

Figure 3.16 Short-circuit current, open circuit voltage and maximum three-phase power for 18-coil stator

Figure 3.17 Short-circuit current, open circuit voltage and maximum three-phase power for 21-coil stator

Figure 3.18 Short-circuit current, open circuit voltage and maximum three-phase power for 27-coil stator

Loading torque

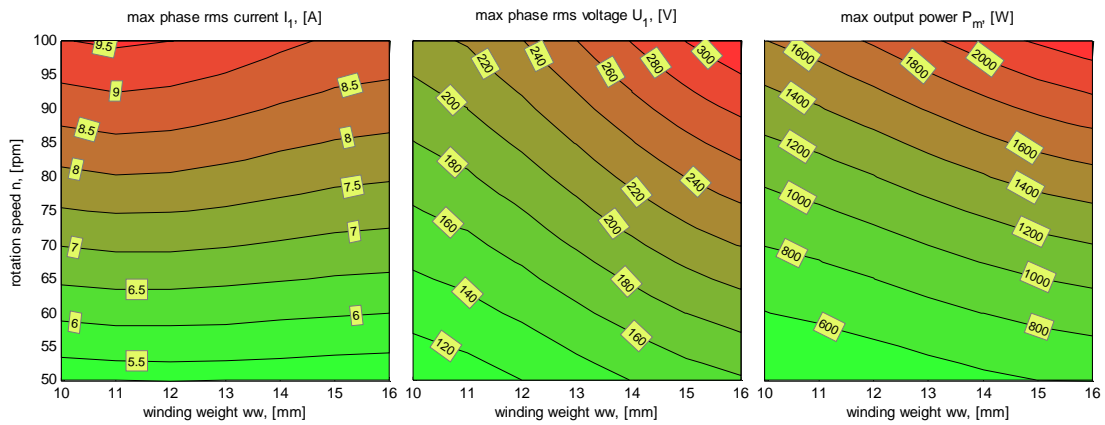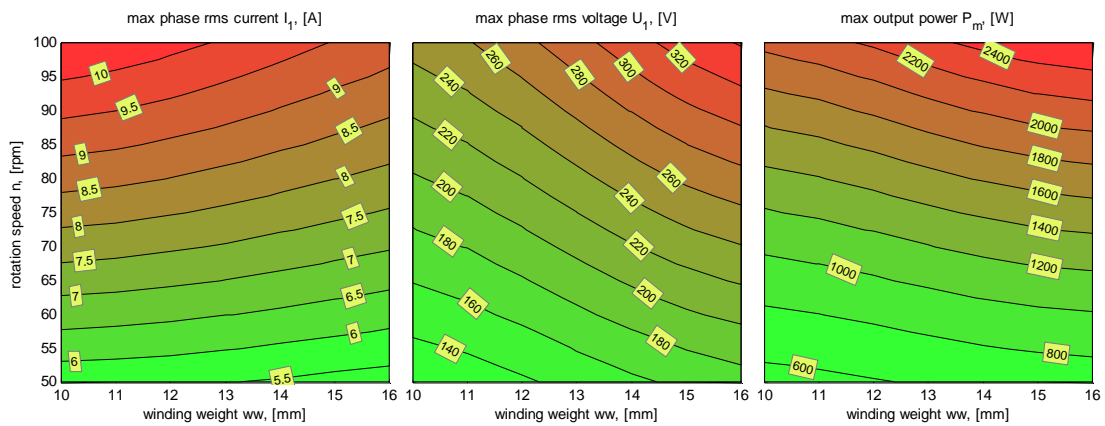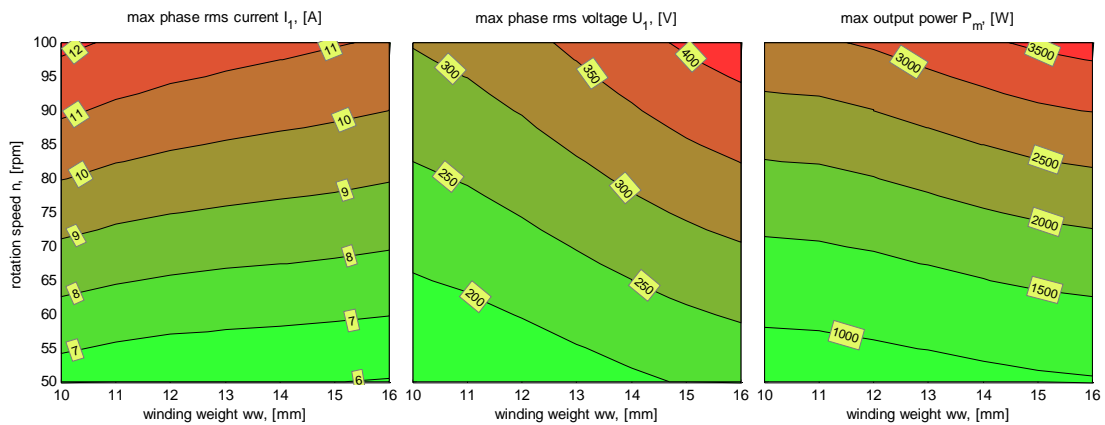The drag torque due to the resistive load is calculated as the power over speed and current. In the similar manner the electromagnetic torque is calculated wit 3DFE model. In this FE model a two different current levels are defined based on the winding cross-section area that is perpendicular to the current direction, the fill factor of the winding and the current density of the conductor. From the resulting total current, which is based on winding area, fill factor (*50% selected*) and current density (*5 and 10 A/mm²*), the real current in the single conductor is calculated. The calculated values from 3D FE are shown in Table 3.7 and Figure 3.19, and compared to calculations based on the load torque, which is calculated as the extracted power from the load resistance according to equivalent circuit Figure 3.20 and from the power consumption on the load as well as from the winding resistance Figure 3.21. The comparative generator load torque over the load resistance (Figure 3.20) or the whole unit (Figure 3.21) is calculated for the coil thickness (W) of *14 mm*. The difference between the torque and the current values between the 3D FE model and the equivalent circuit representation is due to the difference between the coil area definitions.

Table 3.7 Torque estimation from 3D FE magnetostatic calculation

	Ns=18				Ns=21				Ns=27			
Coil thickness W, mm	10	12	14	16	10	12	14	16	10	12	14	16
Number of turns N, turn	266	304	361	418	266	304	361	418	266	304	361	418
Current at 5 A/mm² I_5, A	1.06	1.12	1.09	1.08	1.06	1.12	1.09	1.08	1.06	1.12	1.09	1.08
Torque at 5 A/mm² T_5, Nm	78.1	93.3	105	114	62.2	76.0	87.9	98.3	84.7	93.0	95.6	95.8
Current at 10 A/mm² I_{10}, A	2.13	2.23	2.19	2.17	2.13	2.23	2.19	2.17	2.13	2.23	2.19	2.17
Torque at 10 A/mm² T_{10}, Nm	160	188	211	229	126	152	176	197	173	188	192	192
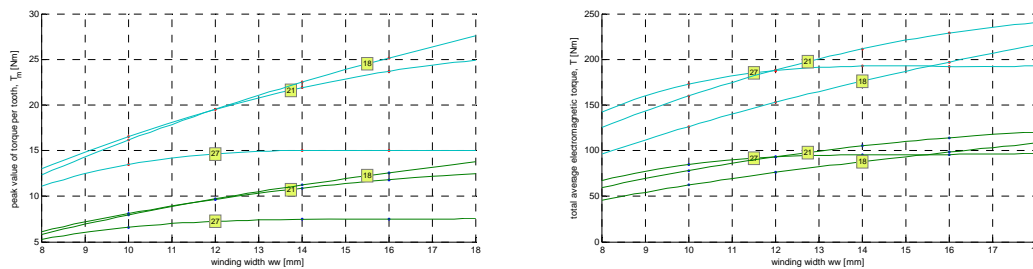
Figure 3.19 Torque estimation from 3D FE magnetostatic calculation: peak torque per teeth (left) and average torque over whole stator (right) at 5 A/mm² (green lines) and 10 A/mm² (cyan lines)
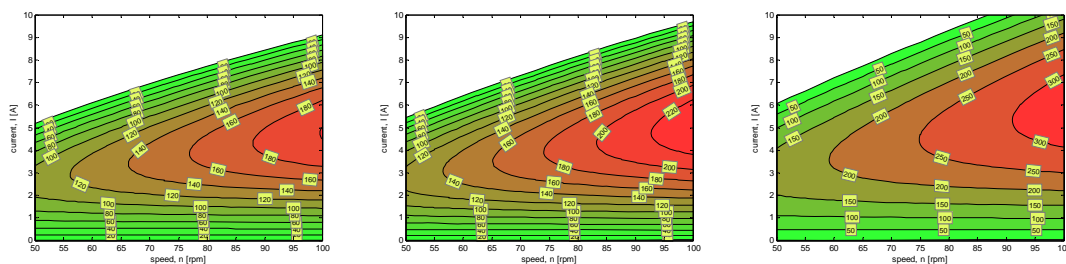
Figure 3.20 Iso-torque lines as result of the extracted active power over the speed a function of speed and current for 18, 21 and 27-coil stator
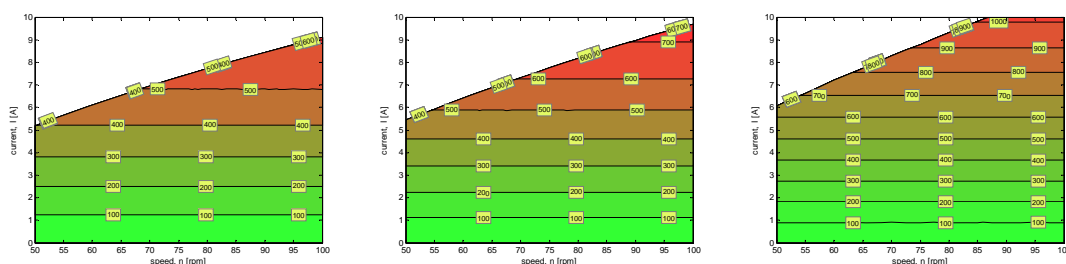
Figure 3.21 Iso-torque lines as result of the extracted active power on the load and lost active power in the winding over the speed a function of speed and current for 18, 21 and 27-coil stator

Stator tooth geometry

27-coil stator is selected as the most promising configuration due to a) three phase symmetry, b) highest induced voltage and load torque, and c) the low cogging torque. Considering the size for the tooth and the coil there are tradeoff between the cross-sectional areas for the magnetic flux and the electric current (Figure 3.22). The large cross-sectional area for the winding can bond more winding turns and have theoretically higher induced voltage or larger cross-sectional area for the same numbers of turns to accommodate more current. The increase of the coil cross section area for current reduces the core cross-section area for the magnetic flux and as an outcome the flux linkage from the rotor reduces and the self inductance is increasing. There is also a thermal aspect that determines the limits for the size or for the electric loading of the coil – the thermal resistance to dissipate heat inside the winding is increasing together with size and there is higher temperature drop across the winding for the same amount of heat losses.
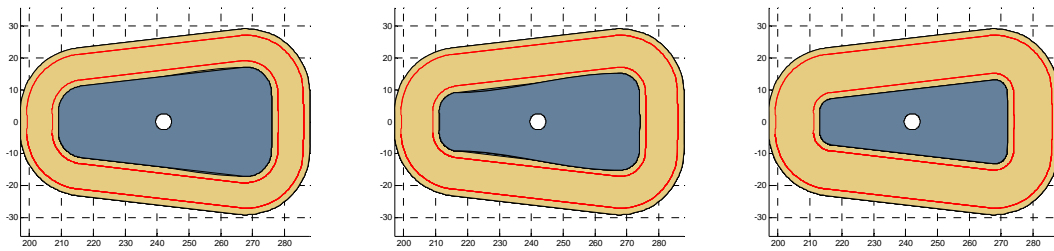
Figure 3.22 Alternative tooth size for 27-coil stator with the coil thickness of 12 (left), 14 (middle) and 16 (right) mm. Red contours indicate the conductor contours used for modeling purposes

Prototype drawings

The technical drawing that is used to build the coils for the stator is shown in Figure 3.23. The coil size is defined by the axial height $H_t=16\ mm$, the radial length $L=93\ mm$ where the outer radius $R_{to}=289\ mm$, and the tangential distance between the adjacent 27 coils of 2 mm. The selected winding thickness in radial and tangential direction, which is 14 mm, defines the size of the stator tooth.
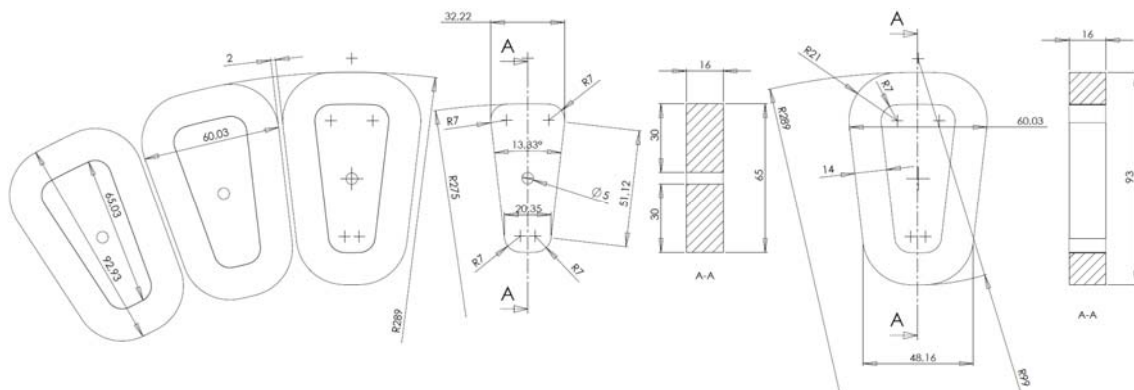
Figure 3.23 technical drawing of the phase segment, a core segment i.e. tooth and the coil

The coil is defined to have a maximum of 1 mm thick main insulation between the core and the coil. This determines the specified thickness of the coil and that is 13 mm. Practically, by using a minimum insulation thickness between the coil and the core the result is the greatest thickness of for the coil and that is 14 mm. Considering the margins, assembling tolerances and the need for the main insulation at least around the teeth the coil thickness of 13 mm is chosen and this is also specified in the winding specification.

Prototyping of the stator

The prototyping process of the stator includes the following steps:

1. Molding of SM²C block (16x260x295 mm) at normal temperature and pressure

2. 7x4 stator teeth are waterjet cut from the SM²C block

3. The teeth to coil periphery is covered with a tape of electric insulation

4. The winding is specified for *332 turns* with *0.71 mm* diameter round copper wire

5. Ready made coils are placed into a mould that is filled with

6. Terminals

Coil fill factor

Theoretical filling of two different types of windings are studied: a) quadrilateral packing, and b) the hexagonal packing. Cross-sections of these two types of windings are shown in Figure 3.24 where the area is 16x14 mm. The round conductor diameter is 0.71 mm and the insulation thickness is chosen 13% of the wire size diameter. Based on the same statement of the packing the reduced cross-section area of 16x13 mm remove winding layer of layer of 19 turns. When following the red and the blue numbers in the figures, the approach of bringing the coil terminals to the outer periphery can be seen. The coil arrangements with both coil terminals in the outer periphery facilitate the planar alignment of the coils and reduce the risk of damaging wire that crosses the coils in the air-gap region. The comparison between the geometric model of the coils and the prototyped coil is in Table 3.8.
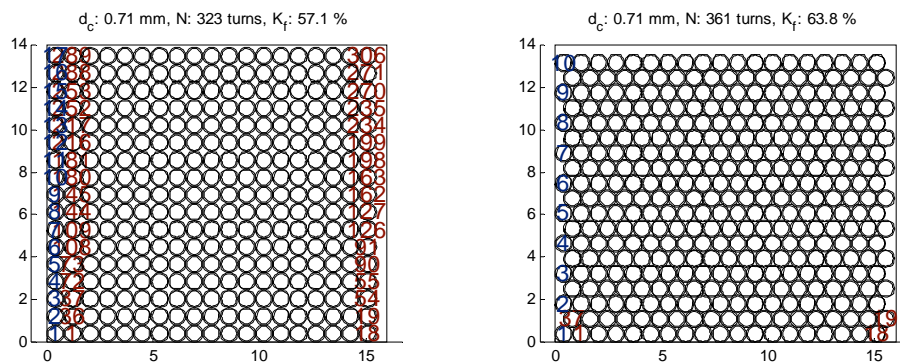
Figure 3.24 Coil fill: (left) quadrilateral and (right) hexagonal wiring arrangement

Table 3.8 Coil filling data

Wire arrangement in the coil	Quadrilateral wire packing	Hexagonal wire packing	Prototyped coil
Available or specified cross-section area	16x14	16x14	16x13
Number of layers in the coil	17	19	-
Number of turns in the coil	323	361	315
Filll factor of coil, %	57.1	63.8	55.7

The prototype coil has a thin layer of insulation between the core and the first layer of the winding wire. The short edges of the coil along the inner and the outer radius are more compressed than the coil along the longitudinal sides and prototype coil has (in all likelihood for all these coils) 315 turns. The coils and their arrangement are seen in Figure 3.25.

Figure 3.25 Coils and their arrangement. One segment of three coils is labeled.

Coil impedance

The impedance of a phase winding, which consists of 9 coils, is calculated with dc resistance where resistivity is 1.75E-8 ohm·m and inductance at the frequency of 10 Hz corresponding to 50 rpm in speed rotors. Since the windings are different due to the cross-section area and the wire packing arrangement Table 3.8, the comparison in Table 3.9 is shown in three columns.

Table 3.9 Estimation of phase resistance and inductance

Wire arrangement in the coil	Quadrilateral wire packing	Hexagonal wire packing	Prototyped coil
Stator tooth cross-section area At, cm²	16.71	16.71	16.71
Average turn length of the coil, cm	21.5	21.5	21.5
Winding phase resistance Rs, Ohm	27.6	30.9	26.9
Winding phase inductance Ls, mH	95.3	119	90.6
Current value in the Ls calculation, A	1.55	1.55	1.55

Every single coil is measured separately with RLC-meter and the results are collected into Table 3.10. There are also applied current in order to detect the polarity of the coil and to arrange them correctly in the mould. The voltage across the coil is added into the table together with the magnetic polarity of the single coil. Measurements are done on clock-wise direction from coil A1.1, which is the first coil on the first section and belongs to the A-phase (Figure 3.25).

Table 3.10 Coil parameters: resistance and inductance according to measurements

coil	current A	voltage V	polarity	L@1kHz, mH	L@120Hz, mH	R@120Hz Ohm	R@1kHz Ohm	R@0Hz Ohm	Z@12Hz Ohm	Z@50Hz Ohm	dU,V	dP,W
A 1.1	1,35	3,9	s	9,86	9,88	22,4	1311	2,89	2,98	4,24	8,95	26,00
A 1.2	1,35	3,9	n	9,84	9,87	22,3	1346	2,89	2,98	4,24	8,95	26,00
A 1.3	1,35	3,9	s	9,83	9,84	22,2	1338	2,89	2,98	4,23	8,95	26,00
B 1.1	1,27	3,9	s	9,83	9,85	22,2	1343	3,07	3,16	4,36	9,48	27,64
B 1.2	1,29	3,9	n	9,81	9,83	22,1	1338	3,02	3,11	4,32	9,34	27,21
B 1.3	1,31	3,9	s	9,79	9,81	21,9	1325	2,98	3,07	4,29	9,20	26,79
C 1.1	1,34	3,9	s	9,82	9,84	22,3	1350	2,91	3,00	4,25	9,01	26,19
C 1.2	1,28	3,9	n	9,94	9,97	22,6	1362	3,05	3,14	4,37	9,41	27,42
C 1.3	1,35	3,9	s	9,79	9,82	22	1327	2,89	2,98	4,23	8,95	26,00
A 2.1	1,34	3,9	s	9,87	9,88	22,3	1350	2,91	3,00	4,25	9,01	26,19
A 2.2	1,27	3,9	n	9,86	9,88	22,4	1352	3,07	3,16	4,37	9,48	27,64
A 2.3	1,24	3,9	s	9,76	9,79	21,9	1319	3,15	3,23	4,40	9,69	28,31
B 2.1	1,36	3,9	s	9,61	9,64	21,3	1287	2,87	2,96	4,17	8,87	25,81
B 2.2	1,34	3,9	n	9,85	9,87	22,4	1359	2,91	3,00	4,25	9,01	26,19
B 2.3	1,32	3,9	s	9,84	9,87	22,3	1349	2,95	3,05	4,28	9,14	26,59
C 2.1	1,31	3,9	s	9,84	9,86	22,4	1357	2,98	3,07	4,30	9,21	26,79
C 2.2	1,36	3,9	n	9,81	9,83	22,3	1347	2,87	2,96	4,21	8,89	25,81
C 2.3	1,31	3,9	s	9,76	9,78	22	1330	2,98	3,07	4,28	9,20	26,79
A 3.1	1,39	3,9	s	8,85	8,87	19,1	1145	2,81	2,88	3,95	8,65	25,25
A 3.2	1,32	3,9	n	9,81	9,83	21,9	1323	2,95	3,05	4,27	9,14	26,59
A 3.3	1,3	3,9	s	9,58	9,6	21,3	1283	3,00	3,09	4,25	9,26	27,00
B 3.1	1,35	3,9	s	9,68	9,7	21,7	1304	2,89	2,98	4,20	8,94	26,00
B 3.2	1,22	3,9	n	9,73	9,75	21,9	1323	3,20	3,28	4,43	9,84	28,77
B 3.3	1,32	3,9	s	9,85	9,87	22,2	1343	2,95	3,05	4,28	9,14	26,59
C 3.1	1,28	3,9	s	9,76	9,78	22	1329	3,05	3,13	4,33	9,40	27,42
C 3.2	1,34	3,9	n	9,78	9,79	22,1	1337	2,91	3,00	4,23	9,01	26,19
C 3.3	1,31	3,9	s	9,82	9,84	22,1	1336	2,98	3,07	4,29	9,20	26,79

According to measurements at 120 Hz the inductance is 9.783mH with standard deviation of 0.198mH and the resistance 21.9852 Ohm with standard deviation of 0.6538 Ohm. By excluding the data from A3.1 the outcome is 9.8181mH with standard deviation of 0.0781mH and the resistance 22.0962 Ohm with standard deviation of 0.3143 Ohm. By assuming that the inductance is quadratic to the number of turns for the determined space ($L=\mu N^2 A/l$) then the reduction of winding turns from 315 to 300 brings the inductance from 9.818 mH to 8.905 mH. The uncertainty around the number of turns in the coil reduces the possibility to have a deeper study on the manufacturing of single teeth coils for axial flux machines and material properties of SM²C core. The next concern is actually to distribute the coils so that the phase inductance and the resistance become more or less equal between them. Table 3.11 shows the measured resistance and inductances over the phase sections and the complete phase windings.

Table 3.11 Section and winding parameters: resistance and inductance according to measurements

coil	current A	voltage V	polarity	L@1kHz, mH	L@120Hz, mH	R@120Hz Ohm	R@1kHz Ohm	R@0Hz Ohm	Z@12Hz Ohm	Z@50Hz Ohm	dU,V	dP,W
A1	1,39	11,9	sns	33,05	33,08	82,02	5330	8,56	8,92	13,46	26,75	77,05
B1	1,37	11,9	sns	32,84	32,85	80,85	5260	8,69	9,03	13,49	27,10	78,18
C1	1,39	11,9	sns	33,03	33,04	81,92	5330	8,56	8,92	13,45	26,75	77,05
A2	1,39	11,9	sns	33,13	33,14	81,94	5360	8,56	8,92	13,48	26,76	77,05
B2	1,39	11,9	sns	32,21	32,21	78,33	5070	8,56	8,90	13,25	26,70	77,05
C2	1,39	11,9	sns	32,63	32,64	80,19	5250	8,56	8,91	13,36	26,72	77,05
A3	1,41	11,9	sns	31,67	31,68	76,42	4950	8,44	8,77	13,05	26,31	75,96
B3	1,39	11,9	sns	32,39	32,39	78,97	5125	8,56	8,90	13,30	26,71	77,05
C3	1,37	11,9	sns	32,83	32,84	81,03	5290	8,69	9,03	13,49	27,10	78,18
A	1,13	29,1	snssns	98,06	98,17	240,9	14512	25,75	26,79	40,18	80,38	231,77
B	1,12	29,1	snssns	98,19	98,19	240,1	15053	25,98	27,02	40,33	81,05	233,84
C	1,14	29,1	snssns	99,07	99,47	245,6	14760	25,53	26,61	40,35	79,82	229,74

A part from, the measurements in Table 3.10 and Table 3.11 there are the recalculated impedances at 12 and 50 Hz that corresponds to the mechanical speed of the wind turbine 60 and 250 revolutions per minute. Two last columns in the tables show the voltage drop and the power drop across the coil, winding segment or the complete winding at 3A rms and 12Hz. In case of production observation the winding parameters are measured before and after stator assembling (Table 3.12).

Table 3.12 Phase resistance and inductance before and after stator assembling

Winding parameters	In-prior to soldering and moulding			After to soldering and moulding		
Phase label	A	B	C	A	B	C
Resistance (dc), R@0Hz Ohm	25.75	25.98	25.53	25.8	25.0	24.9
Resistance (dc+ac), R@120Hz Ohm	240.9	240.1	245.6	146.86	156.49	195.3
Resistans (dc+ac), R@1kHz kOhm	14.5	15.1	14.8	6.76	5.90	4.92
Inductance, L@120Hz, mH	98.17	98.19	99.47	92.9	94.75	99.33
Inductance, L@1kHz, mH	98.06	98.19	99.07	103.62	102.11	97.63

Machine assembling

AFPMSM consists of double-sided surface mounted PM rotors and a plate of molded 27 single tooth coils. The rotor halves are mounted so that they are parallel and the distance between them $H_m=73.4\ mm$. As a consequence, the magnetic air-gap between the machine parts is 2x6.7 mm. The actual gap is $g=2.7\ mm$ larger than it is assigned as the ideal air-gap.

Figure 3.26 Determination of air-gap and montage of the machine with focus on upper and lower air-gap

The reasons for the larger air-gap are the forces between the machine parts, variation in tolerances, stiffness of the stator body and mounting accuracy. The air-gap or distance between the upper rotor and the stator varies between *1* and *3 mm* and lower air-gap between *6* and *10 mm*, when rotating the rotor. There is less chance to improve the situation as the magnetic forces bends the stator plate so that it reduces the lower air-gap to zero and brings the machine parts into the contact. Some efforts have been done by reinforcing the stator plate and minimizing the air-gap. As the consequence a larger and mechanically stable air-gap has been selected and new electromagnetic analysis is carried out in parallel to the experimental evaluation. The expected magnetic air-gap is 6.7 mm.

Induced voltage of 24-pole 27-coil AFPMSM as a function of gap

3D FE analyses of a single tooth coil have been used to calculate flux linkage and the induced voltage, also the forces and the torque. The air-gap distances between the stator core and the permanent magnets, which are in both air-gaps, have been changed. Figure 3.27 shows the flux linkage per turn and induced voltage at estimated number of turns and at *50 rpm*. The title of voltage waveforms shows the rms voltages at different air-gaps and the values are written into the legend box in mm.
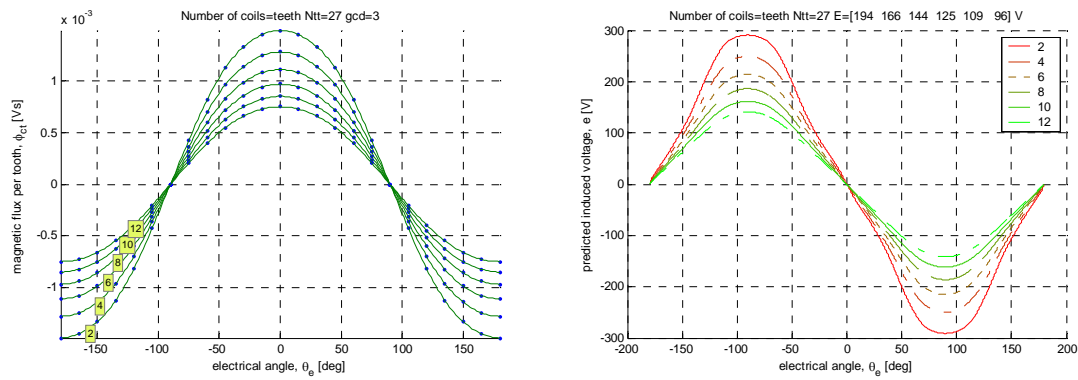
Figure 3.27 Magnetic flux linkage and induced voltage of 24-pole 27-coil AFPMSM as a function of gap

The measured open circuit voltage is between 129-133V and the value is between *125* and *144 V* as the expected *6* and *8 mm* air-gap at 10Hz (Figure 3.28).
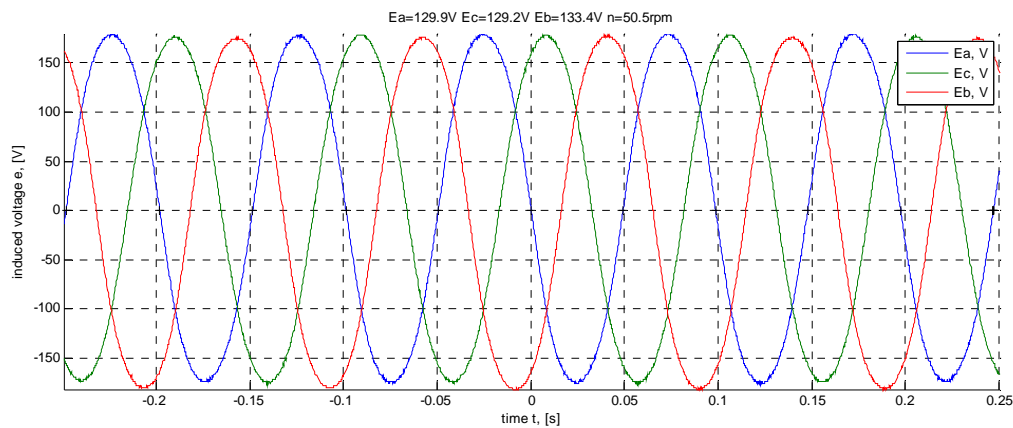

Figure 3.28 Measured open circuit voltage

Cogging torque of 24-pole 27-coil AFPMSM as a function of gap

The cogging torque is calculated from the applied torque waveforms to a single tooth. These waveforms (Figure 3.29, left) are shifted 1/27 period and added together (Figure 3.29, right) in order to predict the resultant cogging torque as a function of rotor position.
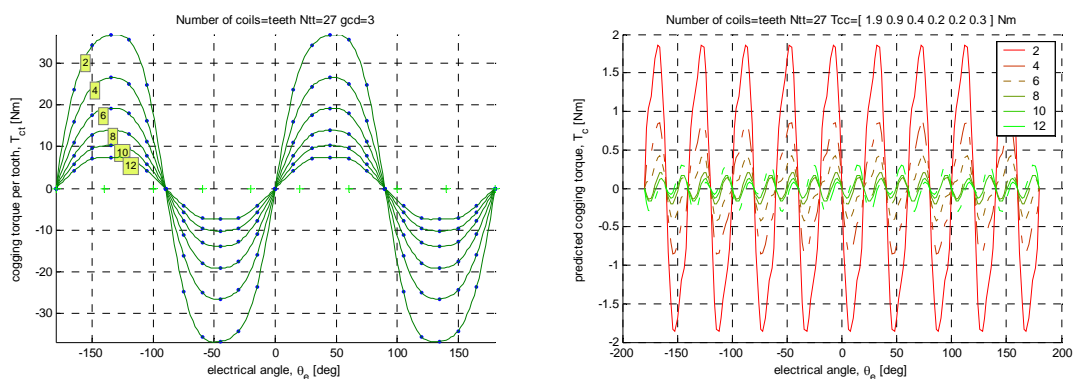

Figure 3.29 Cogging torque per stator tooth and the resultant cogging waveform of 24-pole 27-coil machine

The measurement indicates that the cogging has 24 peaks in the range of *10* to *14 Nm*, which is considerably higher that the theoretical calculations stated. Anyhow the cogging torque is still small compared to starting torque needed or the braking torque and can be reduced by careful balancing of the machine assembly.

Generator performance of 24-pole 27-coil AFPMSM as a function of gap

Once again the machine parameters such as flux linkage, the internal resistance and the inductance are used to determine the power characteristics of the AFPMSM in generator operation at resistive load. This time these characteristics are calculated as a function of the air-gap (the magnetic gap between rotor and stator) at *50 rpm*.
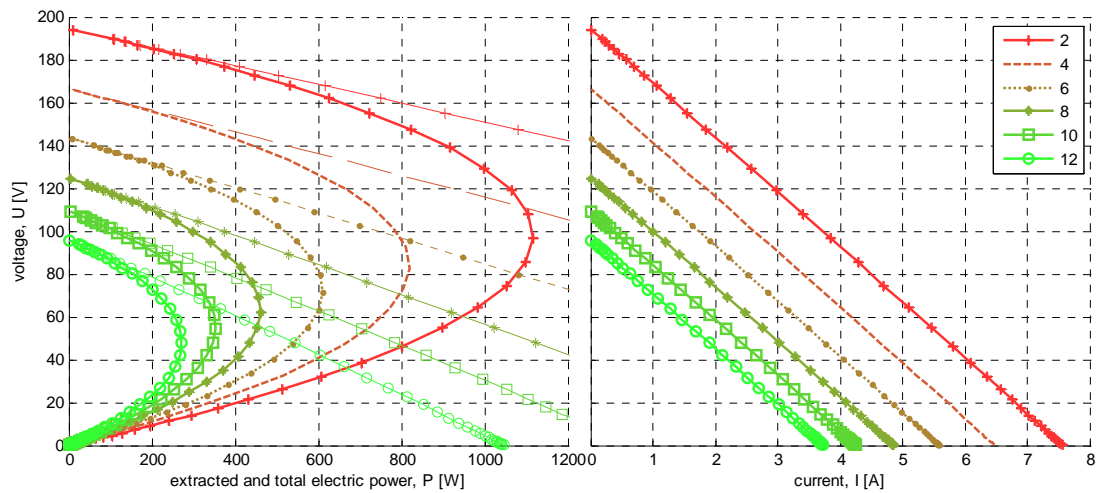

Figure 3.30 Voltage-Power and Voltage-current characteristics as a function of gap. Extracted power is shown as solid lines and the total electric power as thin lines on the voltage-power diagram.
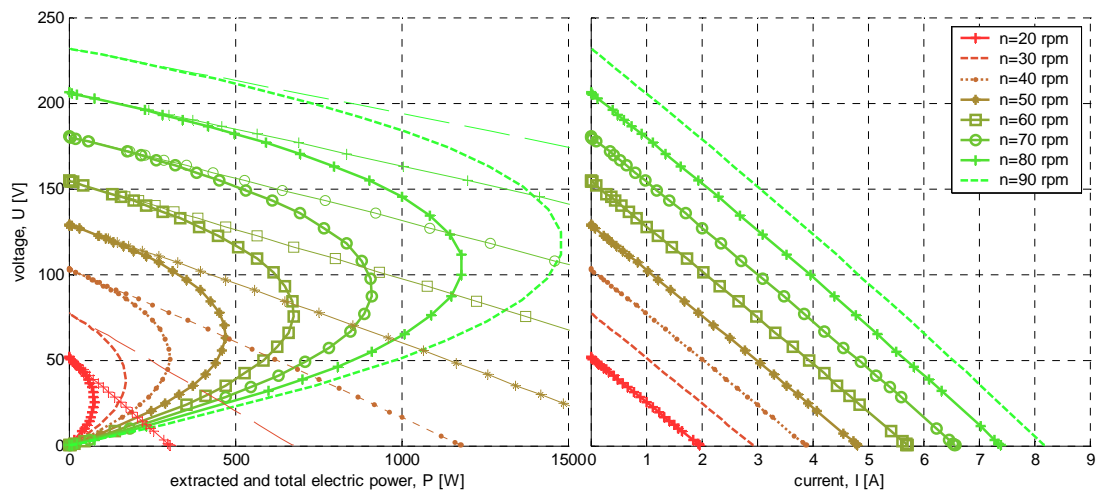

Figure 3.31 Power and Voltage-current characteristics as a function of speed for the prototyped machine with 6.7 mm gap. Extracted power is shown as solid lines and the total electric power as thin lines on the voltage-power diagram.

Power output as a function of rotor speed and machine montage

This section gives a theoretical expectation on short-circuit current, open circuit voltage and maximum 3-phase power over resistive load as a function of rotor speed and machine montage. Hereby depending on montage different air-gap length can occur.
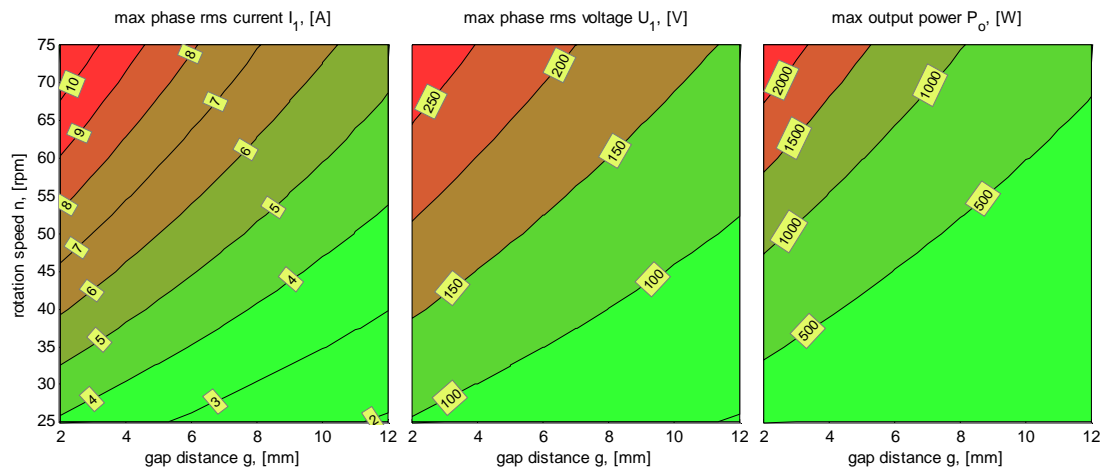
Figure 3.32 Short-circuit current, open circuit voltage and maximum three-phase power for 24-pole 27-coil machine.

Laboratory measurements

The experimental laboratory setup consists of frequency converter driven asynchronous machine as the primary power source to the AFPMSM in generator operation, belt transmission between the machines and (mainly) resistive 3-phase load consisting of lamps and ballast resistors. Power meter is used to measure 3-phase voltages, currents and powers per phase. There are also current and voltage probes connected to the scope for recording the waveforms of the currents and voltages.
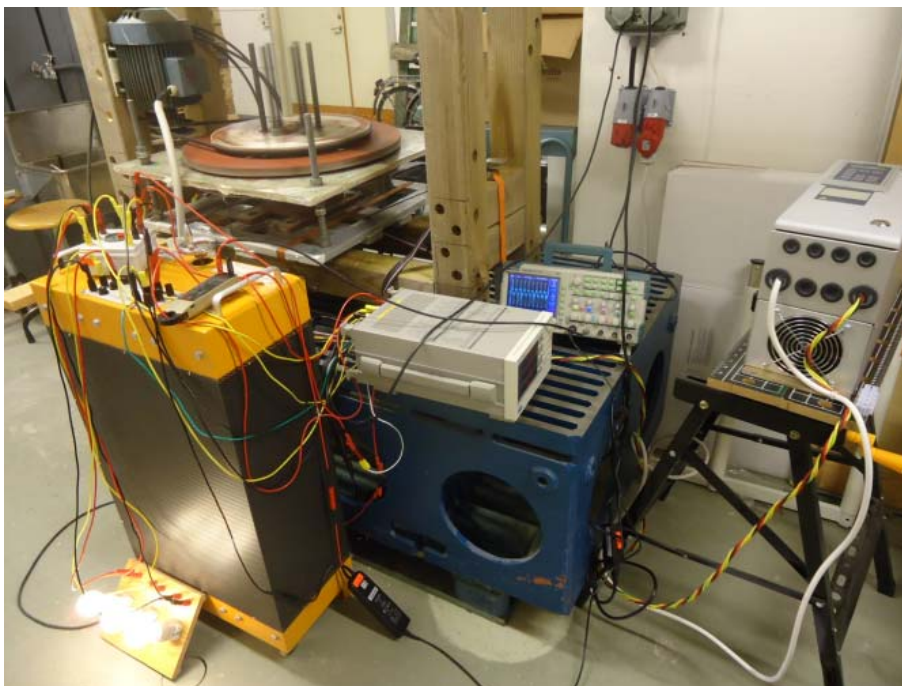
Figure 3.33 Experimental setup at ongoing load test.

There are two different measurements that carried out in the laboratory conditions: 1) no-load measurements of terminal voltage and system input power and 2) measurements of voltage, current and power at loaded conditions.

The load test is carried out as following: 1) Initial speed of the idling machine is selected by frequency converter, 2) The load is switched on and the maximum load point is detected. As the asynchronous motor is not infinitely strong to provide the power needed, the rotation speed is

dropping obviously when the load is increasing. This limits clearly the assessment of the machine capability at higher loading. Having the rotation speed in mind, the peak power detection is made in range of 50 to 100 rpm, which is also the predefined operation range of the machine. There are two measurement cycles recorded in the tables (Table 3.13 and Table 3.14) as the readings from the power meters showing ca *327W* at *77rpm* and *449W* at *90rpm*. This power estimation is slightly underestimated when comparing the values to the instantaneous measurements of voltages and currents (Figure 3.34). Also as it is mentioned before the driving motor is not powerful enough to keep the speed in order to test the prototype machine.

Table 3.13 Records from the power meter from 100 rpm

F, Hz	n, rpm	Ua, V	Ub, V	Uc, V	Ia, A	Ib, A	Ic, A	Pa, W	Pb, W	Pc, W
20	100	251	254	256	0	0	0	0	0	0
19.0	95	232	234	236	0.21	0.21	0.214	49.0	49.5	50.4
18.87	94.4	231	233	234	0.227	0.228	0.231	52.3	53.2	54.0
15.46	77.3	176	177	178	0.614	0.610	0.624	108	108	111.2
14.53	72.7	164	167	168	0.658	0.654	0.651	108	106	108
13.50	67.5	150	152	153	0.692	0.678	0.689	105	103	105

Table 3.14 Records from the power meter from 120 rpm

F, Hz	n, rpm	Ua, V	Ub, V	Uc, V	Ia, A	Ib, A	Ic, A	Pa, W	Pb, W	Pc, W
24	120	301	304	306	-	-	-	-	-	-
22	110	279	281	284	0.234	0.235	0.239	65.4	66.3	68.7
18	90	207	209	211	0.72	0.71	0.73	148	148	153
17.5	87.5	199	200	201	0.72	0.71	0.73	146	143	149
16.78	83.9	184	187	188	0.76	0.74	0.76	141	139	143
15.9	79.5	177	179	180	0.76	0.74	0.76	135	134	137
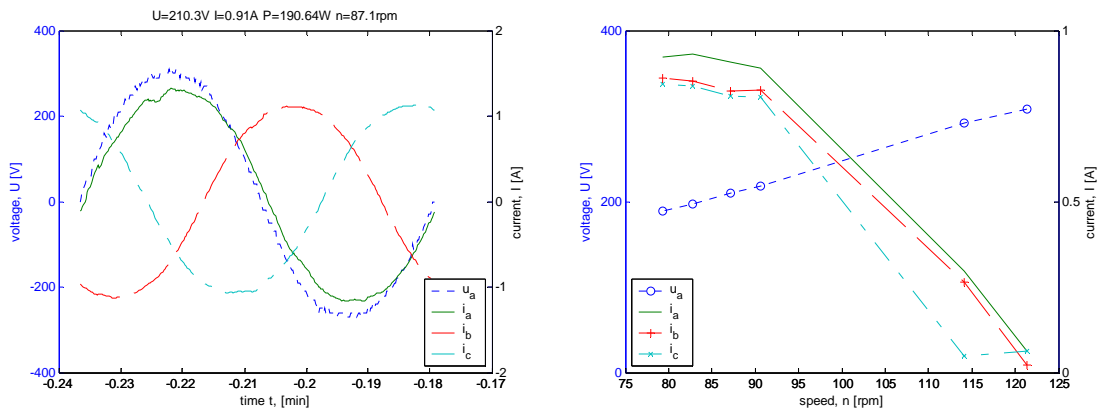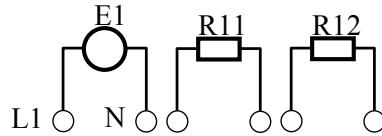
Figure 3.34 operation point recorded by scope where a single voltage probe and three current probes are connected

Field study

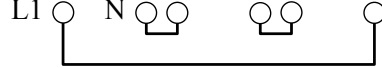There is also an extensive field study done where the speed (wind and turbine) and the extracted power is measured. The measurements are not presented here, just the connection scheme (Table 3.15) that is used to extract a few operation points in order to study the system characteristics.

Table 3.15 Terminal connections for different external loading

	Schematic representation	Description
Circuit	E1 R11 R12 L1 N	Schematic representation of emf source of a single phase winding (E1) and two available resistance for this phase (R11 and R12)
Open	L1 N	There is no closed circuits between sources and loads
Series	L1 N	Both load resistances are connected in series $R_{tot}=2R$
Single	L1 N	Only one resistance is used $R_{tot}=R$
Parallel	L1 N	Both load resistances are connected in parallel $R_{tot}=R/2$

3.4   Summary

The predecessor of 18-coil 24-pole coreless AFPMSM is redesigned to successor of 27-coil 24-pole SM²C core AFPMSM. Reduction of cogging and increase of power capability are the main paths in the design. There is a slight reduction of copper used in the stator and considerable increase of breaking torque capability when comparing the first prototype with the second prototype. The coil data and mounting data is provided in Table 3.16.

Table 3.16 Winding data of the prototype machines: 1) 18-coil 24-pole coreless, 2) 27-coil 24-pole SM²C core

	Prototype 1	Prototype 2
Number of coils	18	27
Diameter of wire	0.55	0.71
Number of turns per coil	833	315
Resistance per coil @ 0 Hz, Ω	19.9-22.2	2.97-3.15
Resistance per coil @ 120 Hz, Ω	128.58-128.49	
Resistance per coil @ 1 kHz, kΩ	8.057-8.149	
Inductance per coil @ 120 Hz, mH	56.69-56.60	9.97
Inductance per coil @ 1 kHz, mH	56.68-56.59	9.61-9.94
Axial distance between the magnets, mm	27	29.4
Distance between the coil and magnets, mm	4	6.7
Flux linkage, Vs	2.81	2.05
Flux linkage peak per coil and winding turn, mVs	0.79	1.02

Even if the machine characteristics at the maximum power output are not measured, they are constructed according to known data of open circuit voltage, stator resistance and inductance (Figure 3.35). As the efficiency is not included, the power curve does not show the power requirement to the wind turbine, which might cause the wind turbine to drop the speed due to high load. From power harvesting point of view either higher speed or the narrower air-gap increase the extracted power of the generator. The maximum flux linkage per coil as a function of the gap is presented in Table 3.17. The difference of winding factor is the values presented in Table 3.16 and in Table 3.17.
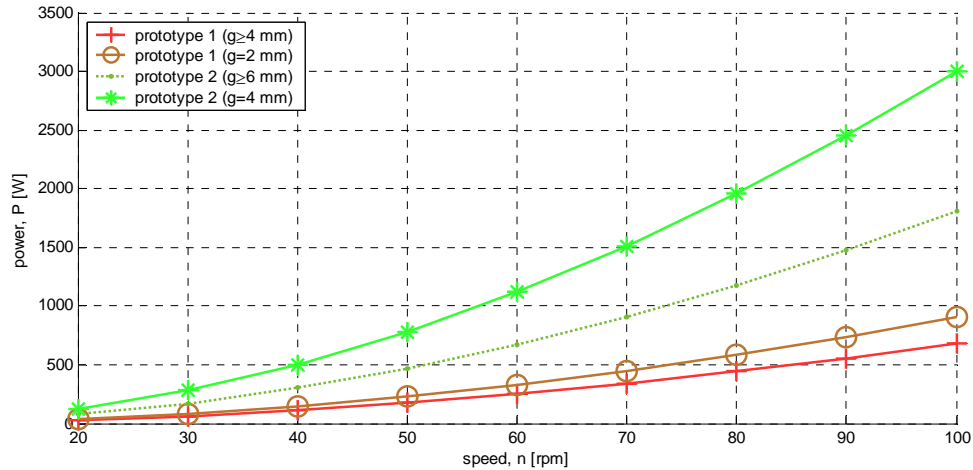
Figure 3.35 Speed-Power characteristic of the axial flux permanent magnet synchronous machine without core (original 18-coil) and with SM²C core (successor 27-coil) shows the maximum extracted power as a function of speed for 24-pole machine. There are two air-gaps for the 27-coil machine: real and reachable by improvement.

Table 3.17 Peak flux linkage per coil for 18-coil 24-pole machine and 27-coil 24-pole machine based on Finite Element Analysis

	18-coil 24-pole	18-coil 24-pole	27-coil 24-pole
Gap, mm	Ψ_{max} coreless, Vs	Ψ_{max} SM²C, Vs	Ψ_{max} SM²C, Vs
1	1.176	2.105	
2	1.108	1.922	1.540
3	1.045	1.765	
4	0.988	1.631	1.318
5	0.935	1.512	
6	0.887	1.408	1.143
7	0.842	1.316	
8	0.800	1.233	0.992
9	0.761	1.158	
10	0.725	1.090	0.865

From machine design and mounting point of view the mechanical loads that causing axial attraction, cogging and vibration depends on the air-gap distance, which in turn influences the starting torque, braking torque and power capability of the machine and makes this parameter on of the most critical in the design and in the practical evaluation. From cost point of view the considerable amount of permanent magnets necessitates finding less PM material topologies for AF or RF machine construction.

4   Hybrid excited radial flux machine

Hybrid excitation is defined as a combined excitation of different sources such as permanent magnets and electro magnets. With the growing size of the electrical machines it is not obvious longer, whether the permanent magnet excitation is the most attractive in the terms of the compactness and the excitation field strength that they can provide. On the contrary, concerning to the permanent magnets, usually the high specific price of the material is noticed and not the high energy density with a low heat loss density. The outcome can be disgraceful as without permanent magnets the machines can be bigger, heavier, probably not as efficient, and require a lot more copper to offset what one save in magnets. Therefore the tradeoff between the different types of magnetizations, which are based on permanent magnet and (temporal) electromagnet, is set into the focus of the research continuation. The advantages of the permanent and temporal magnet excitation are not only the cost related issues rather than added value of excitation field regulation: enhancing and weakening.

This part of the research is not directly connected to the initial goal of Damia-2. It is rather naturally grown out from the project in order to explore for alternative attractive solutions to meet the application need.

4.1   Excitation specification

The first stride in the investigation of the permanent magnet (PM) and electromagnet (EM) based excitation is to analyze some larger RF machines with different size and the number of poles. In this study the distributed three phase winding is selected in the inner stator. There are 3 slots per phase and per pole. The core material is no longer SM²C, but laminated steel. It is worth to highlight one design experience related to SM²C, which is that the high number of poles does not have magnetically any advantages as the material is as poor magnetic conductor as it is and it leaks magnetically even more than the other materials that can attract the air-gap field to link with the windings. Therefore the simulation model in 2D FE is built, where the active length of the machine is $H_{act}=0.1\ m$, and the focus are on two series of analyses when comparing PMSM and EMSM:

1. Same size of machine, with radial thickness of 10 cm at different outer radius of machine. The material and geometry specification of *16-pole 42-slot* synchronous machines with PM (Figure 4.1) and EM (Figure 4.2) excitation are shown for preselected machine diameter of $D_m=700\ mm$. The radial height of the machine is selected to be $d_m=100\ mm$ and the number of poles is changed from $N_p=12$ to 28.

2. The stators are identical and the outer rotor with surface mounted PM or salient pole EM excitation is adapted to the selected gap radius, so that the excitation is designed according to needs: magnetic and the thermal. The material and geometry specification of *24-pole 72-slot* synchronous machines with PM (Figure 4.5) and EM (Figure 4.6) excitation are shown for preselected gap diameter of $D_g=800\ mm$. The radial height of the stator is selected to be $d_m=100\ mm$, the rotor thickness is selected $d_{rt}=25\ mm$ for PM rotor and $d_{rt}=45\ mm$ for EM rotor and the number of poles is changed from $N_p=20$ to 36.

Red circle on the contour maps (Figure 4.3, Figure 4.4, Figure 4.7 and Figure 4.8) indicate the geometric specification of the electrical machine presented in Figure 4.1, Figure 4.2, Figure 4.5 and Figure 4.6 respectively. The peak power is picked from generator load characteristics (Eq 1.5) by assuming that the machine rotates at $n=50\ rpm$ and is loaded with pure 3-phase resistive load. The torque is calculated from the peak power and the power losses are related to the load current in the stator, the excitation current in the rotor when the excitation coil is present and the power losses in the stator core due to the remagnetisation process.
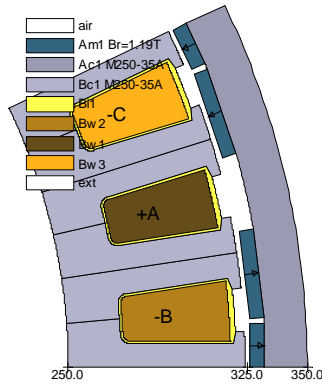
Region	A, [cm²]	∑A, [cm²]	V, [dm³]	material	ρ, [kg/m³]	M, [kg]
Am1	2.23	93.61	0.94	N35	7400	6.93
Ac1	27.14	379.98	3.80	M250-35A	7600	28.88
Bc1	9.85	827.62	8.28	M250-35A	7600	62.90
Bi1	11.39	68.42	0.68	insulation	1200	0.82
Bw2	9.76	136.64	2.09	copper	8900	18.61
Bw1	9.76	136.64	2.09	copper	8900	18.61
Bw3	9.76	136.64	2.09	copper	8900	18.61

Figure 4.1 Surface mounted PM excited synchronous machine (same machine size)
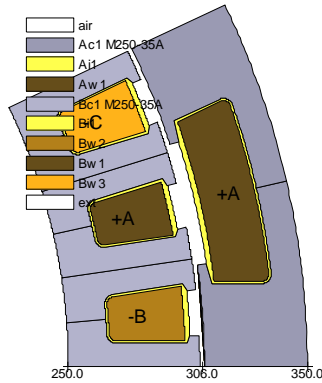
Region	A, [cm²]	∑A, [cm²]	V, [dm³]	material	ρ, [kg/m³]	M, [kg]
Ac1	20.89	584.81	5.85	M250-35A	7600	44.45
Ai1	19.67	37.90	0.38	insulation	1200	0.45
Aw1	16.97	237.54	3.55	copper	8900	31.63
Bc1	7.20	604.55	6.05	M250-35A	7600	45.95
Bi1	7.73	55.66	0.56	insulation	1200	0.67
Bw2	6.40	89.66	1.34	copper	8900	11.94
Bw1	6.40	89.66	1.34	copper	8900	11.94
Bw3	6.40	89.66	1.34	copper	8900	11.94

Figure 4.2 Salient pole EM excited synchronous machine (same machine size)
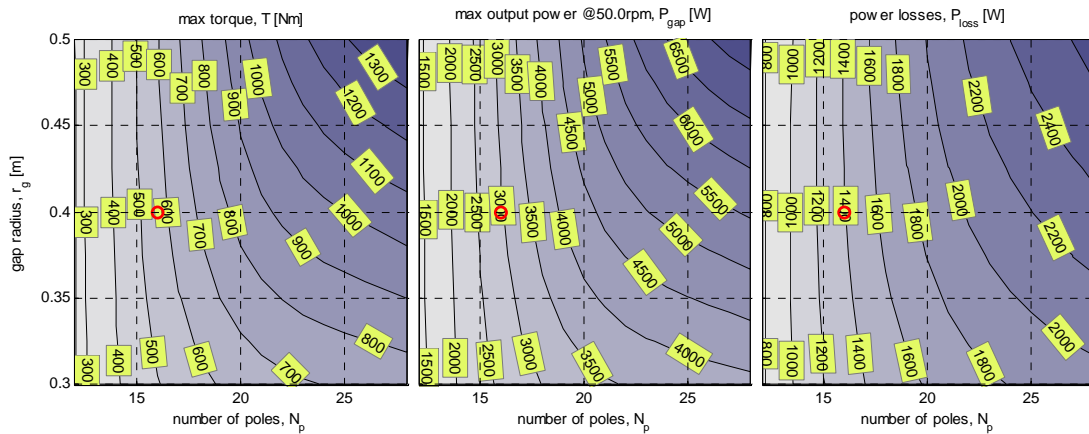

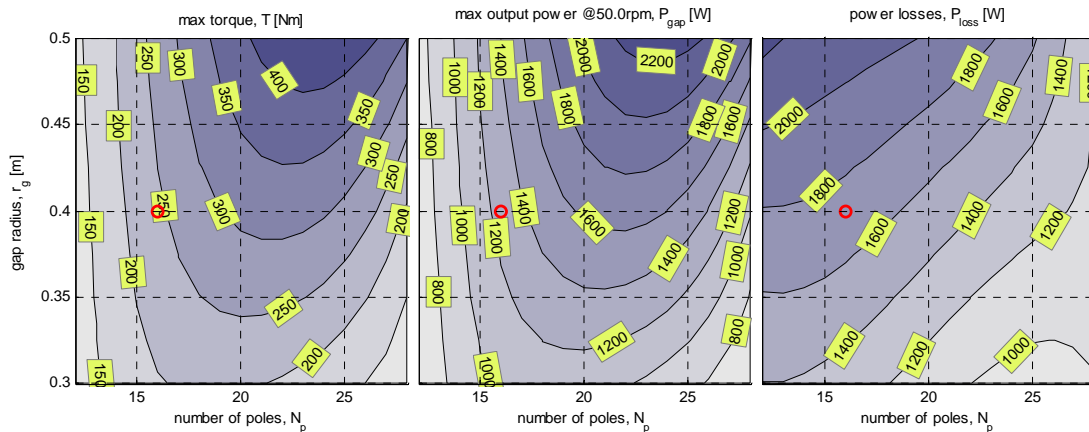*Figure 4.3 torque, power @ 50 rpm and power losses of PMSM (same machine size)*

Figure 4.4 Calculated torque, power @ 50 rpm and power losses of EMSM (same machine size)
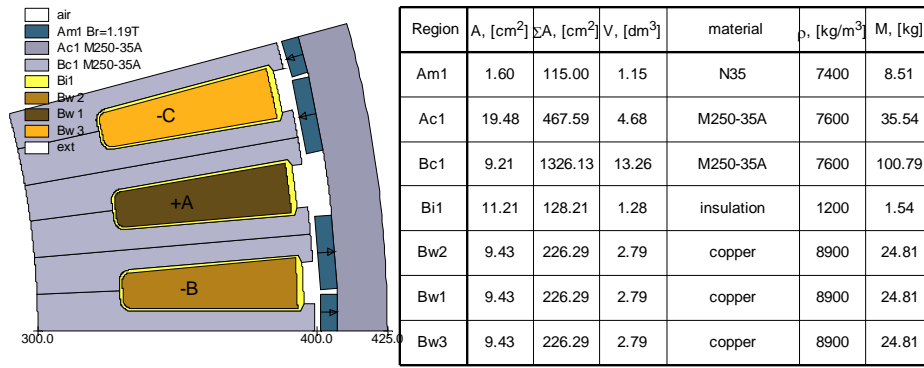
Region	A, [cm²]	∑A, [cm²]	V, [dm³]	material	ρ, [kg/m³]	M, [kg]
Am1	1.60	115.00	1.15	N35	7400	8.51
Ac1	19.48	467.59	4.68	M250-35A	7600	35.54
Bc1	9.21	1326.13	13.26	M250-35A	7600	100.79
Bi1	11.21	128.21	1.28	insulation	1200	1.54
Bw2	9.43	226.29	2.79	copper	8900	24.81
Bw1	9.43	226.29	2.79	copper	8900	24.81
Bw3	9.43	226.29	2.79	copper	8900	24.81

Figure 4.5 Surface mounted PM excited synchronous machine (same stator size)

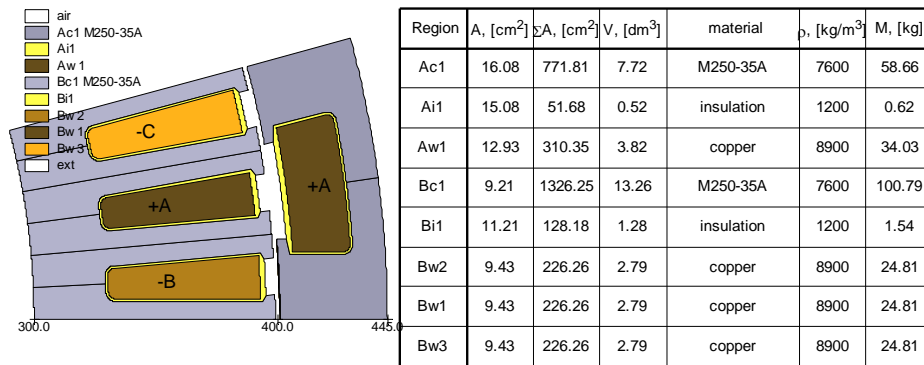| Region	A, [cm²]	∑A, [cm²]	V, [dm³]	material	ρ, [kg/m³]	M, [kg]
Ac1	16.08	771.81	7.72	M250-35A	7600	58.66
Ai1	15.08	51.68	0.52	insulation	1200	0.62
Aw1	12.93	310.35	3.82	copper	8900	34.03
Bc1	9.21	1326.25	13.26	M250-35A	7600	100.79
Bi1	11.21	128.18	1.28	insulation	1200	1.54
Bw2	9.43	226.26	2.79	copper	8900	24.81
Bw1	9.43	226.26	2.79	copper	8900	24.81
Bw3	9.43	226.26	2.79	copper	8900	24.81

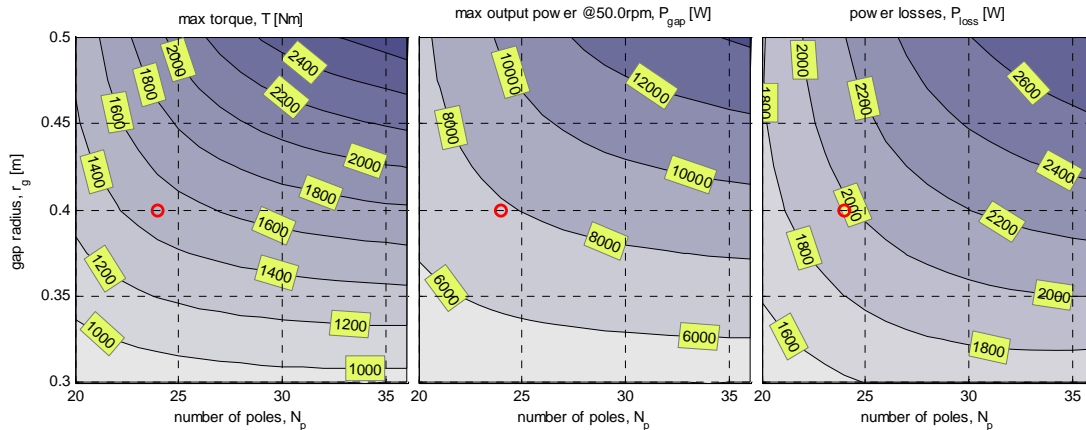*Figure 4.6 Salient pole EM excited synchronous machine (same stator size)*

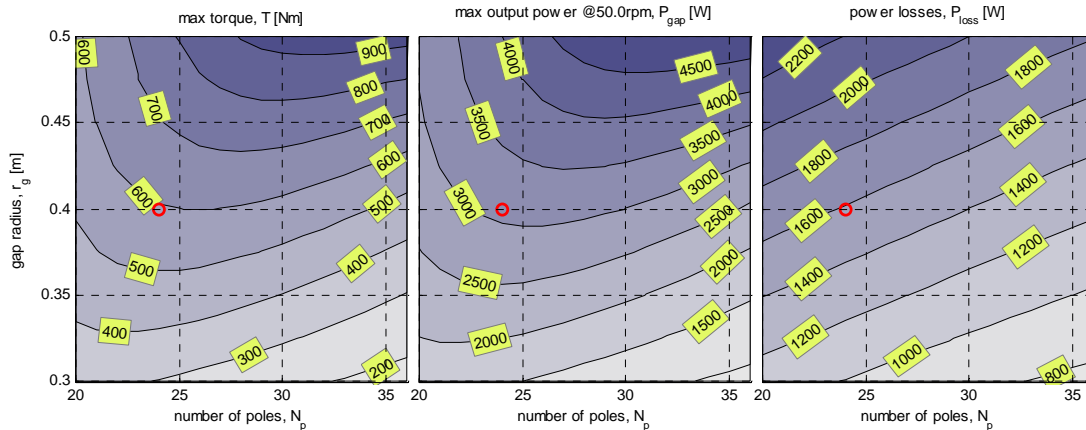*Figure 4.7 Calculated torque, power @ 50 rpm and power losses of PMSM (same stator size)*

Figure 4.8 Calculated torque, power @ 50 rpm and power losses of EMSM (same stator size)

It could be argued whether the previous design constrains favored PM excitation as
1. both the stator and the rotor of the EMSM became under dimensioned for the equal size of the machine, and
2. EM rotor is not designed for the same magnetization as the PM rotor for the equal size of stators.

4.2   *Design of a direct driven generator with hybrid magnetization*

From the last design review of PMSM and EMSM it is obvious that the direct replacement of the magnetization system does not bring directly to the satisfying solution of high torque capability or considerably lower cost. Having the main focus on the torque requirement and the selected volumetric size of the active part of the machine (Figure 4.9) brings to a number of possible solutions of outer rotor (Figure 4.10, left) and inner rotor (Figure 4.10, right)
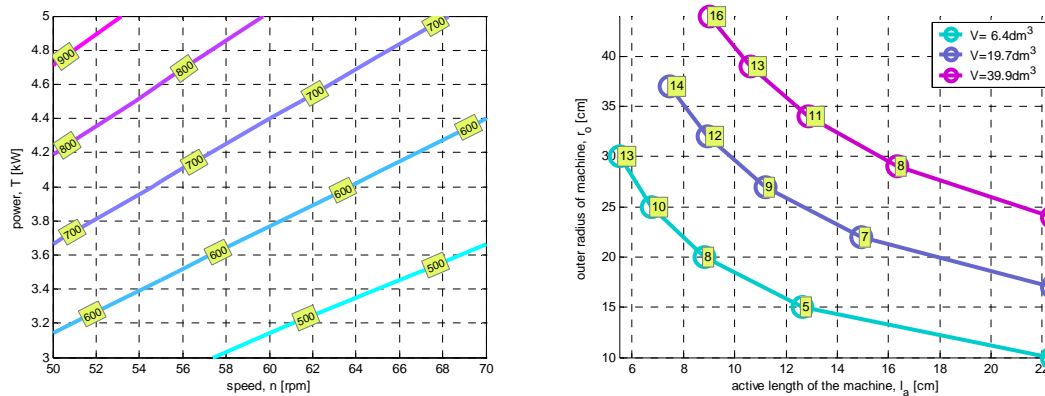

Figure 4.9 Torque requirement (left) and size specification (right) of the synchronous machine
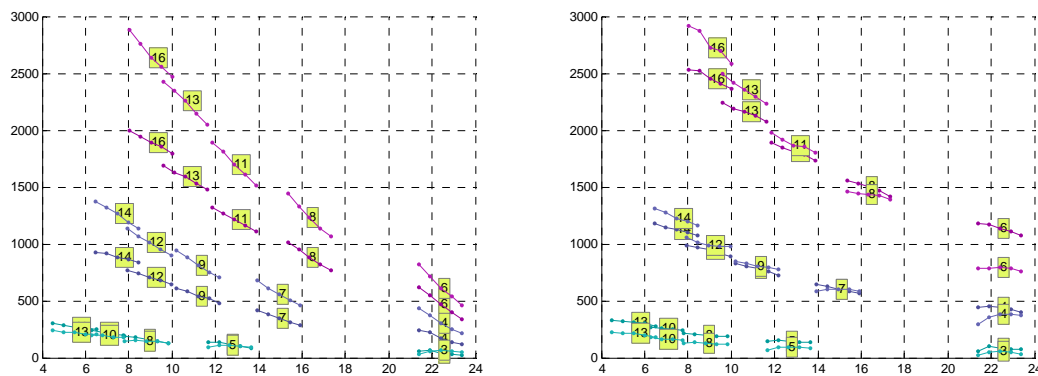

Figure 4.10 Electromagnetic torque in Nm in vertical axis and the active length of the machine in cm in horizontal axis for the outer (left) and inner (right) rotor configuration with electric (light lines) and permanent magnet (dark lines) excitation calculated at different number of poles (presented as dots on the lines)

This calculation is carried out for the benefit and favor of EMSM as the stator size as well as the machine size is kept constant in order to make visible the other side of the prejudiced comparison. The magnetic loading for the outer and for the inner rotor machine is shown, respectively, in Figure 4.11 and Figure 4.12.

These calculations are carried out differently. In this calculation the current density is predefined in the coils. The thermal analysis is carried out in parallel but not accounted in this graphs. Without going deeply in to the thermal design and cooling capability that is related to the specific loss density when selecting the current density and the operational temperatures, the current density in the conductor is $J_c=4A/mm^2$ and coil fill factor in the pre-insulated slot is $K_f=50\%$. The outcome is an electromagnetic torque as an outcome of vector controlled synchronous machine. Also the machine length in axial direction (axial height) is no longer constant as this is varied according to the predefined volume that is defined by D_o/D_i-H_{act} that is the outer radius, the inner radius and the axial height of the machine.
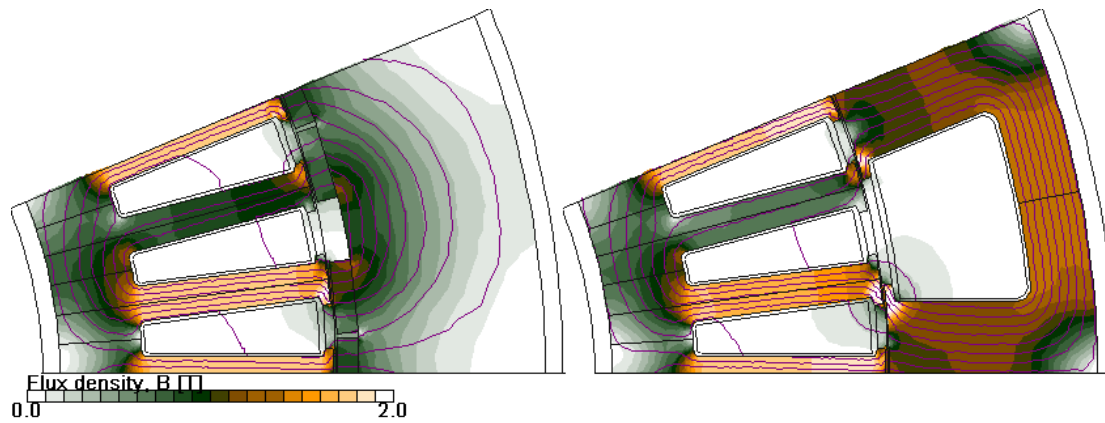
Figure 4.11 Magnetic flux density distribution of PMSM (left) and EMSM (right) with outer rotor
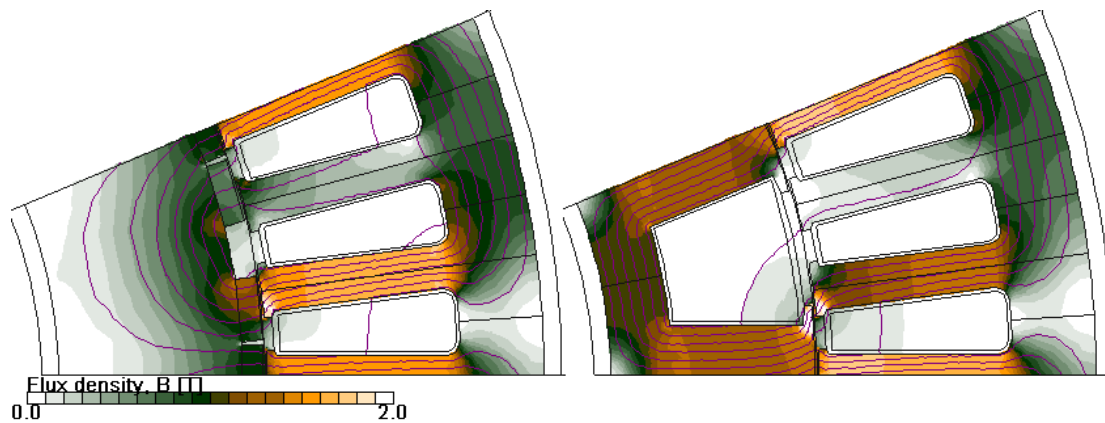

Figure 4.12 Magnetic flux density distribution of PMSM (left) and EMSM (right) with inner rotor

The ideal torque requirement (Figure 4.9, left) for the electrical machine according to the rated power and rated speed specification does not include the additional mechanical input needed to overcome power losses. The actual torque requirement is higher or the delivered power lower. When it comes to relate the torque to the machine size is that the volumetric size specification (Figure 4.9, right) considers the active part and that excludes mechanic support and end windings. The valuable connection in the graphs is the lower-right corner where the starting point is a designed and existing (high-speed) prototype with insert PMSM. According to this analysis (Figure 4.10) the EMSM can over perform PMSM if PMSM has to follow strictly the volumetric constrains to the rotor and the stator.

Based on this introductory analysis the HMSM synthesis is carried out:

1. PMSM and EMSM is combined together to become HMSM

2. The same size of the machine parts facilitates immerging PM and EM excitations

3. The PM excitation is reduced to 2 to 4 poles rest is EM

4. Number of stator slots and remaining PM-poles cause cogging and is selected with care

5. Concentrated windings with same size are preferred in order to facilitate production

The alternate arrangement of EM and PM poles that composes HM excitation is presented by Thomas A Lipo in Wisconsin 90-es and since that the topology has been rather out of sight among research efforts. Anyway, Figure 4.13 shows the principle where one PM pole pair has been replaced with electromagnets (Figure 4.13, left), and PM-EM arrangement is proposed for 32-pole 30-slot (or coils) synchronous machine with concentrated windings (Figure 4.13, right). The arrangement with rotor coils and excitation allows even to change the number of poles and therefore change electric frequency and voltage for given speed that can be part of future studies and analyses.
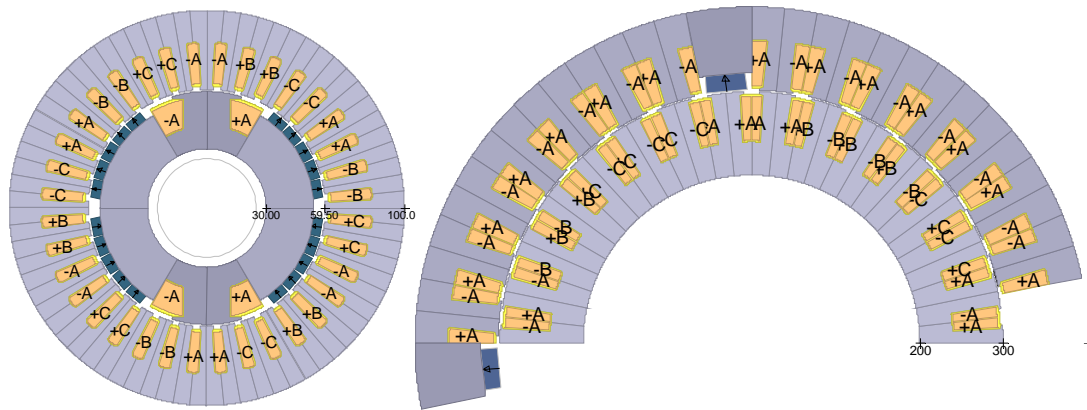
Figure 4.13 Synthesized HMSM for the reference point of 6-pole 36-slot IPMSM (left) and 32-pole 30-slot for wind power application

There is no value of the design process that does not concern the production; therefore the design for manufacturability is the important issue when choosing the initial dimensions for the machine. Concerning the dimensions of the electromagnetic steel plate, laser or water jet cutting of the complete stator and rotor the outer diameter of the core is chosen D_o=600 mm. As the inner cavity is large enough (D_i=400 mm and H_{act}=100 mm) to build another machine with the same principle it is suggested to use the material for a smaller prototype with another configuration. Anyway the large machine is the main concern and the CAD drawing (Figure 4.14) is made to analyze the production aspects of a large electrical machine.
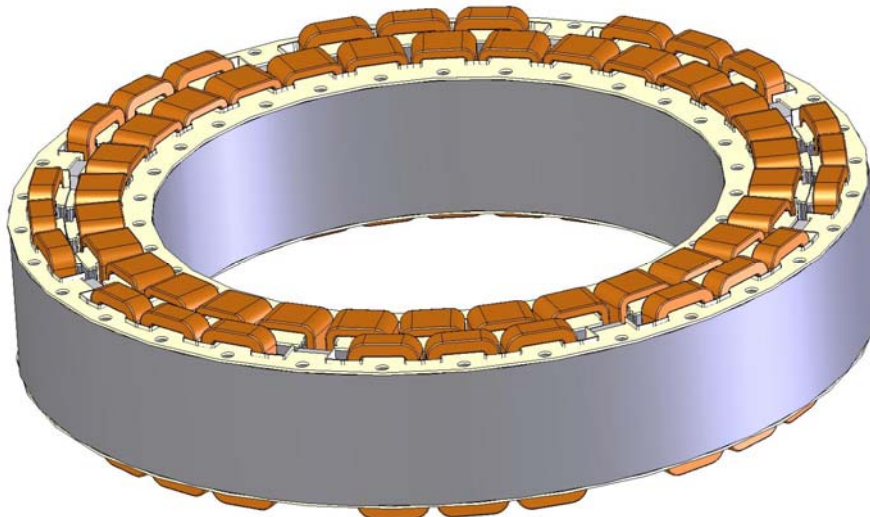

Figure 4.14 Outer rotor 32-pole 30-slot HMSM

The detailed view of the machine that according to the first assumption can have 2, 4, 8 poles for permanent magnets is shown in Figure 4.15. It is decided that the teeth has the same dimensions, though different height in radial direction, for the stator as well as the rotor. This could facilitate the prototyping. The constant tooth width (or slightly conical) could facilitate both assembling as well as the heat transfer from the compact pre-wound coils. Liner insulation, and (likely unnecessary) side insulation is shown. The magnetic core of M330-50A grade of electromagnetic steel can be made of sectors or whole sheets that include all slots, mounting holes, locking grooves and so on.
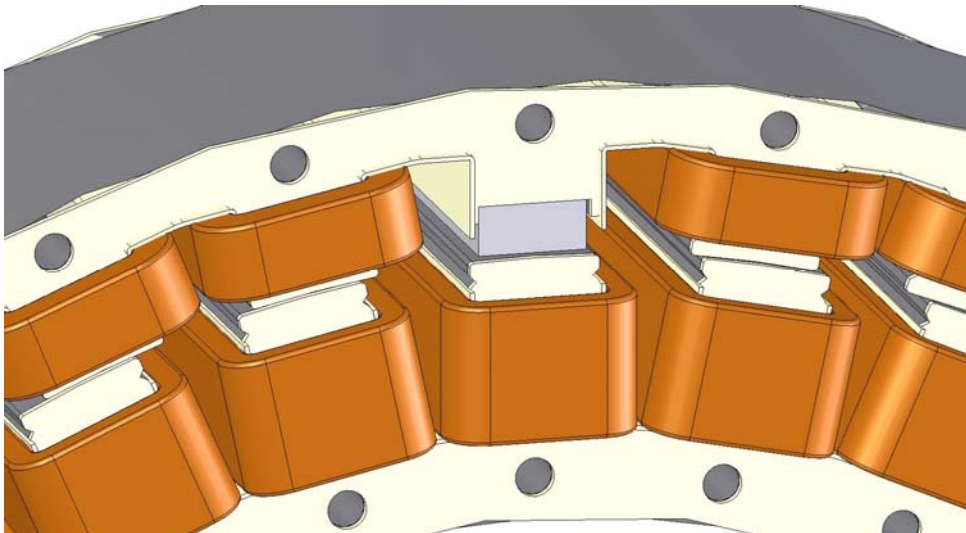
Figure 4.15 Detail view of Outer rotor 32-pole 30-slot HMSM

A more detailed view of the machine geometry is shown in Figure 4.16. Most of the details are included in 2D FEA when the machine characteristics are calculated.
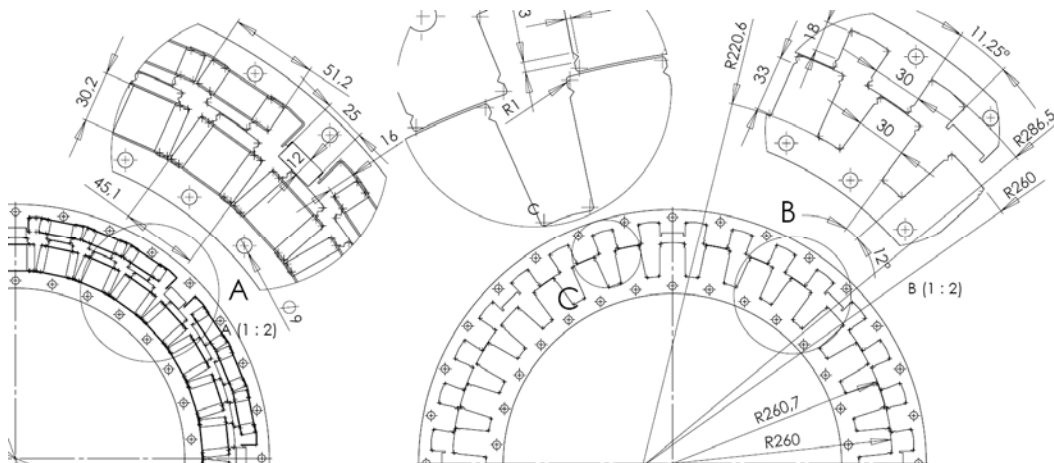

Figure 4.16 Detailed views and dimensions on the initial design of HMSM

The 2D FEA is used to determine

1. All flux linkages, self and mutual inductances of the stator and rotor as a function of current and rotor position

2. Torque as a function of a function of current and rotor position

3. Magnetic loading and magnetization energy losses in the magnetic core

This information is then used to find out the amount and the placement of the permanent magnets, which have two concerns: balanced radial forces and minimized resultant tangential forces i.e. minimized cogging.

The summa of excitations of the machine are determined by initial PM and add on EM excitation

$$\psi = \psi_{pm} + i_f L_f = \psi_{pm} + \frac{\omega_n \psi}{R_f} L_f \quad 4.1$$

Based on the machine parameters the machine performance is estimated as the extracted power over the load resistance

$$P = \frac{3}{2} \omega^2 \left(\frac{\psi_{pm} + i_f L_{sf}}{R_{load} + R_s + j\omega L_s} \right)^2 R_{load} \quad 4.2$$

4.3   Large D600 machine

The large Ø600 mm HMSM topology specification is set up according to number of poles (N_p), number of coils or stator slots (N_c) and number of permanent magnet poles (N_m). The machine is selected to be outer rotor machine but could be as well as inner rotor machine. The calculated results from 2D FE provides information about flux linkages, stator winding parameters and torque such as load torque and cogging torque (Table 4.1). The additional parameters that are related to the outcomes from the 2D FEA is the estimation of the power and the power losses.

Table 4.1 Machine magnetic coupling, stator winding parameters and cogging

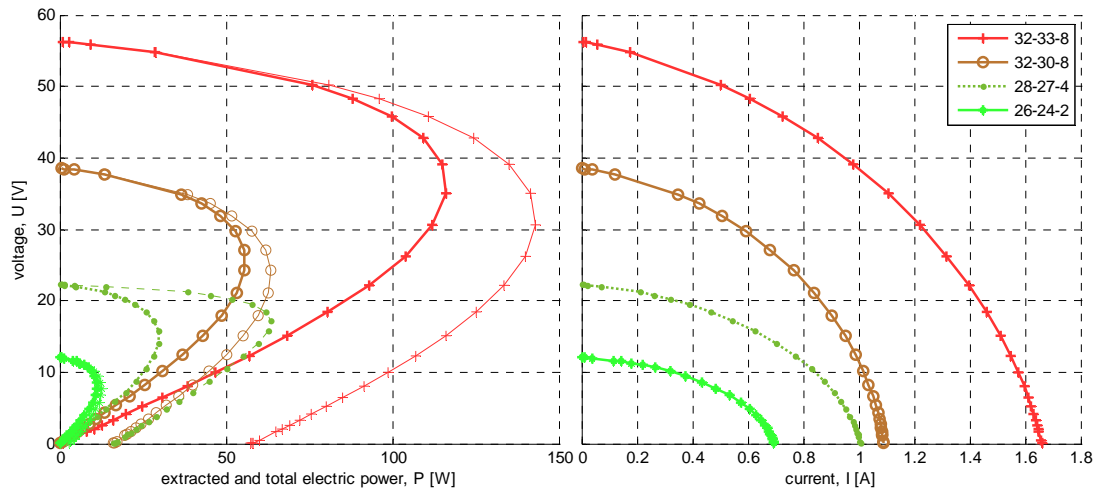| Configuration	PM flux linkage	HM flux linkage	Phase resistance	Phase inductance	PM/HM cogging	HM copper losses
Np-Nc-Nm	Ψ_r/Ψ_s [Vs]	Ψ_r/Ψ_s [Vs]	Rr/Rs [Ohm]	Lr/Ls [H]	Tcog [Nm]	W
32-33-8	0.58/0.95	6.82/3.26	7.36/3.48	0.62/0.36	4/10	736
32-30-8	0.60/0.65	6.40/3.05	7.36/2.26	0.58/0.38	25/55	736
28-27-4	0.03/0.43	5.86/2.66	5.25/1.42	0.58/0.11	7/14	525
26-24-2	0.027/0.25	5.31/2.40	4.9/0.97	0.52/0.23		490

Figure 4.17 Generator characteristics with PM excitation only
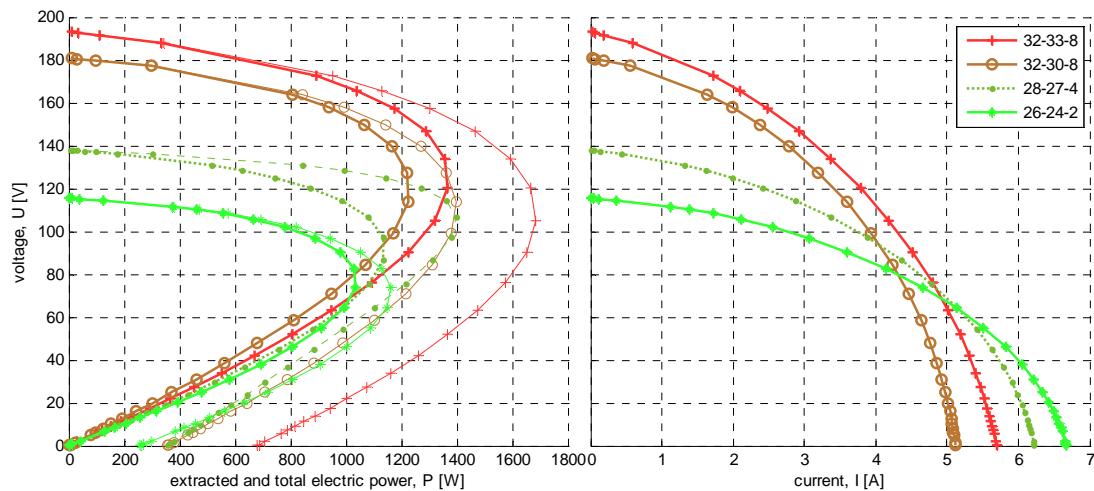

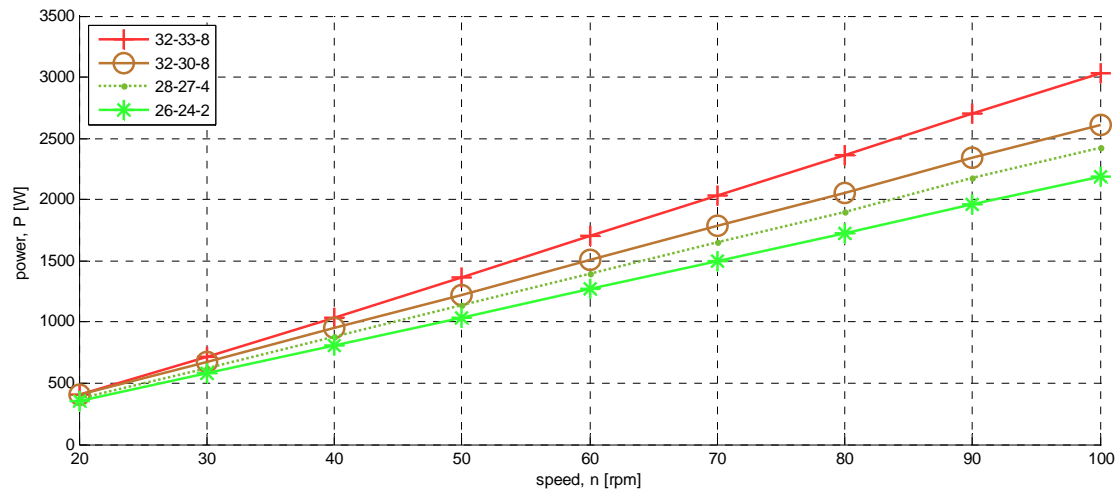*Figure 4.18 Generator characteristics with HM characteristics*

Figure 4.19 maximum power as a function of turbine speed

The simulation results is based (often) on the complete machine due to low periodicity. Large models causes a large computation time and therefore also the resolution of the obtained data is partly minimal. Anyhow following options are used in the models

1. each coil either in rotor or stator have 100 turns

2. Excitation current is changed from 0, 0.25, 0.5, 0.75 and 1.0 or alternatively 0.0 and 1.0 times the maximum current of 20 A

3. current density, power loss density and power losses are calculated from the applied current

4. Saturation occurs around 0.5 times the set current

5. A few steps over the electric period is calculated and this information can be limited in order to specify exactly the cogging

6. Cogging is clearly larger for the machines where the magnets and stator teeth can be in pairs

7. PM excitation is used to power up the HM excitation

8. Generator characteristics show the extracted power from the terminal and the power drop across the stator windings. The characteristics do not show other types of losses not even the excitation losses in the excitation windings.

9. Following section show the magnetic flux density distribution over a few selected large machines. Whole machine and detailed view is shown at PM and HM excitation conditions without any current in the stator windings.

Table 4.1 and following figures give the overview of the different machine configurations. The preferred construction is 33-slot 32-pole machine with 8 magnets. The obtained parameters are selected when the current in the excitation coils is *10 A (1000 Aturns)*. The selection of the excitation current is chosen according to magnetic saturation that becomes significant in the range of *15* to *20 A* and the power losses produced in the winding. The cross section of the excitation coil is *160 mm^2* and has to carry *10 A/mm^2* with *62.5%* fill factor with in the insulated coil. The heat load of *1.5 MW/m^3* at average temperature of *100°C* is considered here as demanding and not harming.

28-pole 27-slot machine

Geometry specification:

Ns=27; Np=28; Npm=4; wss=10e-3; wws=10e-3; wrs=16e-3; wwr=14e-3;

Figure 4.20 Complete 28p27s view: PM excited unloaded and HM excited loaded machine

Figure 4.21 Section 28p27s view: PM excited unloaded and HM excited loaded machine

32-pole 30-slot machine

Geometry specification:

Ns=30; Np=32; Npm=8; wss=6e-3; wws=7e-3; wrs=12e-3; wwr=10e-3;

Figure 4.22 Complete 32p30s view: PM excited unloaded and HM excited loaded machine

Figure 4.23 Section 32p30s view: PM excited unloaded and HM excited loaded machine

32-pole 33-slot machine

Geometry specification:

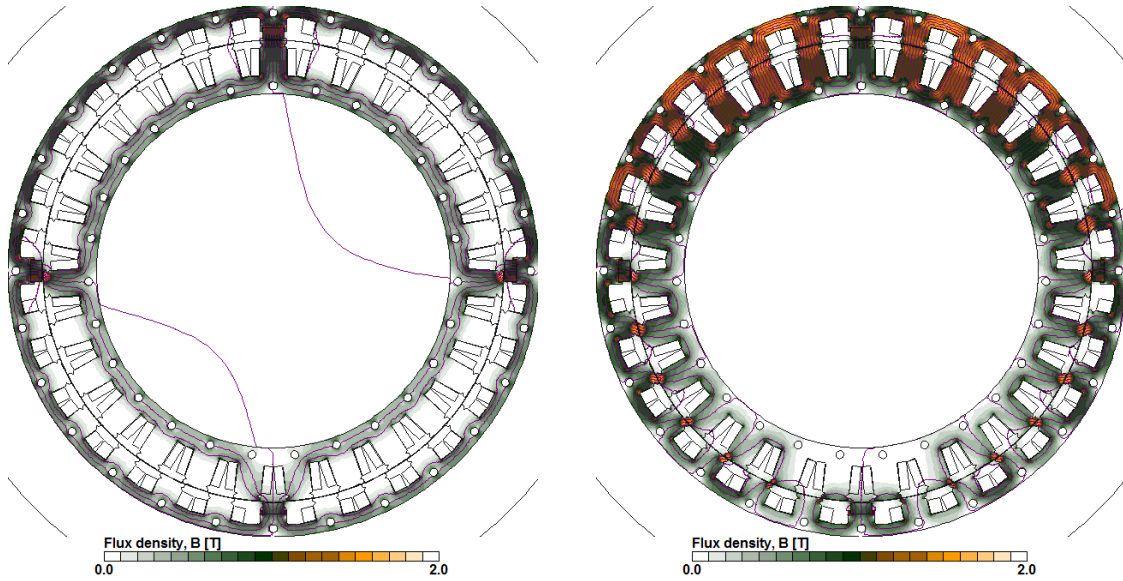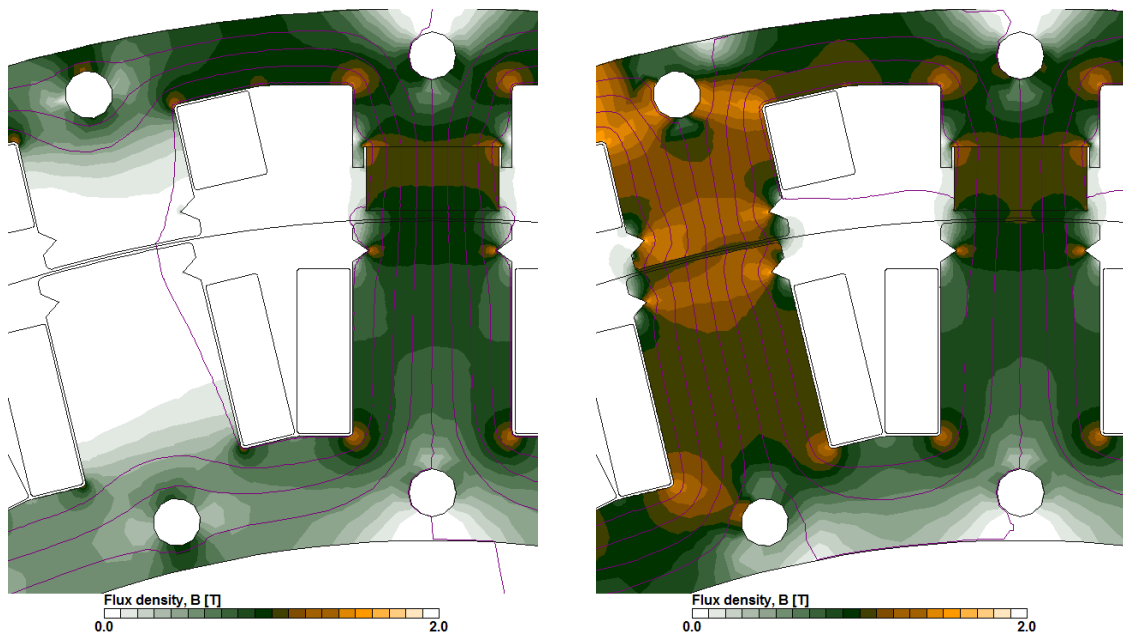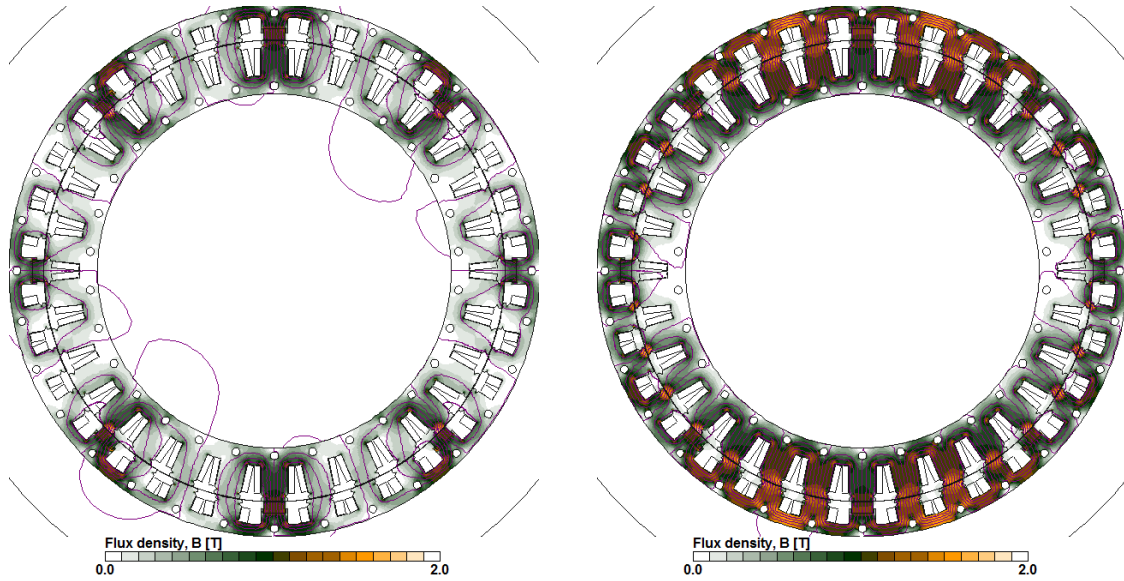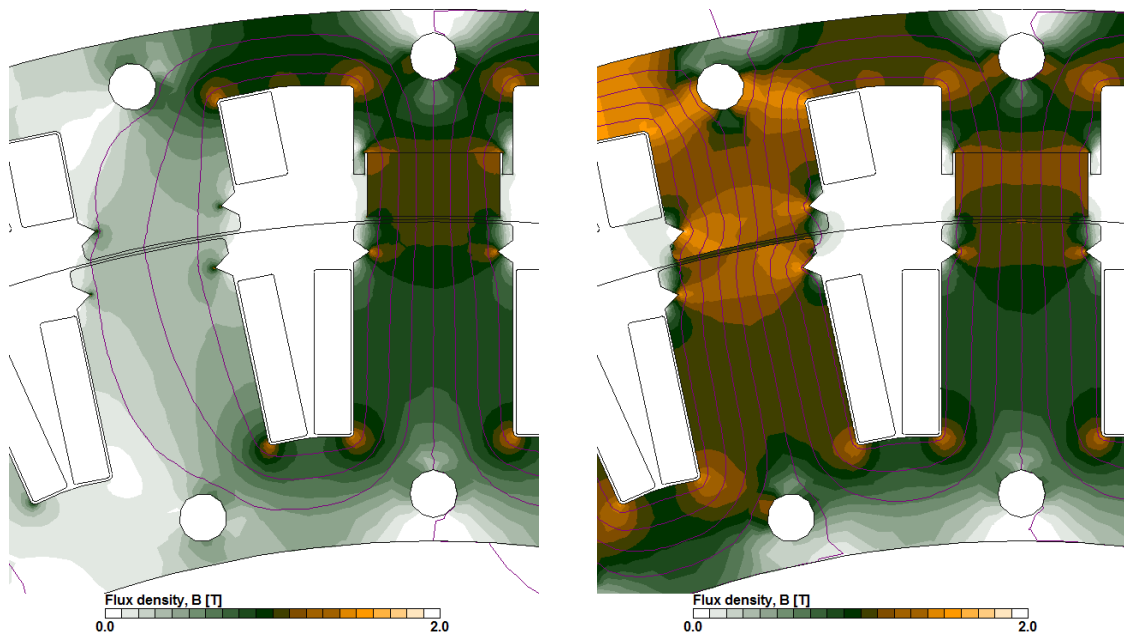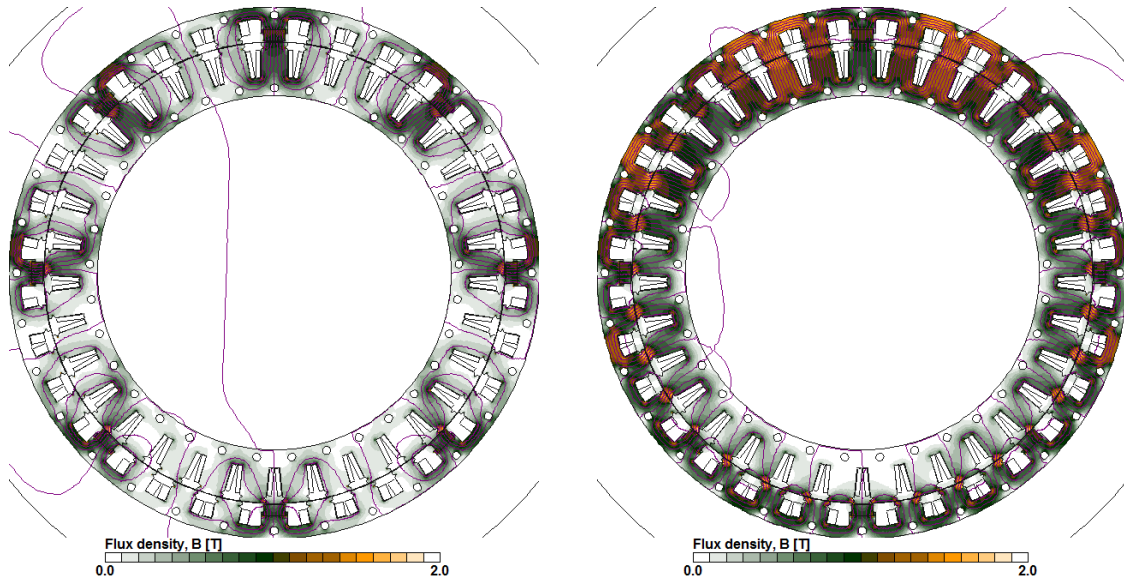Ns=33; Np=32; Npm=8; wss=5e-3; wws=5e-3; wrs=12e-3; wwr=10e-3;

Figure 4.24 Complete 32p33s view: PM excited unloaded and HM excited loaded machine
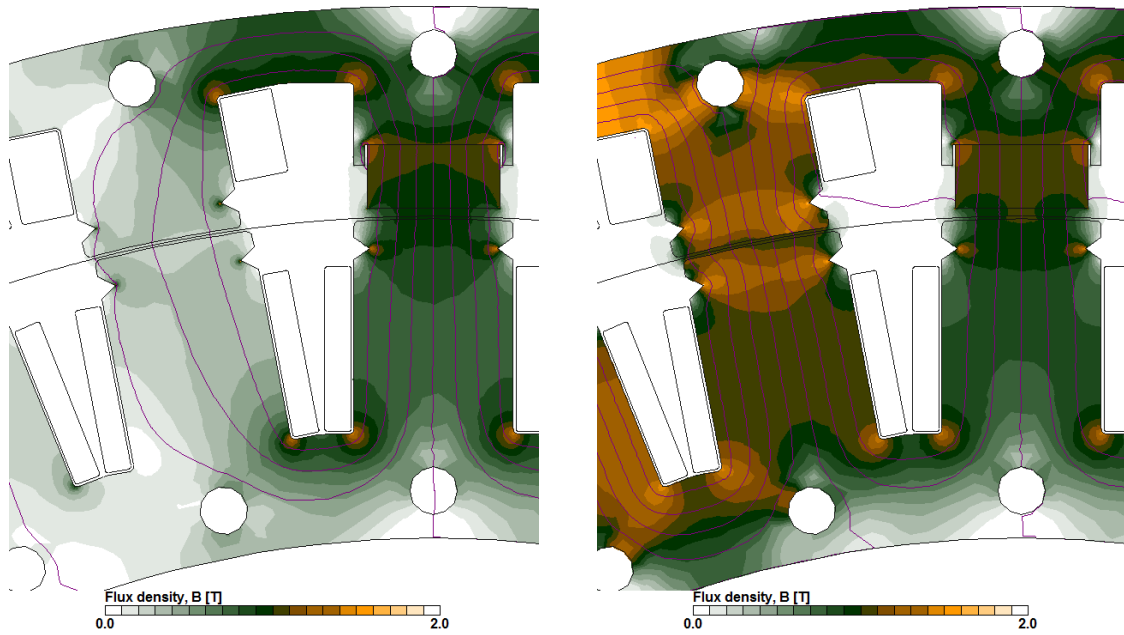

Figure 4.25 Section 32p33s view: PM excited unloaded and HM excited loaded machine

4.4   Small D400 machine

The small Ø400 mm HMSM topology specification is set up according to number of poles (N_p), number of coils or stator slots (N_c) and number of permanent magnet poles (N_m). The machine is selected to be outer rotor machine but could be as well as inner rotor machine. The calculated results from 2D FE provides information about flux linkages, stator winding parameters and torque such as load torque and cogging torque (Table 4.2).

Table 4.2 Machine magnetic coupling, stator winding parameters and cogging

Configuration	PM flux linkage	HM flux linkage	Phase resistance	Phase inductance	PM/HM cogging	HM copper losses
Np-Nc-Nm	$\Psi r/\Psi s$ [Vs]	$\Psi r/\Psi s$ [Vs]	Rr/Rs [Ohm]	Lr/Ls [H]	Tcog [Nm]	W
22-21-2	0.0165/0.13	4.26/1.46	4.96/2.08	0.42/0.11	15/53	495
20-21-4	0.0139/0.26	3.55/1.70	3.63/2.08	0.35/0.07	15/25	363
20-18-4	0.0143/0.13	3.21/1.55	3.63/1.27	0.32/0.02		363

4.5   Summary

The main goal for the WG is to provide a HMSM machine design for direct driven axial flux wind turbine for household supply that takes advantage of less PM material and self-excitation. The actual challenge here is that the machine supposes to be directly coupled, to rotate at low speed (50 rpm at full load), deliver a few kW and to be inexpensive. In order to do that the advantage of open slot, premade coils and distributed concentrated windings are taken in order to take most benefit of design for manufacturing.

The machine design bases on the previously defined 0.6 m diameter radial flux machine. In this design four cases of interest are present. There are from 26-pole to 32-pole machines with different number of stator coils and number of PM-poles. The focus on the magnetic analysis is the torque and torque ripple (especially cogging). The machine parameters are obtained at the nominal load (current) conditions and used to estimate generator characteristics. In the table of parameters and machine configuration there is the power need for the nominal EM excitation.

This analysis example shows the challenging application area of wind power harvesting where the low-speed wind turbine is connected directly to a HMSM and most of the power that the machine is able to generate is actually consumed by the hybrid excitation. The generator characteristics are presented at 50 rpm for PM excited machine and for HM excited machine. The characteristics show the extracted power and current from the no-load machine to short-circuit. The maximum power of the best configurations is in range of 1.2 to 1.4 kW where more than half of the power is needed to supply the HM excitation. In spite of technical features the machine is not considered to be attractive to the specified application.

Our experience on HMSM for wind power is based on the fact that everything what we could save in magnets we paid in a larger machine and field supply

5 Conclusions and future work

From manufacturing point of view Damia-2 for wind power application has shown that the molding technique establishes a considerable alternative to build large electromagnetic devices.

5.1 Specification and topology selection

This has not been an easy task to provide a high torque low speed machine for wind power application. Even the effort on designing a hybrid magnetized synchronous machine with high permeability core has not (theoretically) over performed the designed and prototyped SM²C stator for a double sided axial flux PM wind generator (PMWG).

5.2 Design and production

The design and production experience has clearly shown the benefit of using low permeability material for coreless machines when looking backwards on axial flux double sided PMWG. The cogging is minimized but the mechanical construction should be improved in order to reduce the air-gap and increase the extracted power.

References

[1]   Ahmed, A.A.; Abdel-Latif, K.M.; Eissa, M.M.; Wasfy, S.M.; Malik, O.P. "Study of characteristics of wind turbine PMSG with reduced switches count converters", Electrical and Computer Engineering (CCECE), 2013 26th Annual IEEE Canadian Conference on, On page(s): 1 - 5 (483KB)

[2]   Ahsanullah, K.; Dutta, R.; Rahman, M.F. "Review of PM generator designs for direct-drive wind turbines", Universities Power Engineering Conference (AUPEC), 2012 22nd Australasian, On page(s): 1 - 6, Volume: Issue: , 26-29 Sept. 2012, (1091KB)

[3]   Baroudi J.A., V.Dinavahi, and A.M.Knight,"A Review of Power Converter Topologies for Wind Generators" Renewable Energy, Vol. 32, No.19, Jan.2007, pp.2369-238, (213KB)

[4]   Bianchi N. and A. Lorenzoni "Permanent magnet generators for wind power industry: An overall comparison with traditional generators", Proc. Int. Conf. Opportun. Adv. Int. Elect. Power Gen., pp.49 -54, 1996, , (607KB)

[5]   Chen Y. , P. Pillay and A. Khan "PM wind generator topologies", IEEE Trans. Ind. Appl., vol. 41, no. 6, pp.1619 -1626 2005 (856KB)

[6]   Chen Z, Spooner E, "Wind turbine power converters: A comparative study,". In: Proceedings of IEE seventh international conference on power electronics and variable speed drives, September 1998. p. 471–6.

[7]   Chen Z.,J.M.Guerrero and F. Blaabjerg, "A Review of the State of the Art of Power Electronics for Wind Turbines" IEEE Trans. Energy Conversion,Vol.24, No.8,Agust.2009, , (957KB)

[8]   Chinchilia M., S.Arnaltes, and J.Burgos, "Control of Permanent-Magnet Generator Applied to Variable-Speed Wind-Energy Systems Connected to the Grid," IEEE Trans. Energy conversion, Vol.21, No.1, March.2006, Chi06.pdf, (176KB)

[9]   Corbus D. and D. Prascher "Analysis and comparison of test results from the small wind research turbine test project", 43rd AIAA Aerospace Sciences Meeting Exhibit—Collection ASME Wind Energy Symp. Tech. Papers, 2005

[10] Datta R., V.T. Ranganathan, "A method of tracking the peak power points for a variable speed wind energy conversion system," IEEE, Trans Energy Conver, 18 (2003), pp. 163–168

[11] Esmaili R. , L. Xu and D. Nichols "A new control method of permanent magnet generator for maximum power tracking in wind turbine application", Proc. IEEE Power Eng. Soc. Gen. Meeting, vol. 3, pp.2090 -2095 2005 (1122KB)

[12] Gerlando A. D. , G. Foglia , M. F. Iacchetti and R. Perini "Analysis and test of diode rectifier solutions in grid-connected wind energy conversion systems employing modular permanent-magnet synchronous generators", IEEE Trans. Ind. Electron., vol. 59, no. 5, pp.2135 -2146 2012 (2625KB)

[13] Goto H., H.-J. Guo and O. Ichinokura "A micro wind power generation system using permanent magnet reluctance generator", Proc. 13th Eur. Conf. Power Electron. Appl., pp.1 -8 2009 (292KB)

[14] Haque Md. E., M. Negnevistsky, and K. M. Muttaaqi, "A Naval Control Strategy for a Variable Speed Wind Turbine With a Permanent Magnet Synchronous Generator," IEEE Trans. Industry Applications, Vol.46, No.1, Jun/Feb.2010, Haq10.pdf, (1333KB)

[15] Huang H, Chang L, A new DC link voltage boost scheme of IGBT inverters for wind energy extraction. In: Proceedings of IEEE Canadian conference on electrical and computer engineering, vol. 1, March 2000. p. 540–4.

[16] Hyong Sik Kim; Lu, D.D.-C. "Review on wind turbine generators and power electronic converters with the grid-connection issues", Universities Power Engineering Conference (AUPEC), 2010 20th Australasian, On page(s): 1 - 6, Volume: Issue: , 5-8 Dec. 2010, (417KB)

[17] Jang S. M. , H. J. Seo , Y. S. Park , H. I. Park and J. Y. Choi "Design and electromagnetic field characteristic analysis of 1.5 kW small scale wind power generator for substitution of Nd-Fe-B to ferrite permanent magnet", IEEE Trans. Magn., vol. 48, no. 11, pp.2933 -2936 2012, (1082KB)

[18] Jang S. M. , H. K. Kim , J. Y. Choi and K. J. Ko "Analysis and comparison for rotor eddy current losses of permanent magnet synchronous generator according to dc and ac load conditions", J. Appl. Phys., vol. 105, no. 7, pp.07F109-07F109-3 2009, (248KB)

[19] Jang S. M. , M. M. Koo , Y. S. Park , J. Y. Choi and S. H. Lee "Characteristic analysis on the influence of misaligned rotor position of double-sided axial flux permanent magnet machine and experimental verification", IEEE Trans. Magn., vol. 48, no. 11, pp.2941 -2944 2012, (960KB)

[20] Jiawei Chen; Jie Chen; Chunying Gong "New Overall Power Control Strategy for Variable-Speed Fixed-Pitch Wind Turbines Within the Whole Wind Velocity Range", Industrial Electronics, IEEE Transactions on, On page(s): 2652 - 2660 Volume: 60, Issue: 7, July 2013 (635KB)

[21] Karbakhsh, M.; Abutorabi, H.; Khazaee, A. "An enhanced MPPT fuzzy control of a wind turbine equipped with permanent magnet synchronous generator", Computer and Knowledge Engineering (ICCKE), 2012 2nd International eConference on, On page(s): 77 - 82 (456KB)

[22] Khan M. , P. Pillay and K. Visser "On adapting a small PM wind generator for a multi-blade, high solidity wind turbine", Proc. IEEE Power Eng. Soc. Gen. Meeting, vol. 3, pp.2096 2005 (730KB)

[23] Khazaee, A.; Zarchih, H.A.; Ebrahimi, M. "Robust maximum power point tracking control of permanent magnet synchronous generator for grid connected wind turbines", Renewable Energy and Distributed Generation (ICREDG), 2012 Second Iranian Conference on, On page(s): 75 - 79 (381KB)

[24] Ko K. J. , S. M. Jang , J. H. Park , H. W. Cho and D. J. You "Electromagnetic performance analysis of wind power generator with outer permanent magnet rotor based on turbine characteristics variation over nominal wind speed", IEEE Trans. Magn., vol. 47, no. 10, pp.3292 -3295 2012, (1067KB)

[25] Kowal, D.; Dupre, L.; Sergeant, P.; Vandenbossche, L.; De Wulf, M. "Influence of the Electrical Steel Grade on the Performance of the Direct-Drive and Single Stage Gearbox Permanent-Magnet Machine for Wind Energy Generation, Based on an Analytical Model", Magnetics, IEEE Transactions on, On page(s): 4781 - 4790 Volume: 47, Issue: 12, Dec. 2011 (613KB)

[26] Koyanagi A, Nakamura H, Kobayashi M, Suzuki Y, Shimada R, Study on maximum power point tracking of wind turbine generator using a flywheel. In: Proceedings of IEEE PCC'02, vol. 1, April 2002. p. 322–7.

[27] Lee Hak-Jun; Seung-Ki Sul "Wind power collection and transmission with series connected current source converters", Power Electronics and Applications (EPE 2011), Proceedings of the 2011-14th European Conference on, On page(s): 1 - 10, Volume: Issue: , Aug. 30 2011-Sept. 1 2011, (1096KB)

[28] Li S., T.A.Haskew, and L.Xu, "Conventional and Novel Control Designs for Direct Driven PMSG Wind Turbines" Electric Power System Research, Vol.80, Oct.2009, pp.328-338.

[29] Li, H. and Z. Chen "Overview of different wind generator systems and their comparisons", IET Renew. Power Gener., vol. 2, no. 2, pp.123 -138 2008, (425KB)

[30] Luise, F.; Pieri, S.; Mezzarobba, M.; Tessarolo, A. "Regenerative Testing of a Concentrated-Winding Permanent-Magnet Synchronous Machine for Offshore Wind Generation—Part II: Test Implementation and Results", Industry Applications, IEEE Transactions on, On page(s): 1791 - 1796 Volume: 48, Issue: 6, Nov.-Dec. 2012, (1518KB)

[31] Mehrzad D.,J.Luque,M.C.Quenca," Vector Control of PMSG for Grid Connected Wind Turbine Application," Project for Master's Thesis, Institute of Energy Technology, Alborg University, Spring.2009.

[32] Milivojevic N., I. Stamenkovic and N. Schofield "Power and energy analysis of commercial small wind turbine systems", Proc. IEEE Int. Conf. Ind. Technol., pp.1739 -1744 2010, (752KB)

[33] Miller A. , E. Muljadi and D. Zinger "A variable speed wind turbine power control", IEEE Trans. Energy Convers., vol. 12, no. 2, pp.181 -186 1997 (452KB)

[34] Nicolas C, Lafoz M, Iglesias J. Guidelines for the design and control of electrical generator systems for new grid connected wind turbine generators. In: Proceedings of IEEE IECON'02, vol. 4, November 2002. p. 3317–25.

[35] Park Y. S. , S. M. Jang , J. H. Choi , J. Y. Choi and D. J. You "Characteristic analysis on axial flux permanent magnet synchronous generator considering wind turbine characteristics according to wind speed for small-scale power application", IEEE Trans. Magn., vol. 48, no. 11, pp.2937 -2940 2012, (1168KB)

[36] Park, Y.-S. et all "Comparative Investigation on Integrated System of Permanent Magnet Synchronous Generator and Power Converter Based on Machine Topology for Small-Scale Wind Power Application" IEEE Trans Magn, Vol 49 n 7, July 2013, (1135KB)

[37] Park, Y.-S.; Koo, M.-M.; Jang, S.-M.; Park, H.-I.; Choi, J.-Y. "Characteristic Analysis of Grid-Connected PM Wind Power Generators based on Transfer Relations and Performance Evaluation", Energy Conversion, IEEE Transactions on, On page(s): 969 - 978 Volume: 28, Issue: 4, Dec. 2013 (1629KB)

[38] Pena RS, Cardenas RJ, Clare JC, Asher GM. Control strategies for voltage control of a boost type PWM converter. In: Proceedings of IEEE PESC'01, vol. 2, June 2001. p. 730–5.

[39] Polinder H.,F.F.A.V.der Pijl,Gert-Jan de Vilder,and P.J.Tavner, "Comparison of Direct-Drive and Geared Generator Concept for Wind Turbines," IEEE Trans. Energy Conversion, Vol.21, No.3, September.2006 , Pol06.pdf, (508KB)

[40] Pucci, M.; Cirrincione, M. "Neural MPPT Control of Wind Generators With Induction Machines Without Speed Sensors", Industrial Electronics, IEEE Transactions on, On page(s): 37 - 47 Volume: 58, Issue: 1, Jan. 2011, (1497KB)

[41] Pyrhonen, J.J.; Alexandrova, Y.; Semken, R.S.; Hamalainen, H. "Wind power electrical drives for permanent magnet generators — Development in Finland", ELEKTRO, 2012, On page(s): 9 – 16, (1769KB)

[42] Qiao W., L.Qu,and R.G.Harely, "Control of IPM Synchronous Generator for Maximum Wind Power Generation Considering Magnetic Saturation," IEEE Trans. Industry application, Vol.45, No.3, May/Jun 2009.

[43] Rahman, M.A. "Advances of interior permanent magnet (IPM) wind generators", Electrical Machines and Systems, 2008. ICEMS 2008. International Conference on, On page(s): 2228 - 2233, Volume: Issue: , 17-20 Oct. 2008, (1692KB)

[44] Raju AB, Chatterjee K, Fernandes BG, A simple maximum power point tracker for grid connected variable speed wind energy conversion system with reduced switch count power converters. In: Proceedings of IEEE PESC'03, vol. 2, June 2003. p. 748–53.

[45] Schiemenz I, Stiebler M, Control of a permanent magnet synchronous generator used in a variable speed wind energy system. In: Proceedings of IEEE IEMDC'01, 2001. p. 872–7.

[46] Sharaf A. and M. El-Sayed "A novel hybrid integrated wind-PV micro co-generation energy scheme for village electricity", Proc. IEEE Int. Elect. Mach. Drives Conf., pp.1244 -1249 2009 (444KB)

[47] Sitapati K. and R. Krishnan "Performance comparisons of radial and axial field, permanent-magnet, brushless machines", IEEE Trans. Ind. Appl., vol. 37, no. 5, pp.1219 -1225 2011 (176KB)

[48] Sopanen, J.; Ruuskanen, V.; Nerg, J.; Pyrhonen, J. "Dynamic Torque Analysis of a Wind Turbine Drive Train Including a Direct-Driven Permanent-Magnet Generator", Industrial Electronics, IEEE Transactions on, On page(s): 3859 - 3867 Volume: 58, Issue: 9, Sept. 2011,(413KB)

[49] Svensson J. Simulation of power angle controlled voltage source converter using a linear quadratic method in a wind energy application. In: Proceedings of IEEE workshop on computers in power electronics, August 1996. p. 157–63.

[50] Tan K., and S.Islam, "Optimum Control Strategies in Energy Conversion of PMSG Wind Turbine System without Mechanical Sensors," IEEE Trans. Energy conversion .Vol.19, No.2, Jun.2004. , pp. 392–399 (752KB)

[51] Thongam J. , P. Bouchard , H. Ezzaidi and M. Ouhrouche "Wind speed sensorless maximum power point tracking control of variable speed wind energy conversion systems", Proc. IEEE Int. Elect. Mach. Drives Conf., pp.1832 -1837 2009, (733KB)

[52] Xu Yang; Patterson, D.; Hudgins, J. "Permanent magnet generator design and control for large wind turbines", Power Electronics and Machines in Wind Applications (PEMWA), 2012 IEEE, On page(s): 1 - 5 (213KB)

[53] Ying Zhu; Ming Cheng; Wei Hua "Sensorless maximum power point tracking in dual power flow wind energy conversion system", Power Electronics for Distributed Generation Systems (PEDG), 2012 3rd IEEE International Symposium on, On page(s): 58 – 63, (218KB)

[54] Yu Zou; Elbuluk, M.E.; Sozer, Y. "Stability Analysis of Maximum Power Point Tracking (MPPT) Method in Wind Power Systems", Industry Applications, IEEE Transactions on, On page(s): 1129 - 1136 Volume: 49, Issue: 3, May-June 2013 (1304KB)

[55] Zhang Jianhua; Tian Ye; Ren Mifeng; Zhang Jinfang; Hou Guolian "A novel approach to control PMSG-based wind energy systems", Control Conference (CCC), 2012 31st Chinese, On page(s): 6736 - 6740, Volume: Issue: , 25-27 July 2012, (161KB)

[56] Zhao N. , Z. Q. Zhu and W. Liu "Rotor eddy current loss calculation and thermal analysis of permanent magnet motor and generator", IEEE Trans. Magn., vol. 47, no. 10, pp.4199 -4202 2011 (682KB)